[American Journal of Science, Vol. 307, June, 2007, P. 901–953, DOI 10.2475/06.2007.02]

THE NEOPROTEROZOIC OTTFJÄLLET DIKE SWARM OF THE MIDDLE ALLOCHTHON, TRACED GEOCHEMICALLY INTO THE SCANDIAN HINTERLAND, WESTERN GNEISS REGION, NORWAY

KURT HOLLOCHER*, PETER ROBINSON**, EMILY WALSH***, and MICHAEL P. TERRY§

ABSTRACT. The Ottfjället swarm of Late Neoproterozoic mafic dikes, cutting Neoproterozoic sandstones, became a key, 30 years ago, to the tectonics of the Scandian Caledonides. The sandstones were deposited in basins related to opening of Iapetus, and intruded by dikes in distal parts of the Baltoscandian margin close to the developing spreading axis. The sandstones and underlying basement rocks were transported, from west of the present Norwegian coast, to as far east as western Sweden during the Silurian-Devonian Scandian Orogeny. The sandstones with dikes make up the Särv Nappe, up to 2 km thick in Sweden, and the quartzites and amphibolites of the Sætra and equivalent nappes in Norway. These form the upper part of the Middle Allochthon. The lower part of the Middle Allochthon includes Middle Proterozoic basement gneisses and rapakivi granites, containing mafic rocks in some places. The dike-bearing quartzite is a key unit due to contrast with similar rocks lacking dikes at lower tectonic levels derived from inboard parts of Baltica.

The Sætra Nappe and equivalents are well constrained on lithotectonic grounds in Norway at Oppdal, Leksdal, and Orkanger. It was also suspected to occur in deep, narrow synclines in the Western Gneiss Region where interlayered feldspathic quartzite and amphibolite are in correct tectonostratigraphic sequence, locally with a total thickness of only 1 to 3 m, and locally with dikes converted to eclogite. To test correlations, 127 samples of mafic rocks were collected from 14 areas west and southwest of Trondheimsfjord into the Western Gneiss region toward Ålesund. Samples include mafic rocks in quartzites and others, some clearly dikes, from the underlying 1190 Ma rapakivi granite/augen gneiss of the Risberget Nappe and adjacent basement gneisses.

Typical Sætra dikes in the Oppdal quarries, and mafic rocks from other quartzites and related rocks, have La_n/Sm_n ratios of 1.0 to 1.8, and Nb/La ratios of 0.8 to 1.4 (Oppdal group). Most REE patterns are moderately LREE-enriched with no or very small, mostly negative, Eu anomalies. All have similar multi-element patterns typically with small positive P anomalies, negative Zr-Hf anomalies and an absence of Nb-Ta anomalies, showing that the dikes are unrelated to arcs and have no notable continental crust component. A subset of Sætra, Risberget, and basement dikes is distinguished by higher La_n/Sm_n ratios of 1.8 to 2.5, but otherwise has very similar characteristics (Ystland Group). These data support correlation of the Sætra Nappe quartzite and dikes into highly deformed parts of the Western Gneiss Region and correlation of nearby dike-rich parts of basement gneiss with the Middle Allochthon.

One sample in quartzite at Ura, at an unusual tectonostratigraphic position, has $La_n/Sm_n = 0.7$, $Nb/La = 0.6$, and a multi-element pattern different from Sætra dikes, suggesting it is unrelated to the Ottfjället dikes. Non-Sætra-like amphibolites also occur in the Risberget Nappe, and have La_n/Sm_n ratios of 1.4 to 3, all Nb/La ratios <0.6, and multi-element patterns with sharp negative anomalies for Nb-Ta, P, Zr-Hf and Ti. These are probably Mesoproterozoic magmas and cumulates emplaced into the rapakivi granite protolith of the augen gneiss.

Data from this and earlier studies of correlative nappes in adjacent regions can be geographically partitioned into transitional MORB-like compositions with relatively

*Department of Geology, Union College, Schenectady, New York, 12308, USA; hollochk@union.edu
**Geological Survey of Norway, N-7491, Trondheim, Norway
***Geology Department, Cornell College, Mount Vernon, Iowa, 52314, USA
§Department of Geology and Geological Engineering, South Dakota School of Mines and Technology, Rapid City, South Dakota, 57701, USA

low LREE enrichment to the north and south, and more LREE-enriched alkaline compositions concentrated at about the latitude of northern Trondheimsfjord (~64°N). We interpret the zone of alkaline rocks to have been influenced by a nearby source of hot-spot-related enriched mantle during Late Neoproterozoic rifting of Baltica from Rodinia, with striking geochemical and spatial parallels to the modern Mid-Atlantic region.

INTRODUCTION

The Scandinavian Caledonides is a large-scale thrust-related orogen involving Silurian to Devonian (Scandian) transport of a series of allochthons over hundreds of kilometers (Gee, 1975; Gee and Sturt, 1985) onto Archean to Mesoproterozoic basement of the paleocontinent Baltica. The Western Gneiss Region is an enormous tectonic window exposing Baltoscandian Proterozoic basement, surrounded by the Caledonian thrust nappes. In the northwestern part of this region, mafic rocks of the same basement and of some cover nappes have been metamorphosed to high-pressure and ultra-high-pressure eclogites (Griffin and others, 1985; Terry and others, 2000). In a very general classification, the allochthons are divided into Lower, Middle, Upper, and Uppermost (Roberts and Gee, 1985), each characterized by complex features of stratigraphy, metamorphism, and deformation history. Tectonostratigraphic correlations and a general description of the allochthons adjacent to the northern part of the Western Gneiss Region (fig. 1) are given by Tucker and others (2004).

All the rocks studied here are thought to have belonged to the Middle Allochthon, which has two main elements in central Sweden and Norway, summarized briefly as follows: The lower part consists of Mesoproterozoic variegated basement gneisses and monotonous metamorphosed rapakivi granite, now augen gneiss, in 1659 to 1642 Ma and 1190 to 1180 Ma age groups (Handke and others, 1995). In the central Caledonides in Sweden, this unit is called the Tännäs Augen Gneiss Nappe (Röshoff, 1978); in central Norway, the same unit is called the Risberget Nappe and locally includes bodies of metamorphosed anorthosite and gabbro. These rocks likely belong to the distal basement of the pre-Silurian Baltoscandian margin, and for the most part are unlike the Baltican basement exposed in originally more proximal, eastern locations. This interpretation is supported by the 1190 to 1180 Ma age in the augen gneisses, which is unknown in the autochthonous to para-autochthonous gneisses of the region. Locally, these gneisses are cut by metamorphosed basaltic dikes in various states of deformation (Röshoff, 1978). The upper part consists of metamorphosed Neoprotoerozoic sandstones and diabase dikes introduced in detail below.

In central Sweden, the Ottfjället swarm of Neoproterozoic mafic dikes, cutting Neoproterozoic sandstones in the Särv Nappe of the Middle Allochthon, became a key, 30 years ago, to the tectonics of the Scandinavian Caledonides (Gee, 1975, 1978). The sandstones, including tillites of the Early Vendian (Ediacaran) Varangerian Ice Age (Kumpulainen and Nystuen, 1985; Knoll and others, 2006), were deposited in extensional basins in distal parts of the Baltoscandian margin related to opening of the Iapetus Ocean. The dikes intruded the sandstones and underlying basement close to the developing Iapetus spreading center (Andréasson and others, 1998; Siedlecka and others, 2004), during a later stage of the extension (Gee, 1975; Gee and others, 1985; Vidal and Moczydłowska, 1995; Siedlecka and others, 2004). The sandstones and dikes typical of the Särv Nappe, and the Sætra and equivalent nappes in Norway, are keys due to their contrast with similar sandstones lacking dikes at lower tectonic levels derived from more inboard parts of Baltica.

The dike swarm in the Särv Nappe at Ottfjället cuts a sandstone succession that is locally 2 km thick. Together with the dikes, the host sandstones are exposed in klippen that form prominent mountain plateaus held up by the resistant quartzite and dikes (Gee and Kumpulainen, 1980). Dike abundance can be sparse, but in some places in

Sweden dikes can make up 60 to 100 percent of the unit (Andréasson and others, 1998). The dikes are up to several meters thick and cut bedding at large angles, except in mylonitic shear zones near the nappe base where dikes can be traced down to mafic layers only 1 to 2 cm thick. The dike-bearing quartzites were later traced into regions in Norway with more deformation and metamorphism, for example in the areas of Leksdal (Gee, 1977; Andréasson and others, 1979), Oppdal (Krill, 1980), Orkanger (Gee and Wolff, 1981), and Sørli (Beckholmen and Roberts, 1999). In southern parts of central Norway, the unit is called the Sætra Nappe (Krill and Röshoff, 1981) and in northern parts the Leksdal Nappe (Andréassson and others, 1979; Beckholmen and Roberts, 1999).

In the Western Gneiss Region, other highly deformed feldspathic quartzites with interlayered amphibolite, in correct tectono-stratigraphic position, were long suspected to correlate with the Särv Nappe (Gee, 1980; Krill, 1980; Rickard, 1985; Krill 1987; Tucker, 1986) even where tectonically thinned to 1 to 3 m (Krill and Sigmond, 1986; Robinson 1995a, 2003; Terry and Robinson, 2003a, 2003b), or where the dikes are now eclogite (Robinson and Panish, 1994; Robinson, 1995b). Near these are similar mafic dikes intruding earlier metamorphosed Proterozoic basement rocks or 1190 Ma rapakivi granites of the Risberget Nappe with its mafic suite (Gee and Wolff, 1981; Tucker, 1986; Robinson, 1995a; Terry and Robinson, 2003a; Robinson and others, 2003). Despite the great power of lithostratigraphic similarity and sequence in these proposed correlations, doubts and questions have remained. Hence, we determined to investigate the correlations using geochemistry of the metamorphosed mafic igneous rocks.

This paper is warmly dedicated to the late Professor John Rodgers, a master of the tectono-stratigraphy of all mountain belts, particularly this one. The second author gained John as friend and consultant on matters of New England geology beginning around 1960, and partly through John and three of his former students, Ed Hansen, Alan Krill, and Bob Tucker, was introduced to the Scandinavian Caledonides. In August 1991, John visited the outcrops near Brattvåg, described here, and was enthusiastic about the proposed correlations, now supported in greater detail.

SAMPLE COLLECTIONS AND GEOLOGIC RELATIONSHIPS

Diabase Dikes in the Sætra Nappe

The most famous Norwegian locality of the Sætra Nappe is the Engan flagstone quarries near Oppdal (figs. 1 and 2A), described by Krill (1986), where the demonstrably crosscutting diabase dikes (fig. 2A) of presumed Late Neoproterozoic age are highly deformed and involved in a regional scale recumbent fold. We began here by collecting 15 dike specimens (299 – 313) to serve as a reference population, and then proceeded to areas progressively more deformed and metamorphosed. Below, we follow a geographically similar outline to describe the locations and characteristics of the rocks we studied that are assigned to the Sætra Nappe. This is followed by a description of sampled mafic dikes cutting adjacent areas of basement gneiss and the metamorphosed rapakivi granite of the Risberget Nappe, and a description of other mafic rocks of uncertain origin in the Risberget Nappe. See Appendices 2 and 3 for supplemental information.

North from Oppdal (fig. 1) the best locality for sandstone with diabase is in the small quarry at Almlia along the southeast-facing shore north of Orkanger, on the northwest limb of the Trondheim syncline. Here, 15 samples (240 – 253) were taken from highly deformed but cross-cutting dikes (fig. 2B). Additional dikes (363 – 366) were collected from the southwest end of a huge road cut in quartzite on highway E39, adjacent to the Vasslivatnet reservoir, in a synclinal belt extending from Orkanger southwest toward Vinjeora.

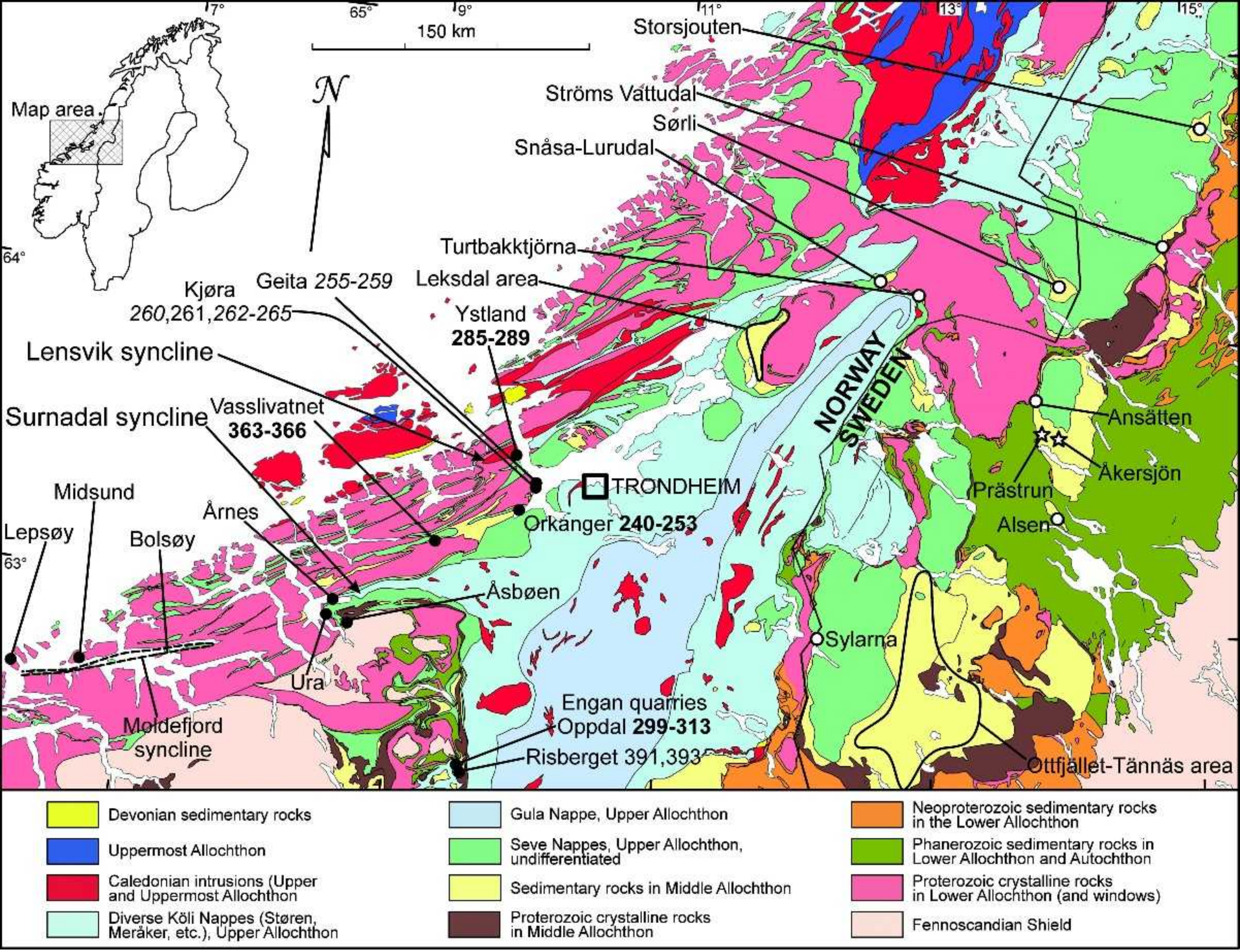

Fig 1. Gelogic map of the Trondheim region including west-central Sweden. Sample locations of this study are shown as filled circles, except those in the Moldefjord Syncline which are encompassed by a dashed outline of the syncline. Data from other studies (Appendix 1) are shown with open circles, or stars where geochemical data are unavailable. Sample numbers are shown if not located on more detailed maps. Sample number type: Dike samples in Saetra Quartzite, bold; Saetra-like dikes in basement or augen gneiss of the Risberget Nappe, italics; and not-Saetralike dikes in augen gneiss of the Risberget Nappe, plain (***94***, *103*, 102, respectively). Modified from Tucker and others (2004).

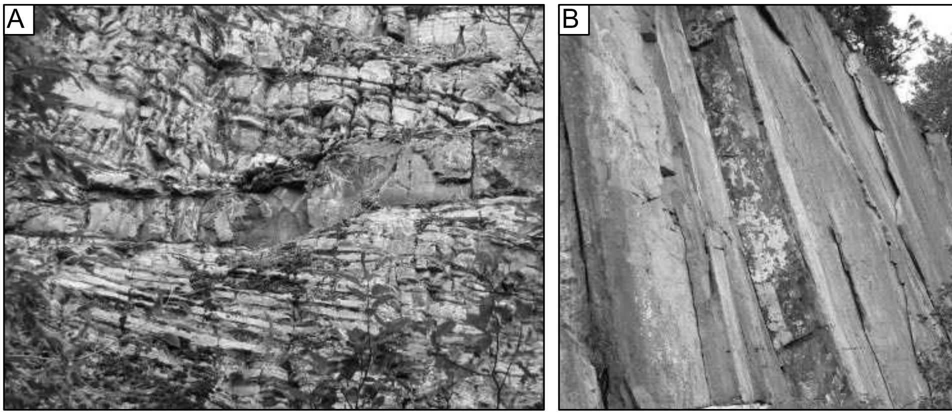

Fig. 2. Outcrop photographs of the Oppdal and Orkanger sample localities. (A) Oppdal, Eidsvoll flagstone quarry access road showing dike (sample 301) cutting horizontal quartzite bedding. (B) View in flagstone quarry at Almlia near Orkanger, showing dike in schistose quartzite (samples 240–253).

There is a superbly exposed section on the steep northwest limb of the Surnadal syncline southwest of Vasslivatnet (Grammeltvedt, 1995) at Årnes (fig. 3). Road cuts include basement, Risberget Nappe, Sætra Nappe quartzite and amphibolite, Blåhø Nappe mica schist and amphibolite, and Støren Nappe fine-grained epidote amphibolite and marble (Krill and Röshoff, 1981; Rickard, 1985; Krill, 1987). Six amphibolite samples (333 – 338) were collected from the Sætra Nappe here.

The Sætra Nappe is present but poorly exposed on both limbs of the Moldefjord syncline (fig. 3) east of Molde, including exposures on the north limb in the subsea Fannefjord Tunnel and in forest exposures near the hinge at Kortgarden (Robinson, 1995a). Extensive exposures on the south limb on the south shore of Moldefjorden from Dragneset west beyond Brattvåg (fig. 4) were sampled in four places.

The easily accessible exposure at Dragneset (fig. 5) has a 34.6 m continuous section of the Sætra Nappe, though the base against the Risberget is not exposed here

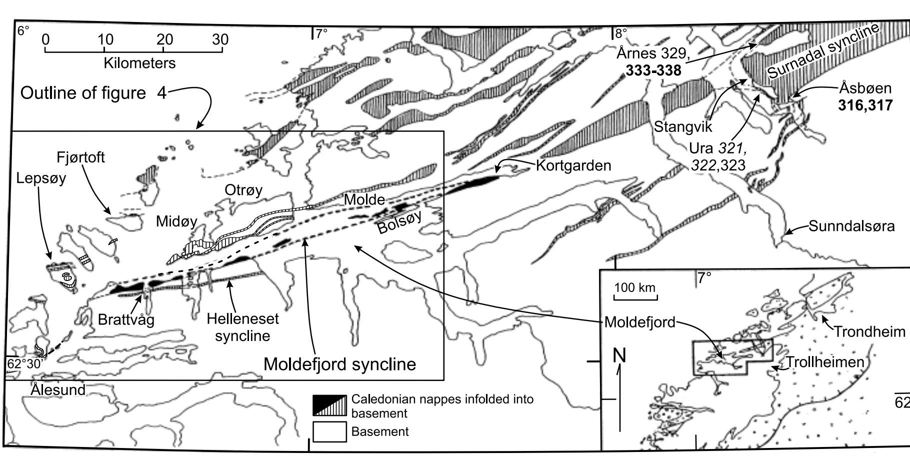

Fig. 3. Geologic index map of the Moldefjord (black) and Surnadal synclines and surrounding areas. Area of detailed index map, figure 4, is marked. Modified from Robinson (1995a, his fig. 1). Sample number symbols as in figure 1.

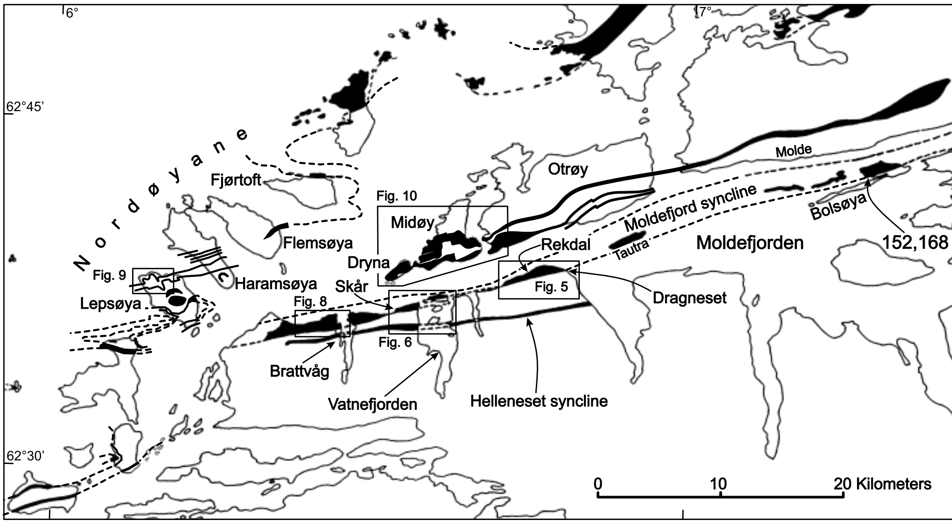

Fig. 4. Index map showing locations of detailed sample location maps for the Moldefjord and Helleneset synclines, and nearby areas. Modified from Robinson (1995a, his fig. 2). Sample number symbols as in figure 1.

and the top contact with the overlying Blåhø Nappe is in a 10.8 m covered interval. A measured section (PR station 354, August 27, 1991) through essentially vertical layers from south to north (base at bottom) gives an impression of the unit and shows the positions in the section of 6 analyzed samples.

2.2 m: Quartz-rich laminated quartzite with <5% amphibolite.
1.2 m: Fine-grained porphyritic amphibolite with abundant sulfide. **Sample 99**, 32.5 m in measured section, 25 cm from base of layer.

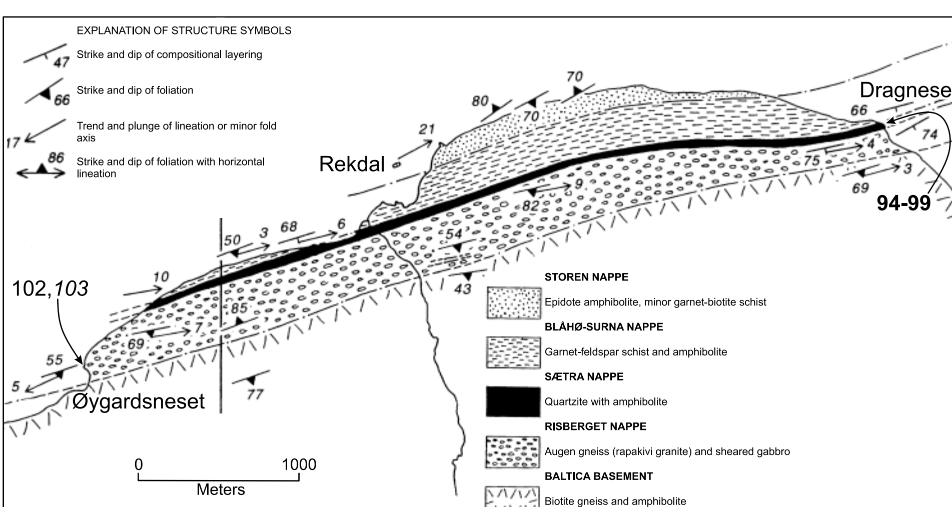

Fig. 5. Geologic map of the Rekdal area, showing sample locations at Dragneset and Øygardsneset. Modified from Robinson (1995a, his fig. 12). Sample number symbols as in figure 1.

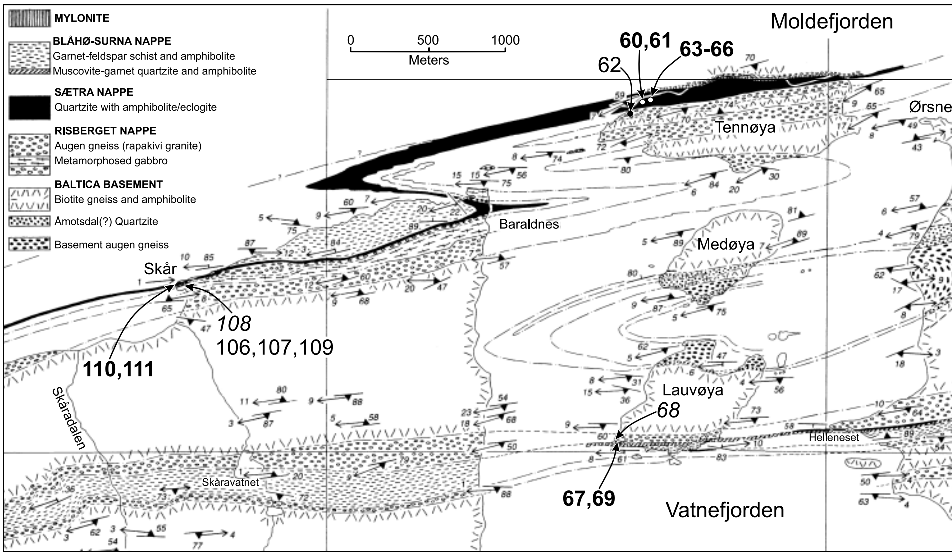

Fig. 6. Geologic map of the Vatnefjord area, showing sample localities at Tennøya, Skår, and Lauvøya. Modified from Robinson (1995a, his fig. 10). Sample number symbols as in figure 1, structure symbols as in figure 5.

3.0 m: Quartzite and amphibolite in about equal proportions. **Sample 98**, 28.5 m in measured section is from a boudin 0.6 m thick at base of zone and contains abundant epidote and sulfides.
7.4 m: Quartzite with a few amphibolites up to 25 cm.
6.2 m: Quartzite with 5% amphibolite, a few layers up to 10 cm, mostly <2.5 cm.
1.2 m: Porphyritic amphibolite with relict plagioclase phenocrysts, small garnets, pyrite. **Sample 97**, 14 m in measured section.
2.2 m: Quartzite with 5% thin amphibolite.
0.3 m: Amphibolite with sparse garnet, pyrite. **Sample 96,** 11.05 m in measured section, center of layer.
0.3 m: Quartzite with very thin amphibolite.
0.5 m: Porphyritic amphibolite with relict plagioclase phenocrysts.
1.5 m: Amphibolite 80%, quartzite 20% in 2.5-5 cm layers.
1.2 m: Thick amphibolite. **Sample 95**, at 7.65 m in measured section, 25 cm from base.
1.2 m: Quartzite with 20% thin amphibolite.
6.2 m: Amphibolite 90%, quartzite 10% or less. **Sample 94**, 3.2 m in measured section, 3 m below top.

West of Dragneset, the next extensive exposures of the Sætra Nappe are on the north shore of Tennøya, Vatnefjorden (fig. 6). Here, the base against the Risberget Nappe is well exposed, also the north contact against the late-Scandian Brattvåg mylonite zone. Here is where eclogite boudins were first found in the Sætra Nappe (Robinson, 1995a; fig. 7C). Unlike the typical amphibolites, rarely >1m thick, the eclogite boudins are as much as 6m thick, indicating that the eclogite metamorphism took place before the mafic layers were converted to the present amphibolite assemblage and deformed into thin layers. Six samples (60 – 61, 63 – 66) of variably retrograded eclogite were collected including three from a single boudin (see Appendix 2).

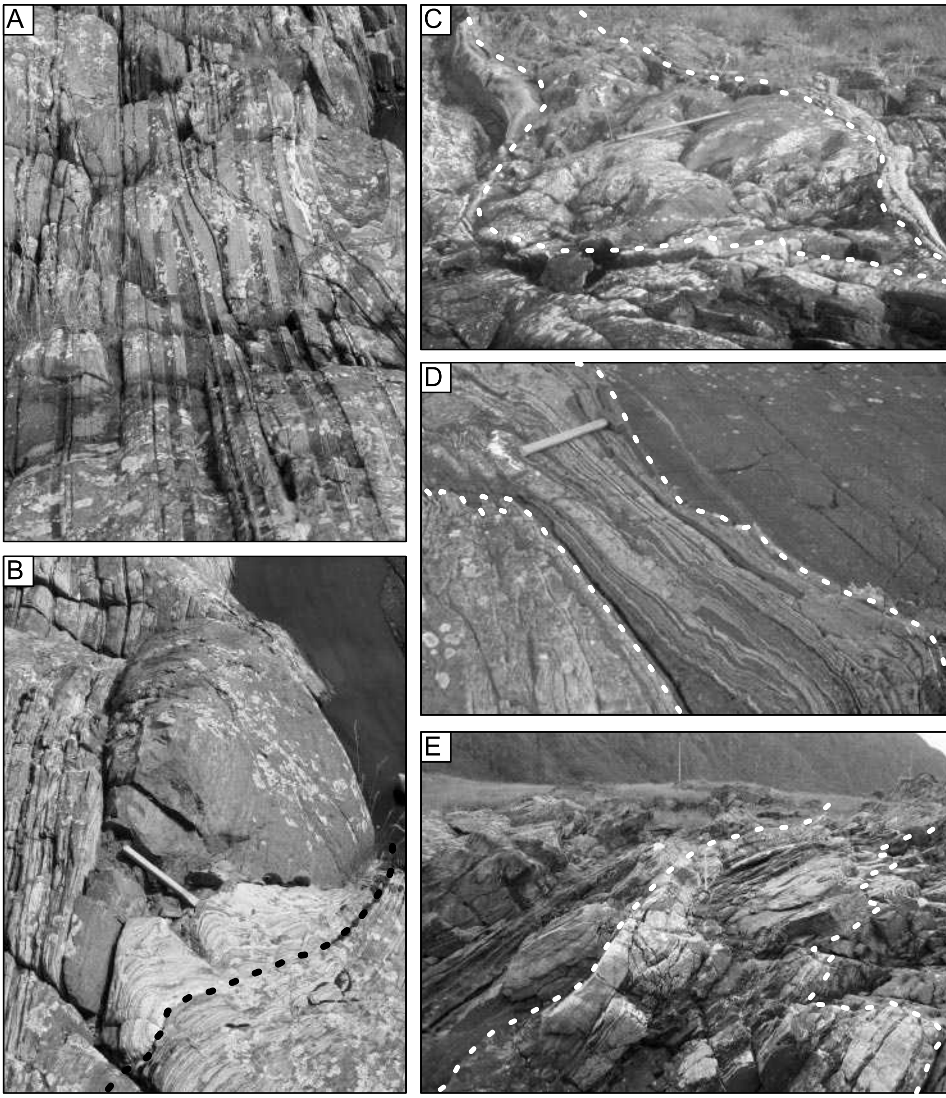

Fig. 7. Outcrop photographs of dikes in quartzite of the Sætra Nappe in the Vatnefjord area and on Lepsøy. (A) Typical isoclinal folds in quartzite and amphibolite at Skår, Moldefjord syncline. (B) Retrograded eclogite boudin in basal quartzite of Sætra Nappe at Skår. Contact with mylonitic Risberget Augen Gneiss is along the black dashed line. Note the sinistrally sheared tail of amphibolite on the eclogite (sample 110). (C) Retrograded eclogite boudin (within white dashed lines) in quartzite of the Sætra Nappe on the north coast of Tennøy (near samples 60, 61, 63-66). (D) Quartzite of the Sætra Nappe (between white dashed lines) that is only a maximum of 1.5 m thick on the northwest margin of a 10 m thick retrograded eclogite boudin (upper right, samples 67, 69) on the north limb of the Helleneset syncline, Lauvøya. The boudin is considerably thicker than the common thickness of the entire Sætra Nappe on Lauvøy. Gray rock to lower left is mylonitic Risberget Augen Gneiss. (E) 1.5 m thick layer of Sætra quartzite and amphibolite (between white dashed lines, sample 93) at Hellevik, between the Blåhø Nappe (left) and basement sausage rock (right).

The outcrop at Skår (figs. 6, 7A, and 7B) is described and illustrated by Robinson (1995a, his fig. 11). It gives 100 percent exposure of all 10 m of the Sætra Nappe, including several eclogite boudins up to 0.95 m thick near the base and many amphibolites from <1 cm thick to 30 cm thick near the top. Sample 110 is from the 0.3

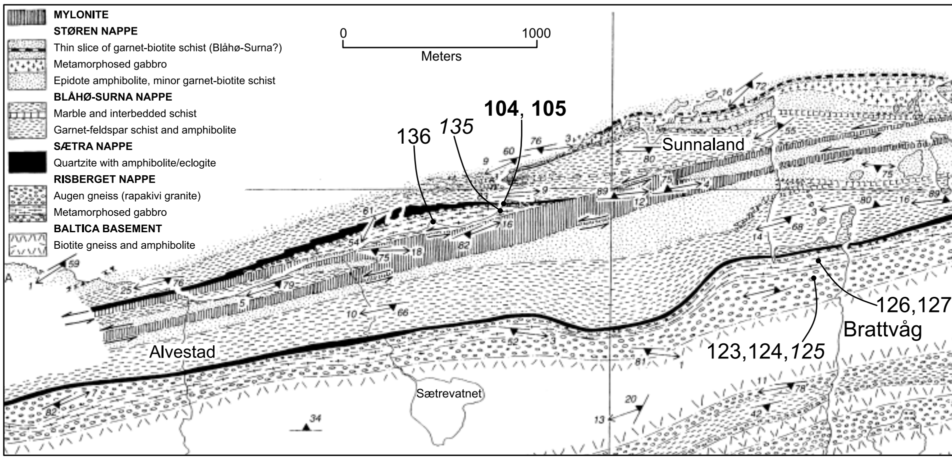

Fig. 8. Map showing sample locations in the Brattvåg area, south limb of the Moldefjord syncline. Modified from Robinson (1995a, his fig. 6). All Sætra localities lie in a tectonic slice of north-facing strata north of a major mylonite zone. Sample number symbols as in figure 1, structure symbols as in figure 5.

m-thick southern tail of an eclogite boudin 0.95 thick (fig. 7B) that is 0.3 m above the basal contact with the underlying Risberget Nappe, here a highly sheared augen-bearing mylonite, also with thin mafic layers that are probably also deformed basaltic dikes (Robinson 1995a, his fig. 11C). Sample 111 is from the highest amphibolite in the section, a plagioclase porphyry in the core of an anticlinal fold, 0.6 m below the 5 to 15 cm marble that lies on the contact with the Blåhø Nappe (Robinson 1995a, his fig. 11F).

There are many exposures of the very thin Sætra Nappe near Brattvåg (fig. 8) and two samples were collected from an exposure west of Sunnaland (PR station 195). This belt on the south limb of the Moldefjord syncline is repeated by sinistral shear on the Brattvåg mylonite zone. The section is 7 m thick and contacts with underlying Risberget and overlying Blåhø are well exposed. Sample 105 is fine-grained amphibolite within 1.5 m of the contact with the underlying Risberget. Sample 104 is porphyritic amphibolite in a boudin 0.6 m thick, 2.3 m above sample 105, and 3 m below a thin marble on the Blåhø contact.

The narrow Helleneset syncline traces for 25 km from south of Dragneset to west of Brattvåg (fig. 4). Characteristically, the syncline has a core of Blåhø Nappe rocks with a thin belt of highly sheared Risberget Nappe rocks on both limbs. A belt of the Sætra Nappe a few meters thick occurs locally on the north limb, including the southwest tip of Lauvøya (PR station 843) in Vatnefjorden (fig. 6). Here a boudin of layered, retrograded eclogite ~10 m thick (samples 67 and 69) and <1 m of quartzite appears to constitute the entire Nappe (fig. 7D).

The north coast of Lepsøya (Terry and Robinson, 2003a, their figs. 2, 6, and 7) has three narrow synclinal belts of rocks assigned to the Blåhø Nappe (fig. 9), from north to south A, B, and C, deeply infolded between belts of basement rocks. The basement rocks north of belt A, between A and B, and between B and C are eclogite-free, but the basement south of belt C contains abundant eclogite, implying a significant tectonic contact. Along the northern boundary of belt A and in a narrow isoclinal anticline within belt A, there are nearly continuous belts of quartzite with amphibolite that closely resemble Sætra Quartzite in the Moldefjord syncline. Principal differences are that there is no eclogite, the quartzites are generally more quartz-rich, and the unit is

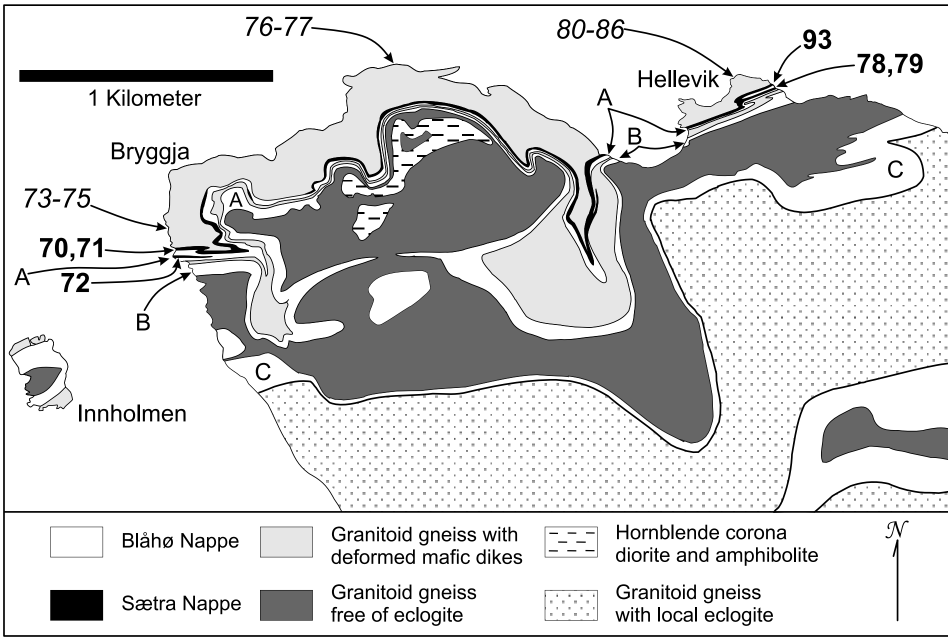

Fig. 9. Map showing sample locations on northern Lepsøy. (A), (B), and (C) represent belts of the Blåhø Nappe (see text). Modified from Terry and Robinson (2003a, their fig. 6). Sample number symbols as in figure 1.

only ~1 m thick. Stratigraphic arguments that these rocks belong to the Sætra Nappe involve lithic similarity and stratigraphic position between Blåhø rocks above and basement below. In addition, there is commonly a marble/calc-silicate layer 1 to 20 cm thick between the quartzite and the Blåhø Nappe, also common in the Moldefjord syncline (Robinson, 1995a).

Early work on the islands of Midsund (Carswell and Harvey, 1981, 1985) implied that all the rocks are pre-Caledonian basement of two types; orthogneisses of intrusive igneous origin, and paragneisses of sedimentary and volcanic origin. However, Robinson, beginning 1992 – 1993, suspected that the 'paragneisses' represent the Blåhø Nappe that lies in narrow synclines between belts of basement (fig. 10). The widespread occurrence of marble and diopside calc-silicate rock, usually <1 m thick, on the contact is similar to the occurrence of marble and calc-silicate at the base of the Blåhø Nappe in the Moldefjord syncline and reinforces this hypothesis. At Oksvollneset the same contact has ~1 m of quartzite with interlayers of diopside calc-silicate and amphibolite (figs. 11A and 11B), diagnostic of the Sætra Nappe. Three samples (183 – 185) came from the thickest parts of the amphibolite layers.

The Lensvik syncline near Ystland (Tucker, 1986) in the Trondheimsfjord region (fig. 1) is a broad northeast-plunging fold in basement overlain by a substantial thickness of Blåhø schists, amphibolites and calc-silicate rocks, and in turn overlain by low-grade amphibolites intruded by gabbros and tonalites assigned to the Støren Nappe. Very thin quartzites with amphibolite occur between Blåhø above and basement below on both shores of Trondheimsfjord. A layer of quartzite and amphibolite 1 to 3 m-thick is exposed at the southern end of a road cut in the south limb of the fold at Ystland. Five amphibolite samples (285 – 289) were taken here.

Krill (1987) mapped a separate synclinal belt of quartzites and augen gneisses southwest of and parallel to the Surnadal syncline (fig. 3) where it is involved in the

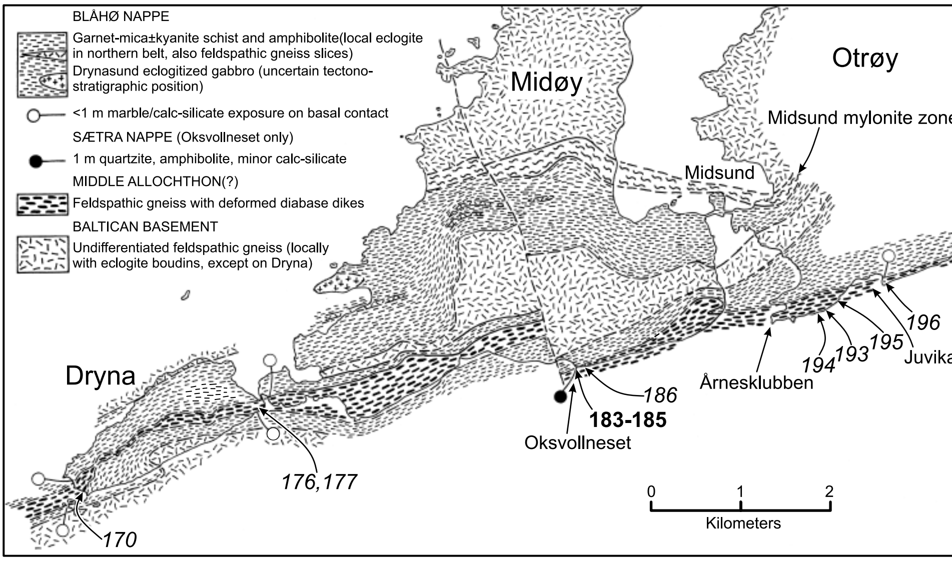

Fig. 10. Geologic map showing sample locations on Dryna, Midøy, and Otrøy, Midsund Kommune. Belts of Blåhø Nappe mica schists and amphibolites separate belts of basement rock (locally with eclogite), and basement sausage rocks (lacking eclogite). Special locations showing marble or Sætra Quartzite on contacts between Blåhø rocks and basement sausage rocks are indicated. Mapping by Robinson 1993–2006. Sample number symbols as in caption to figure 1.

enormous northwest-directed backfold at Stangvik. Here, near Ura, this belt comes ashore beneath the backfolded Surnadal syncline strata. In this belt, according to Krill, the quartzites and amphibolites of the Sætra Nappe lie on both limbs of the syncline, whereas Risberget Augen Gneiss forms a layer along the axial surface of the syncline. One sample of amphibolite (323) within quartzite was taken to test the correlation.

On the southeast limb of the Surnadal syncline at Åsbøen (fig. 3), in a region shown by Krill (1987) as basement, there are road cuts with quartzite containing dikes,

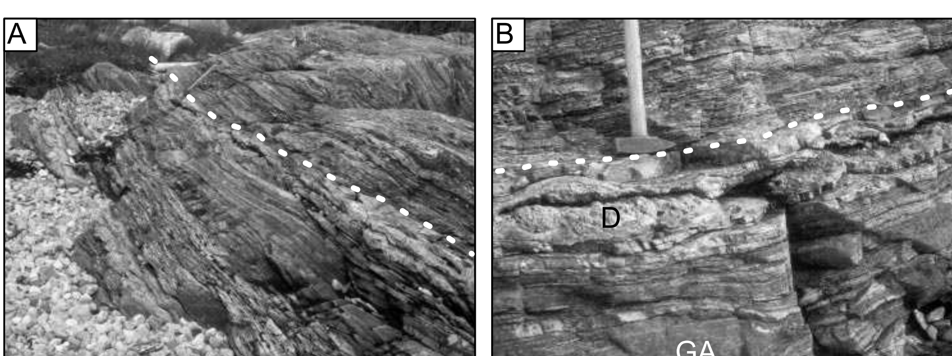

Fig. 11. Outcrop photographs of Sætra Quartzite at Oksvollneset, Midøy. (A) Quartzite 1.5 m thick (samples 183–185) in contact with basement sausage rock to the right of the dashed line. Contact with the Blåhø Nappe is under pebbles to the lower left. (B) Closeup of the same outcrop, showing the contact of Sætra Quartzite with basement gneiss above the hammerhead, a garnet amphibolite boudin in the quartzite (GA, sample 183), and a diopside calc-silicate layer (D).

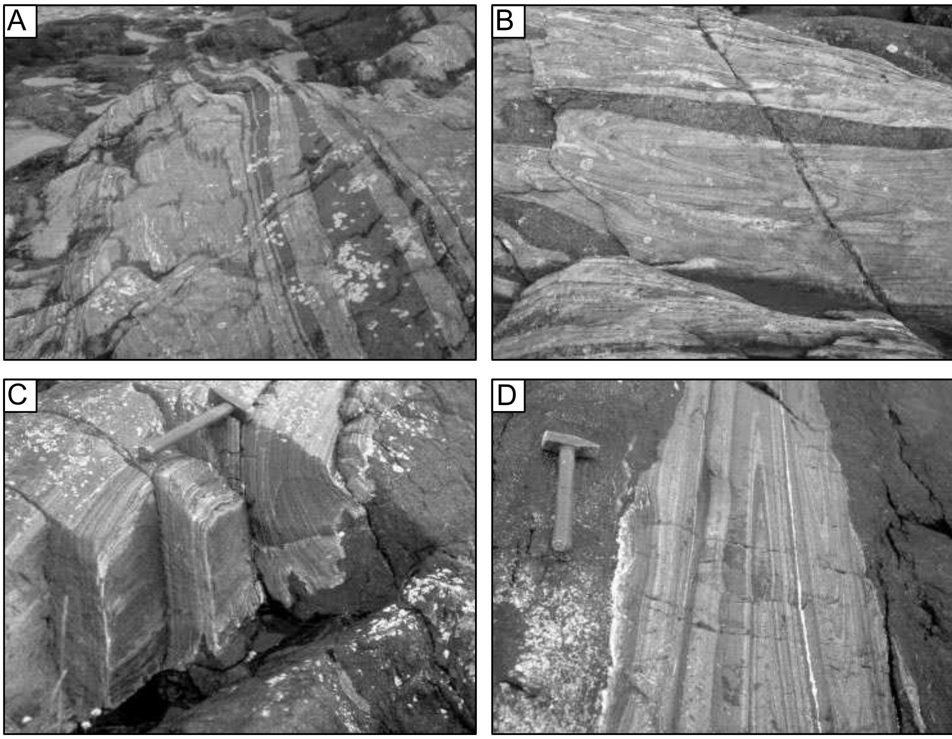

Fig. 12. Outcrop photographs of basement sausage rock, northern Lepsøy and Midøy. (A) Typical outcrop of basement sausage rock northwest of locality 93, figure 9, at Hellevik. (B) Amphibolite dike cutting layering of felsic gneiss, northern Lepsøy, midway between Hellevik and locality 93. (C) Otrøy south coast (sample 193, fig. 10), dike cutting layering in granitoid gneiss. Joint face below the hammerhead is approximately perpendicular to the subhorizontal lineation. (D) Same locality as C, showing dikes cutting layering in felsic gneiss with late folds. Fold axes and mineral lineation are parallel to each other and subparallel to the gently sloping outcrop surface. Although the dikes cut the gneissic layering, they do not appear to truncate the axial surfaces. The folds are interpreted to have nucleated and grown during late Scandian extensional deformation as a result of rheological inhomogeneities between the more rigid dike rocks and the more ductile gneiss.

and augen gneiss like the Risberget Nappe. Two samples of amphibolite (316, 317) in quartzite were collected.

Mafic Rocks in Risberget Augen Gneiss and Other Basement

In addition to quartzite with amphibolite dikes believed or suspected to correlate with the Sætra Nappe, a series of localities with mafic rocks suspected of being correlative with mafic rocks of the Sætra Nappe were found within foliated basement gneisses or Risberget Augen Gneiss. The northernmost belt of basement on Lepsøya (fig. 9), north of belt A of Blåhø rocks, and also the belt between Blåhø belts A and B were described by Terry and Robinson (2003b) as 'gray sausage rock' (fig. 12). The belts consist of rather homogeneous amphibolite in boudinaged layers from centimeters to 3 m-thick, surrounded by laminated gray gneiss (fig. 12A). In rare locations the amphibolites crosscut the gneissic layering (fig. 12B), suggesting that the mafic layers are the remains of an extensive dike swarm that may be an extension of the dike swarm in the nearby Sætra quartzites. This hypothesis was tested with 12 samples from northern Lepsøya, all from the area north of belt A of Blåhø rocks (fig. 9). The basement between Blåhø belts A and B referred to as 'shredded sausage rock', contains few mafic boudins large enough for effective sampling.

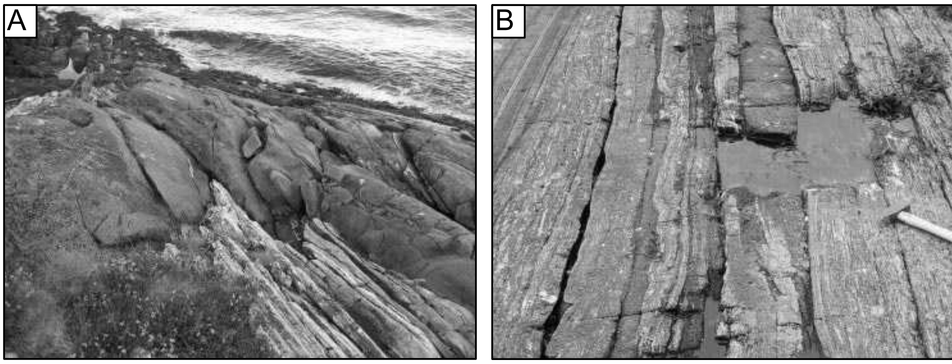

Fig. 13. Outcrop photographs of dike relations in basement and in Risberget augen gneiss. (A) Fold hinge in Sætra-like dike (sample 255) near Geita on Trondheimsfjord shore northeast of Orkanger, showing 90-degree truncation of layering in felsic basement gneiss. (B) Several thin mafic dikes on Lauvøy (sample 68, thickest dike; fig. 6), north limb of Helleneset syncline.

An extensive part of the basement on the southern shores of Dryna, Midøy, and Otrøy (fig. 10) consists of homogeneous amphibolite boudins and layers in heterogeneous, finely laminated, pinkish feldspathic gneiss (figs. 12C and 12D; near Årnesklubben, fig. 10, locality 193). Because these mafic rocks crosscut the gneissic layering, they may be the same as the dikes on Lepsøy and so could be part of the same dike swarm, possibly associated with the Sætra Nappe. Eight samples were taken from these amphibolites (fig. 10).

The outcrops at Kjøra on the shores of Trondheimsfjord (fig. 1), a popular field-trip stop for decades (Gee and Wolff, 1981; Solli and others, 1997, stop 3) have superb examples of Risberget Augen Gneiss cut by a series of mafic dikes, long suspected to be possible correlatives of the Sætra dikes. Northeast along the same coast, near Geita, the augen gneiss gives way to strongly layered and foliated basement gneiss that is cut by texturally identical dikes. In these last outcrops the basement has a strong metamorphic foliation truncated by the dikes, and the dikes have subsequently been folded (fig. 13A). The Risberget Augen Gneiss itself has a protolith age of 1190 Ma at this locality (Handke and others, 1995), considerably younger than the protolith age (1680 – 1650 Ma) of the dominant basement gneiss type in the region (Tucker and others, 1990), and also younger than the last known pre-Scandian metamorphism at 1650 Ma (Tucker and others, 2004).

The physical correlation of dikes in the Risberget and nearby basement implies that they both belong to the same nappe. Because the local, larger basement areas contain no young rocks of Risberget age (1190 Ma), it has always been assumed that the Risberget represents a far-travelled nappe from a different age province within the Fennoscandian Shield. This being so, the metamorphic age of the gneiss cut by the dikes becomes an intriguing question. Was that metamorphism as old as the 1650 Ma Svecofennian, or did it occur in a distant part of the shield that was subject to younger metamorphism, for example Sveconorwegian? It is, of course, first necessary to establish the geochemical correlation of the dikes. This was done with 10 dike samples, 255–259 cutting basement gneiss at Geita, and 260, 262–265 cutting Risberget Augen Gneiss on the coast between Geita and Kjøra. Sample 261 is of a coarse-grained amphibolite boudin in the Risberget Augen Gneiss at Kjøra that is cut by one of the younger dikes (260).

Various mafic rocks are found within the Risberget Nappe in and near the Surnadal syncline (fig. 3), on the south limb of the Moldefjord syncline, and also in the

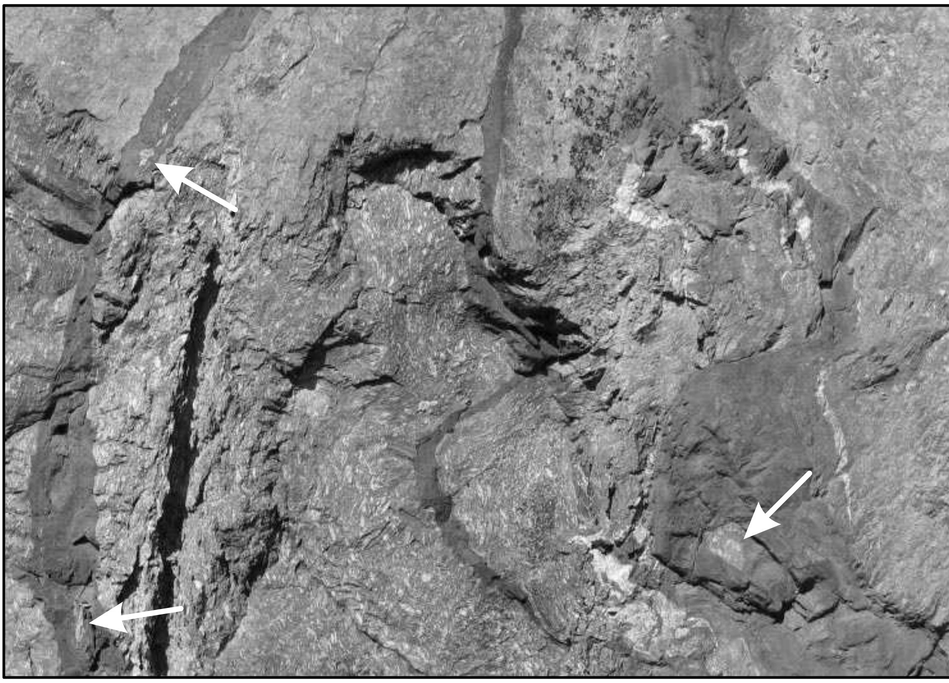

Fig. 14. Outcrop photograph of three deformed dikes in Augen Gneiss of the Risberget Nappe in a huge east-facing artificial exposure near the Brattvåg Ferry landing (fig. 8), south limb of Moldefjord syncline. Sample 123 is from the dike on the right. Arrows point to xenoliths in the dikes.

Helleneset syncline (fig. 4). Some resemble fine-grained dikes as described above (figs. 13B, 14A and 14B), others are part of extensive coarse-grained bodies described by Robinson (1995a) as metamorphosed gabbro (fig. 15). Locally, the so-called gabbro is a mappable member of the Risberget Nappe for tens of kilometers. Similar rocks that are associated with strongly metamorphosed anorthosite occur in the Risberget Nappe near Oppdal (for example, Lutro and others, 1997, stop 1-3A). Both the fine- and coarse-grained mafic rocks were sampled to test their similarity to the Sætra dikes.

Samples from augen gneisses in the Risberget Nappe are as follows. In and adjacent to the Surnadal syncline, mafic rocks in Risberget augen gneiss were collected from Ura (321, 322, fig. 3) and Årnes (329, fig. 3). In the Moldefjord syncline samples were taken from Øygardsneset (102 and 103, fig. 5; Lutro and others, 1997, stop 4.2), Bolsøya (152, 168, fig. 4), Tennøya (62, figs. 6 and 13B), a dike cutting a coarse-grained amphibolite (108, fig. 6) and the mapped metamorphosed gabbro body (106, 107, 109, figs. 6 and 15) at Skår, dikes near Brattvåg Ferry (123, 124, 125, figs. 8, 14A and 14B), the mapped metamorphosed gabbro body near Brattvåg Ferry (126, 127, fig. 8 and fig. 14), and the mapped metamorphosed gabbro body (136, fig. 8) and a dike cutting that body (135, fig. 8) near Sunnaland. A sample was taken from a mafic dike on the north limb of the Helleneset syncline on Lauvøya (68, fig. 6 and fig. 13B). Lastly, two samples were taken from layered mafic rocks in the Risberget Nappe at Oppdal (391, 393).

SAMPLE PREPARATION

Samples were collected during summer 2004 from locations described above. Sample size ranged from 0.5 to 5 kg, depending on homogeneity and grain size. Only fresh, representative, relatively homogeneous material was sampled.

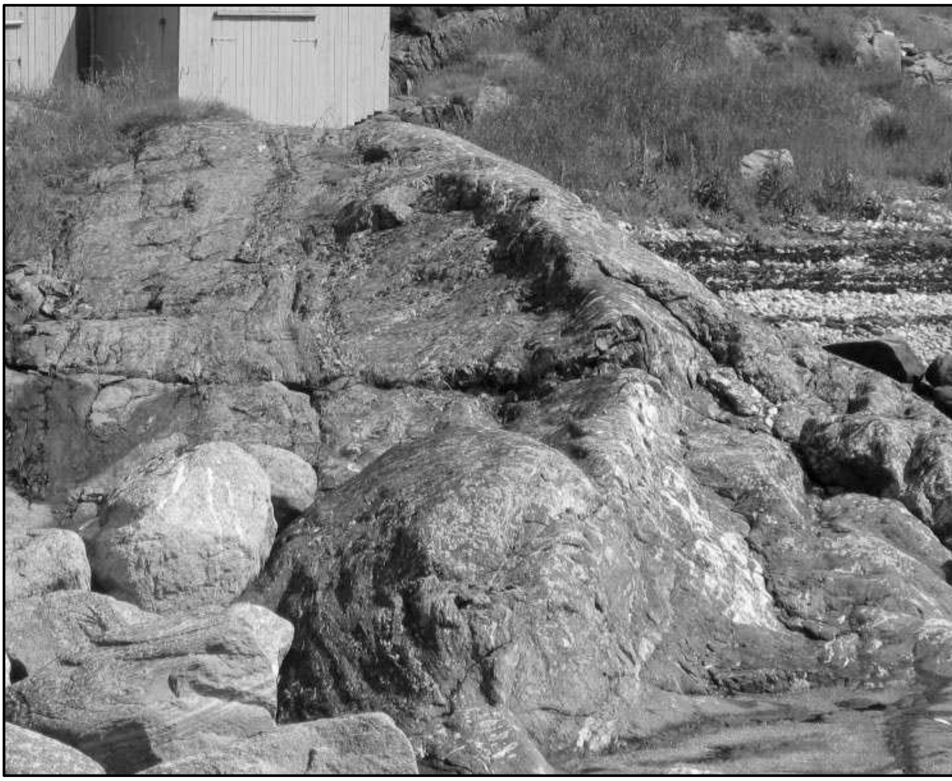

Fig. 15. A 5 m thick boudin of coarse-grained amphibolite (sample 108, fig. 6) in a mapped section of layered amphibolite within the Risberget Nappe at Skår, south limb of Moldefjord syncline. The surrounding layered amphibolite is represented by samples 106, 107, 109.

In the lab, samples were broken and undesirable portions removed with a hydraulic splitter. Fragments were crushed with a hydraulic press between 12 cm tungsten carbide faces, to pass through a 6 mm stainless steel sieve. No wear was seen on the tungsten carbide faces after >400 samples, and Co concentrations as low as 0.9 ppm in granitoid samples (to be reported elsewhere) suggest negligible contamination from the tungsten carbide. Splits of 30 to 100 g were crushed to a fine powder by 5 minutes agitation in a Spex 15 cm aluminum oxide puck mill. This mill also showed no significant wear, and contamination from it is considered negligible.

For major elements, 5 g aliquots were dried at 110°C overnight and analyzed by ICP-OES at Acme Labs, Vancouver, Canada, including analysis of carbon and sulfur by infrared spectroscopy and loss-on-ignition by weight. Several trace elements were also analyzed, but these were not used except as a check on the quality of ICP-MS analyses.

Trace elements were analyzed at the Union College Geology Department. Acids were purified in-house using Teflon sub-boiling stills, water was purified to 18.3 MΩ by ion exchange, and plastic test tubes were pre-cleaned with 1 percent HNO_3 to remove minor copper and zinc contamination. All powdered samples and the standards BIR-1, NIST-688, BCR-2 (basalts), and NIST-278 (rhyolite) were dried at 110°C overnight. 200 mg aliquots of the unknowns and standards were weighed into digestion vessels, and two empty vessels served as process blanks.

Digestions were done in a PicoTrace (Bovenden, Germany) Teflon bomb system using the following procedure. 5 ml of 50 percent HF was added to the samples and the vessels were sealed and heated to 180°C for four days. The long reaction time ensured complete dissolution of possible zircon. Vessels were evaporated to dryness overnight at ~100°C under flowing filtered air. 15 ml of 70 percent HNO_3 was added and the vessels were evaporated to dryness again. 125 ml of HNO_3, 25 ml of 37 percent HCl, 1 ml HF, and 0.3 ml each of 1000 ng/g Rh, In, Re, and Bi internal standard solutions (Inorganic Ventures, Lakewood, New Jersey) were combined and diluted to 500 ml. 15 ml of this mixture was added to each sample. The vessels were again sealed and heated to 150°C overnight. Immediately upon cooling 0.2 ml of each sample solution was transferred into 12 ml polypropylene test tubes, and 10 ml of 1 percent HNO_3 (by volume) was added.

Samples were analyzed immediately with a PerkinElmer Elan 6100 DRC ICP-MS instrument in three sets: V and Cr in DRC mode with 0.4 ml/minute NH_3 gas flowing to the DRC chamber to reduce polyatomic ion interferences; most other elements in normal mode; and Li and Be separately, also in normal mode. Zn and Cu were corrected for TiO^+ and Ba^{2+} interferences, and the lanthanides, Hf, and Ta were corrected for a variety of Ba and lanthanide oxide, hydroxide, and isobaric interferences. Standard concentrations, detection limits, and analytical precision of sample replicates are shown in table 1. Digestion vessels were carefully checked for residual solids after analysis was complete, but none was found.

RESULTS

Petrography

Of the 127 samples we report, representative thin sections were made from 42. Most are amphibolites, including the eight Sætra retrograded eclogites. The eclogites were identified based on abundance of garnet, common presence of relict rutile, and on remnant hornblende- and clinopyroxene-plagioclase symplectites, derived from decomposition and hydration of omphacite and garnet at low pressures.

Nearly all Sætra samples, including the eclogites, contain epidote, with pistacite dominant but with considerable clinozoisite, especially in the eclogites. Many of these rocks have white spots 2 to 6 mm across that look like plagioclase phenocrysts, but these are now polycrystalline clinozoisite. Quartz and sodic plagioclase occur in almost all samples. All samples have abundant titanite, but rutile is rare and occurs as small relics inside garnet or titanite. Garnet-bearing amphibolites come only from the southwestern part of the area: Lepsøy, the Moldefjord syncline, and Midøy (fig. 4). Eclogite samples came from Tennøy and Lauvøy (fig. 6), but Robinson has found eclogite boudins extensively in the Sætra Nappe of the Moldefjord and Helleneset synclines west from Vatnefjord, and at one locality in the Risberget Nappe south of Skårevatnet (fig. 6). Basement sausage rock dikes are all from Lepsøy (fig. 9) or the Midsund area (fig. 10). All have hornblende, quartz, and plagioclase, some have clinopyroxene (coarse, not part of a symplectite), some have small quantities of pistacite, and a few have garnet. Titanite is common but rutile is not generally found.

Amphibolites in the Risberget augen gneiss that are chemically like the Sætra dikes (see table 4) are also mineralogically similar. Most are epidote-quartz amphibolites with abundant titanite but rare rutile. In contrast, Risberget amphibolites that are chemically unlike Sætra dikes (see table 5) are mineralogically subtly distinct. Titanite is much less abundant, and matrix rutile, not armored by titanite or other minerals, is common. Except for Mg-rich samples 261 and 393, this does not seem to be a result of major element composition, such as high Mg/(Mg+Fe) ratios.

Rocks in the southwestern part of the area (Lepsøy, the Moldefjord syncline, and the Midsund area) appear to be at somewhat higher grade amphibolite facies with common garnet and clinopyroxene, and sparse epidote, as compared to regions to the east and northeast that have epidote amphibolite facies assemblages. Retrograded

TABLE 1

Analytical standards, analytical precision, and detection limits

Major elements, weight %	Major element QC standard SO-17			
	Accepted value	Analyzed value	Analytical precision*	Detection limits
SiO_2	61.17	61.43	0.5%	0.02
TiO_2	0.59	0.59	2.3%	0.01
Al_2O_3	13.72	13.85	1.0%	0.03
Fe_2O_3	5.8	5.81	2.8%	0.04
MnO	0.53	0.53	3.0%	0.01
MgO	2.33	2.31	2.8%	0.01
CaO	4.64	4.63	2.4%	0.01
Na_2O	4.09	4.08	2.2%	0.01
K_2O	1.37	1.42	1.4%	0.01
P_2O_5	0.98	0.99	2.9%	0.01
LOI	3.4	3.4	0.0%	0.1
C	2.4	2.40	2.4%	0.01
S	5.3	5.32	2.7%	0.01
SUM	106.32	106.76	2.2%	-

Trace elements, ppm	Trace element standard concentrations†				Median precision‡	Median concentration§	Detection limits††
	BIR-1	NIST-688	BCR-2	NIST-278			
Li	3.4	7	12	47	2%	9.1	0.03
Be	0.58	0.7	1.6	1.9	2%	0.55	0.003
Sc	43.8	37.3	32.8	4.96	2%	38	0.05
V	317	242	415	9	2%	240	0.006
Cr	382	331	14.2	5.9	2%	261	0.02
Co	52	48.7	37	1.5	2%	43	0.003
Ni	169	152	12.1	3.6	2%	84	0.02
Cu	125	96	18	5.3	8%	36	0.05
Zn	71	72	129.5	53	4%	86	0.06
Ga	16	17	22	16.8	2%	17.2	0.007
Rb	0.23	1.91	47.9	127.5	2%	3.7	0.002
Sr	109	169	346	64	1%	183	0.09
Y	16.2	18.4	37.7	39	2%	26	0.002
Zr	15.5	58	188	288	4%	107	0.005
Nb	0.55	5.5	14	18	2%	5.1	0.001
Mo	0.054	0.41	-	3.2	10%	0.24	0.01
Sn	0.65	1.66	2.7	4.16	3%	0.93	0.004
Cs	0.005	0.23	0.96	5.2	1%	0.18	0.000
Ba	7	181	675	918	2%	30.6	0.01
La	0.61	5.21	24.9	31.4	3%	6.0	0.001
Ce	2.07	12.75	53.7	61.4	3%	15.9	0.001
Pr	0.402	1.833	6.8	7.13	3%	2.3	0.0002
Nd	2.45	8.54	28.4	27.6	2%	11.9	0.001
Sm	1.11	2.522	6.63	5.72	2%	3.9	0.001
Eu	0.53	0.99	1.95	0.78	1%	1.37	0.0002
Gd	1.9	3.02	6.68	5.7	1%	4.8	0.001
Tb	0.36	0.515	1.06	0.961	2%	0.76	0.0002
Dy	2.505	3.36	6.44	6.23	1%	4.6	0.001
Ho	0.567	0.724	1.32	1.34	2%	0.97	0.0001
Er	1.683	2.08	3.63	3.97	2%	2.7	0.0004
Tm	0.26	0.317	0.536	0.64	2%	0.39	0.0001
Yb	1.693	2.05	3.39	4.45	1%	2.5	0.001
Lu	0.259	0.312	0.509	0.74	1%	0.39	0.0001
Hf	0.59	1.56	4.88	8.3	2%	2.9	0.0005
Ta	0.039	0.3	0.79	1.26	3%	0.20	0.001
Pb	3	3.26	11	16.4	3%	2.2	0.002
Th	0.03	0.32	5.99	12.4	3%	0.32	0.001
U	0.01	0.32	1.73	4.58	3%	0.16	0.0001

* Major element precision is based on 12 analyses of SO-17/CSB as a quality control standard.

† Trace element concentrations in standards based on a variety of published and unpublished sources.

‡ Median trace element precision based on 16 runs, in each of which one unknown sample was processed and analyzed in duplicate. 2 standard deviations of the mean.

§ Median trace element concentration for the 16 unknown samples analyzed in duplicate.

†† Detection limits are the median for 16 runs, 2 process blanks each run analyzed three times each as unknowns.

eclogites were only found in the southwestern area, and only in the cores of boudins. It is likely that other amphibolites within eclogite-bearing outcrops were also eclogite, but have been retrograded during late Scandian hydration and extensional deformation (for example sample 110, fig. 7B). However the massive amphibolites that constitute metamorphosed mafic dikes on Lepsøy, at Midsund, and at Kjøra and Geita show no features indicating former presence of eclogite. The non-Sætra-like amphibolites in the Risberget, with their generally coarse grain size, sparse titanite, and matrix rutile, may record partially an older episode of amphibolite facies metamorphism.

Geochemistry Introduction

The analyzed samples (tables 2 – 5) range from 45.10 to 63.65 percent SiO_2. The extreme compositions are amphibolites in the Risberget Nappe. Mafic rocks from the Sætra Nappe (table 2) span a narrower basaltic range of 47.32 to 53.45 percent SiO_2. The major-element and some trace element chemistry of mafic rocks from the Sætra Nappe and equivalent units has been discussed adequately at length elsewhere (Andréasson and others, 1979; Solyom and others, 1979; Krill, 1983; Solyom and others, 1985; Beckholmen and Roberts, 1999), and we will not discuss it in any depth for our samples. To summarize, these workers report that the Sætra dikes and their equivalents span a continuous compositional range from tholeiitic to alkaline basalts, with tholeiites dominating the sample population. Comparisons with basalts elsewhere suggest that the Sætra dikes are chemically similar to continental flood and rift-related basalts (Solyom and others, 1985), consistent with the interpretation that the Sætra dikes intruded the Baltica margin during rifting of Rodinia to produce the Iapetus Ocean (for example, Andréasson and others, 1998; Siedlecka and others, 2004).

The emphasis of this paper is on new trace-element analyses of highly deformed rocks metamorphosed to epidote amphibolite, amphibolite, and eclogite facies. Some or all may have undergone post-intrusion chemical alteration (for example, Hollocher, 1985). Because of this, we concentrate on trace elements that are relatively immobile during metamorphism and hydrothermal alteration processes (Lanthanides, Ti, Y, Zr, Nb, Hf, Ta, Th, and to a lesser extent U, P; for example, Humphris and Thompson, 1978; Greenough and others, 1990; Dupuy and others, 1993; Pearce and Peate, 1995; Becker and others, 2000; Mocek, 2001; Polat and others, 2003, metamorphism; but see Ludden and Thompson, 1979; Finlow-Bates and Stumpfl, 1981; Polat and others, 2003, hydrothermal alteration). Our conclusions are based, in general, on broad consistency of element concentrations and ratios rather than on individual samples.

Our initial hypothesis was that the quartzites from which we have samples all belong to the Sætra Nappe, as suggested by mapping, described above. This included all samples plotted in figures 16, 17, and 18, panels A-J, in particular the two Åsbøen samples in panel J that occur in a 12 m-thick quartzite section within an area mapped as basement (Krill, 1987). We further hypothesized that mafic dikes and lenses in basement sausage rocks (table 3) would be similar to those in the Sætra, but that the diverse fine- to coarse-grained mafic bodies in the Risberget Nappe (tables 4 and 5), were likely to be different from the Sætra. Several chemical variation diagrams were used to differentiate between rocks from these different lithotectonic units. Diagrams were supplemented by cluster (hierarchical, Ward, and centroid) and discriminant (linear distances, centroid clusters) analysis using a variety of immobile element concentrations and ratios, as has been useful in other instances (for example, Pearce, 1976; Solyom and others, 1985). These tests demonstrated that a set of mafic rocks in the Risberget Nappe augen gneiss (table 5) is chemically different from the Sætra dikes ($p < 0.01$). However, other Risberget Nappe mafic rocks, dikes cutting basement at Geita, and dikes in the basement sausage rock on Lepsøy and in the Midsund area (table 3), could not be distinguished from one another or from dikes in Sætra Nappe quartzites.

TABLE 2

Chemical analyses of mafic rocks in quartzites, mostly of the Sætra Nappe

Sample	299	300	301	302	303	304	305	306	307	308	309	310	311	312
Place	Oppdal	Oppdal	Oppdal	Oppdal	Oppdal	Oppdal	Oppdal	Oppdal	Oppdal	Oppdal	Oppdal	Oppdal	Oppdal	Oppdal
SiO_2	51.59	49.91	52.42	51.09	51.70	50.60	50.36	51.78	50.84	50.45	50.25	51.05	51.81	51.40
TiO_2	1.49	0.99	1.62	1.50	1.42	0.87	1.94	2.28	1.46	1.70	1.38	1.64	1.44	1.45
Al_2O_3	15.32	14.48	14.40	14.86	14.56	14.42	14.35	12.98	15.04	13.65	15.80	13.70	15.41	14.72
Fe_2O_3	10.10	12.66	10.47	10.06	10.14	11.26	11.54	13.41	10.33	13.40	9.29	13.12	9.72	10.41
MnO	0.17	0.27	0.16	0.18	0.17	0.21	0.17	0.22	0.17	0.22	0.16	0.21	0.15	0.16
MgO	6.67	8.20	6.78	7.11	7.04	7.36	6.44	4.96	6.69	5.87	7.25	6.24	6.84	7.17
CaO	10.29	11.63	10.68	11.26	10.91	12.00	10.87	9.19	11.15	10.63	11.76	10.46	11.37	11.09
Na_2O	2.78	0.15	2.07	1.49	1.32	0.27	2.60	2.29	2.03	0.18	1.50	2.24	2.17	2.26
K_2O	0.89	0.71	0.62	1.70	1.87	2.42	0.79	1.73	1.45	3.01	1.70	0.49	0.31	0.39
P_2O_5	0.17	0.10	0.21	0.17	0.18	0.09	0.27	0.32	0.18	0.22	0.17	0.19	0.16	0.17
CO_2	0.26	0.50	0.15	0.11	0.19	0.11	0.15	0.15	0.19	0.15	0.15	0.11	0.19	0.26
S	0.03	0.15	0.03	0.13	0.11	0.04	0.11	0.16	0.09	0.08	0.10	0.12	0.07	0.01
SUM	99.76	99.75	99.61	99.66	99.61	99.65	99.59	99.47	99.62	99.56	99.51	99.57	99.64	99.49
LOI	1.0	3.7	1.4	1.4	1.5	1.3	1.2	1.2	1.4	1.6	1.2	1.0	1.1	0.9
Li	7.8	62.6	7.4	9.7	10.7	13.2	5.4	9.8	9.6	23.2	13.1	5.0	3.5	3.9
Be	0.7	1.0	0.5	0.6	0.5	0.3	0.5	0.9	0.5	0.8	0.5	0.5	0.5	0.5
Sc	32	48	33	35	31	48	37	34	33	42	32	43	33	34
V	230	272	249	241	221	279	296	360	249	381	209	386	244	258
Cr	233	39	187	251	251	39	81	35	212	45	269	42	245	264
Co	36	72	37	39	39	32	40	37	39	45	36	41	35	34
Ni	42	39	39	51	52	36	30	23	43	30	44	29	43	42
Cu	55	164	36	62	79	81	34	64	57	68	97	31	40	18
Zn	96	124	95	92	90	101	93	117	86	110	93	114	86	84
Ga	19	19	20	19	19	17	20	22	18	19	17	19	18	18
Rb	33	22	20	53	60	86	17	38	31	98	50	10	10	12
Sr	246	336	243	244	247	225	223	176	218	272	258	157	221	205
Y	25	24	27	26	25	21	29	42	25	37	22	35	24	26
Zr	102	59	113	110	108	45	144	183	101	105	97	102	100	106
Nb	10.0	4.8	10.7	9.4	9.0	3.7	15.1	17.6	10.0	12.4	9.2	13.2	9.6	9.3
Mo	0.45	0.13	0.90	0.25	0.33	0.43	0.28	0.75	0.41	1.53	0.29	0.41	0.25	0.25
Sn	0.92	0.60	1.42	1.13	1.10	0.52	1.37	1.62	0.97	1.02	0.85	0.93	0.90	1.16
Cs	0.46	0.78	0.25	2.48	2.64	4.78	0.72	1.51	1.14	5.30	2.53	0.14	0.36	0.18
Ba	239	70	200	190	220	186	110	185	178	253	155	129	89	90
La	8.6	4.0	9.1	8.6	8.4	3.1	12.4	15.8	8.5	10.0	7.9	9.8	8.6	8.7
Ce	21.0	9.7	23.0	21.3	21.0	7.9	30.7	38.2	20.8	23.5	19.8	22.8	20.7	21.6
Pr	3.10	1.47	3.27	3.14	3.08	1.17	4.43	5.49	3.01	3.28	2.90	3.20	3.07	3.11
Nd	14.4	7.0	15.7	14.9	14.4	5.9	20.5	25.7	14.1	15.3	13.7	14.6	14.2	14.7
Sm	4.15	2.36	4.48	4.19	4.14	1.94	5.15	6.90	3.90	4.38	3.68	4.16	3.97	4.10
Eu	1.41	0.91	1.50	1.40	1.37	0.78	1.70	2.16	1.35	1.48	1.25	1.42	1.36	1.34
Gd	4.59	3.13	4.96	4.75	4.60	2.68	5.42	7.45	4.46	5.33	4.04	5.01	4.39	4.56
Tb	0.75	0.57	0.80	0.78	0.76	0.49	0.86	1.20	0.74	0.94	0.65	0.90	0.72	0.76
Dy	4.65	3.92	4.90	4.82	4.72	3.38	5.12	7.49	4.59	6.23	3.94	5.99	4.42	4.69
Ho	0.94	0.86	0.96	0.95	0.94	0.75	1.01	1.51	0.95	1.35	0.79	1.29	0.90	0.95
Er	2.54	2.49	2.53	2.57	2.52	2.14	2.69	4.10	2.58	3.83	2.08	3.71	2.41	2.60
Tm	0.36	0.38	0.36	0.38	0.36	0.33	0.39	0.59	0.37	0.57	0.30	0.56	0.35	0.37
Yb	2.22	2.50	2.17	2.25	2.21	2.12	2.39	3.63	2.23	3.62	1.84	3.56	2.11	2.30
Lu	0.31	0.38	0.31	0.33	0.32	0.33	0.35	0.53	0.32	0.54	0.26	0.53	0.30	0.33
Hf	2.8	1.6	3.1	3.0	3.0	1.3	3.6	4.8	2.7	2.9	2.6	2.9	2.7	2.9
Ta	0.56	0.25	0.59	0.53	0.52	0.19	0.82	0.99	0.56	0.67	0.52	0.71	0.54	0.52
Pb	6.9	21.6	4.5	14.3	14.2	21.3	7.4	7.7	8.4	21.6	14.0	4.2	1.8	2.4
Th	0.88	0.37	1.31	1.29	1.31	0.27	1.11	1.70	0.90	0.94	0.70	0.97	0.81	1.39
U	0.27	0.35	0.44	0.36	0.38	0.15	0.31	0.52	0.31	0.31	0.26	0.28	0.28	0.39
Nb/La	1.2	1.2	1.2	1.1	1.1	1.2	1.2	1.1	1.2	1.2	1.2	1.3	1.1	1.1
La_n/Sm_n	1.3	1.1	1.3	1.3	1.3	1.0	1.5	1.4	1.4	1.4	1.3	1.5	1.3	1.3

* Composition is not Sætra-like.
† Eclogite, retrograded to varying degrees.

Figures 16, 17, and 18 each have 15 panels, A-O, representing the same rock sets. In figure 16, the Nb/La and La_n/Sm_n axes were chosen on the basis of discriminant analysis (see above) showing that these ratios were among the most powerful discriminant vectors. The La_n/Sm_n ratio represents LREE-enrichment relative to MREE,

TABLE 2

(continued)

Sample	313	240	241	242	243	244	245A	245B	246	247	248	249
Place	Oppdal	Orkanger	Orkanger	Orkanger	Orkanger	Orkanger	Orkanger	Orkanger	Orkanger	Orkanger	Orkanger	Orkanger
SiO_2	51.24	51.46	49.24	51.42	50.77	50.14	48.11	49.22	48.28	48.59	49.09	49.76
TiO_2	1.58	1.82	1.13	1.33	1.37	1.00	0.83	1.05	0.86	0.83	1.03	1.35
Al_2O_3	16.38	14.14	16.52	14.62	14.25	15.96	17.71	15.77	16.86	21.12	17.49	15.63
Fe_2O_3	11.32	12.16	9.26	10.17	10.77	9.34	8.26	10.45	8.69	7.25	8.51	10.42
MnO	0.26	0.20	0.17	0.21	0.22	0.16	0.16	0.18	0.16	0.13	0.14	0.17
MgO	6.37	6.51	8.02	6.48	7.16	7.96	8.75	8.16	8.88	5.15	8.08	7.55
CaO	12.41	10.07	12.18	11.49	10.76	11.93	12.65	12.03	12.79	12.51	12.27	11.78
Na_2O	0.01	2.25	2.23	2.31	2.35	2.07	2.12	0.83	2.20	2.91	2.05	2.35
K_2O	0.04	0.74	0.58	0.45	0.98	0.83	0.88	1.72	0.47	0.83	0.64	0.45
P_2O_5	0.21	0.20	0.11	0.14	0.14	0.10	0.11	0.10	0.11	0.10	0.13	0.15
CO_2	0.15	0.15	0.04	0.89	0.90	0.11	0.11	0.11	0.34	0.19	0.22	0.15
S	0.01	0.14	0.15	0.12	0.12	0.12	0.04	0.08	0.10	0.06	0.08	0.09
SUM	99.98	99.84	99.63	99.63	99.79	99.72	99.73	99.70	99.74	99.67	99.73	99.85
LOI	4.2	1.1	1.3	1.4	1.9	1.2	1.8	2.0	1.5	1.5	1.4	1.1
Li	32.8	4.6	5.2	3.0	5.3	5.1	5.2	13.6	4.4	3.8	3.9	3.2
Be	0.5	0.6	0.4	0.3	0.6	0.3	0.3	0.6	0.3	0.3	0.3	0.4
Sc	33	40	34	40	38	41	32	43	36	27	30	37
V	246	318	245	318	350	327	270	400	205	169	201	283
Cr	238	40	327	108	91	435	347	445	285	192	328	240
Co	40	45	43	44	42	43	38	44	40	27	40	43
Ni	46	31	62	44	38	66	95	60	85	50	77	69
Cu	54	81	83	73	80	112	17	75	75	42	75	70
Zn	139	103	82	95	87	63	69	78	64	52	72	87
Ga	24	21	18	19	18	18	16	19	16	18	18	19
Rb	1	20	23	9	37	35	29	76	14	32	25	7
Sr	361	168	234	212	211	185	223	196	203	253	302	220
Y	27	38	22	24	26	22	17	23	19	18	20	26
Zr	108	135	73	81	86	57	60	58	61	54	69	82
Nb	10.6	11.8	8.0	10.3	11.2	5.2	6.8	5.5	6.7	5.5	7.7	9.7
Mo	0.62	0.40	0.34	0.32	0.37	0.21	0.18	0.25	0.24	0.24	0.56	0.38
Sn	1.01	1.28	0.82	0.75	0.91	0.65	0.63	0.75	0.57	0.55	0.70	0.80
Cs	0.08	0.44	0.68	0.20	0.47	1.04	0.80	2.02	0.42	0.74	0.33	0.12
Ba	8	94	79	60	175	88	124	145	47	117	69	43
La	12.1	10.5	7.1	8.4	9.3	5.1	6.3	5.2	6.3	5.1	6.9	8.0
Ce	24.2	25.2	16.1	19.0	20.8	12.1	14.4	12.3	14.3	11.8	15.7	18.5
Pr	3.57	3.54	2.25	2.62	2.90	1.71	1.95	1.76	1.96	1.64	2.21	2.55
Nd	16.8	16.7	10.7	12.5	13.1	8.1	8.8	8.7	8.9	7.7	10.2	12.1
Sm	4.42	4.85	3.02	3.40	3.58	2.48	2.29	2.68	2.36	2.12	2.80	3.23
Eu	1.50	1.64	1.11	1.23	1.30	0.93	0.87	1.02	0.88	0.81	1.02	1.18
Gd	4.97	5.79	3.63	4.04	4.30	3.15	2.69	3.45	2.84	2.63	3.26	3.91
Tb	0.79	0.99	0.60	0.67	0.72	0.55	0.46	0.61	0.50	0.45	0.54	0.65
Dy	4.84	6.40	3.81	4.28	4.50	3.55	2.99	3.98	3.28	2.92	3.51	4.17
Ho	0.97	1.32	0.80	0.89	0.93	0.76	0.63	0.85	0.70	0.61	0.72	0.88
Er	2.64	3.75	2.20	2.45	2.55	2.16	1.75	2.38	1.96	1.71	1.98	2.42
Tm	0.38	0.55	0.32	0.36	0.37	0.32	0.26	0.35	0.30	0.25	0.29	0.36
Yb	2.35	3.48	1.93	2.21	2.31	2.02	1.60	2.21	1.87	1.59	1.82	2.25
Lu	0.35	0.51	0.29	0.32	0.34	0.31	0.24	0.33	0.28	0.24	0.27	0.34
Hf	2.9	3.6	2.0	2.3	2.4	1.6	1.6	1.7	1.6	1.5	1.9	2.2
Ta	0.59	0.63	0.43	0.55	0.58	0.28	0.36	0.30	0.36	0.29	0.40	0.50
Pb	16.1	4.6	5.6	2.6	3.2	7.6	7.3	9.7	5.1	7.5	4.5	4.3
Th	0.90	1.08	0.64	0.81	0.86	0.57	0.57	0.43	0.56	0.48	0.60	0.74
U	0.32	0.34	0.23	0.24	0.30	0.33	0.20	0.26	0.22	0.22	0.25	0.22
Nb/La	0.9	1.1	1.1	1.2	1.2	1.0	1.1	1.1	1.1	1.1	1.1	1.2
La_n/Sm_n	1.7	1.3	1.5	1.5	1.6	1.3	1.7	1.2	1.7	1.5	1.6	1.5

whereas the Nb/La ratio represents expression of the classic Nb-depleted arc or continental crust signatures (for example, Rudnick and Gao, 2003). Chondrite-normalized REE diagrams are shown in figure 17, and multi-element diagrams are shown in figure 18. Only selected samples are shown in figure 18 to avoid too many crossing lines.

Table 2

(continued)

Sample	250	251	252	253	363	364	365	366	333	334	335	336	337
Place	Orkanger	Orkanger	Orkanger	Orkanger	Vassli-vatnet	Vassli-vatnet	Vassli-vatnet	Vassli-vatnet	Årnes	Årnes	Årnes	Årnes	Årnes
SiO_2	49.41	48.63	51.13	51.24	52.14	51.16	51.49	50.56	49.95	51.57	49.62	49.92	50.18
TiO_2	1.33	1.28	1.50	1.79	1.63	1.60	1.66	1.77	1.63	1.90	1.29	1.37	1.55
Al_2O_3	16.10	16.11	14.07	14.35	15.09	13.96	13.88	14.59	14.01	13.87	14.92	14.71	14.10
Fe_2O_3	10.24	10.34	11.75	12.04	12.06	12.17	12.38	12.50	11.95	11.96	10.78	10.71	11.36
MnO	0.17	0.17	0.18	0.21	0.20	0.23	0.23	0.24	0.21	0.20	0.19	0.18	0.20
MgO	7.61	7.29	7.20	6.07	5.62	7.07	6.89	7.68	7.07	6.23	7.62	7.83	7.35
CaO	11.69	10.76	11.31	10.24	12.21	12.56	12.28	11.79	10.67	10.44	11.73	11.19	11.25
Na_2O	2.29	1.13	1.71	2.49	0.01	0.23	0.15	0.03	1.74	2.27	2.64	2.29	2.40
K_2O	0.56	2.69	0.60	0.50	0.58	0.63	0.61	0.39	1.52	0.76	0.80	1.29	0.99
P_2O_5	0.14	0.15	0.16	0.19	0.20	0.18	0.19	0.19	0.17	0.22	0.12	0.14	0.14
CO_2	0.04	1.16	0.07	0.56	0.19	0.19	0.19	0.19	0.60	0.30	0.11	0.26	0.34
S	0.09	0.07	0.15	0.13	0.01	0.01	0.01	0.01	0.03	0.23	0.16	0.11	0.16
SUM	99.67	99.78	99.83	99.81	99.94	99.99	99.96	99.94	99.55	99.95	99.98	100.00	100.02
LOI	1.0	2.2	1.0	1.3	3.5	2.9	3.2	4.1	1.7	0.9	1.0	1.3	1.5
Li	2.8	7.1	2.7	3.6	24.3	12.6	14.8	16.7	12.2	11.2	11.3	11.2	8.4
Be	0.4	1.0	0.4	0.6	1.6	1.0	1.6	1.5	0.6	0.6	0.3	0.4	0.4
Sc	37	35	41	40	41	42	43	45	41	40	46	44	44
V	285	273	310	328	307	326	317	339	316	335	258	280	299
Cr	241	245	72	41	90	103	100	115	119	121	278	239	186
Co	41	38	43	45	41	44	43	45	44	45	46	43	49
Ni	63	60	39	31	40	45	41	55	45	44	65	77	55
Cu	52	46	75	59	76	102	16	5	133	109	115	74	90
Zn	82	84	92	115	102	99	99	114	106	97	82	90	88
Ga	18	18	20	21	27	20	21	24	19	21	18	19	19
Rb	11	109	12	8	23	18	21	16	50	20	27	69	32
Sr	227	251	188	186	536	302	290	363	160	142	194	165	174
Y	25	25	32	36	34	32	34	36	31	43	30	32	32
Zr	83	79	95	128	122	108	120	125	106	153	86	100	106
Nb	9.6	9.2	9.7	11.2	9.8	9.3	9.7	10.7	8.3	16.2	5.1	7.4	7.4
Mo	0.24	0.29	0.20	0.32	0.33	0.63	0.34	0.23	0.42	0.82	0.24	0.31	0.35
Sn	0.83	0.82	0.94	1.24	1.19	1.12	1.22	1.29	1.14	1.74	0.89	1.13	1.09
Cs	0.23	2.56	0.12	0.12	0.19	0.20	0.25	0.16	1.32	0.38	2.05	3.52	0.36
Ba	53	276	65	55	19	48	104	88	217	141	86	172	153
La	8.0	8.1	9.3	9.7	9.2	7.9	8.3	10.1	7.3	14.1	5.1	7.1	6.9
Ce	18.1	18.2	22.1	23.2	21.8	19.4	20.6	23.5	18.4	32.6	13.1	17.4	17.5
Pr	2.55	2.51	3.07	3.30	3.12	2.83	3.00	3.43	2.68	4.46	1.99	2.55	2.58
Nd	11.9	11.8	14.6	15.7	14.9	13.6	14.3	16.2	12.9	20.3	10.0	12.3	12.7
Sm	3.24	3.28	4.14	4.60	4.40	3.96	4.22	4.54	3.90	5.61	3.11	3.66	3.80
Eu	1.18	1.19	1.51	1.56	1.48	1.39	1.45	1.54	1.35	1.89	1.14	1.27	1.35
Gd	3.86	3.94	5.13	5.58	5.41	5.03	5.27	5.56	4.86	6.68	4.09	4.56	4.77
Tb	0.67	0.66	0.87	0.95	0.93	0.86	0.93	0.96	0.85	1.15	0.72	0.80	0.82
Dy	4.30	4.26	5.57	6.10	6.04	5.66	5.99	6.23	5.51	7.53	4.87	5.26	5.40
Ho	0.89	0.89	1.15	1.28	1.27	1.21	1.27	1.30	1.15	1.61	1.06	1.12	1.14
Er	2.42	2.44	3.16	3.52	3.58	3.35	3.58	3.69	3.26	4.57	3.01	3.21	3.21
Tm	0.36	0.36	0.47	0.52	0.53	0.50	0.53	0.54	0.48	0.69	0.46	0.48	0.48
Yb	2.23	2.22	2.86	3.26	3.36	3.10	3.35	3.38	2.96	4.35	2.89	3.07	3.03
Lu	0.33	0.33	0.42	0.48	0.50	0.46	0.50	0.50	0.45	0.65	0.43	0.46	0.45
Hf	2.2	2.2	2.6	3.4	3.4	3.0	3.3	3.4	2.9	4.2	2.3	2.7	2.8
Ta	0.50	0.50	0.52	0.60	0.54	0.50	0.54	0.57	0.47	0.88	0.28	0.39	0.41
Pb	5.8	7.6	6.9	4.8	23.5	11.4	14.5	15.6	6.3	2.7	4.6	3.3	2.2
Th	0.75	0.72	0.77	1.04	0.76	0.66	0.71	1.03	0.67	1.59	0.38	0.63	0.50
U	0.39	0.26	0.29	0.31	0.35	0.24	0.26	0.35	0.28	0.53	0.18	0.32	0.26
Nb/La	1.2	1.1	1.0	1.2	1.1	1.2	1.2	1.1	1.1	1.1	1.0	1.0	1.1
La_n/Sm_n	1.5	1.5	1.4	1.3	1.3	1.2	1.2	1.4	1.2	1.6	1.0	1.2	1.1

Mafic Dikes and Layers in Probable Sætra Quartzites

Figures 16, 17, and 18, panels A-I show data for amphibolites in quartzites that we were reasonably certain belonged to the Sætra Nappe based on lithotectonic stratigraphy, as described above. The Oppdal site has long been correlated with the Sætra Nappe (Krill, 1986) and we used those samples as reference compositions for the other

TABLE 2

(continued)

Sample Place	338 Årnes	94 Drag-neset	95 Drag-neset	96 Drag-neset	97 Drag-neset	98 Drag-neset	99 Drag-neset	60† Tennøy	61† Tennøy	63† Tennøy	64† Tennøy	65† Tennøy	66† Tennøy	110† Skår
SiO_2	49.88	49.40	50.02	53.45	52.44	50.28	50.15	51.90	50.32	50.92	50.78	49.58	51.10	51.24
TiO_2	1.47	1.30	1.85	2.40	2.80	1.69	1.60	2.59	1.73	1.67	1.60	1.58	1.60	1.41
Al_2O_3	14.81	15.32	14.65	11.72	11.97	14.18	14.44	12.27	13.99	13.71	13.73	14.15	13.72	14.01
Fe_2O_3	10.84	10.88	12.91	17.30	17.59	12.56	12.25	16.05	12.73	12.34	12.63	11.86	12.45	11.27
MnO	0.19	0.17	0.21	0.31	0.36	0.23	0.21	0.25	0.20	0.18	0.22	0.20	0.23	0.21
MgO	7.47	7.94	6.02	2.31	2.77	7.02	7.39	4.66	6.58	6.71	6.51	7.45	6.56	7.33
CaO	11.05	11.32	10.41	7.15	7.56	11.15	10.32	8.93	10.65	10.60	10.86	11.36	10.69	10.80
Na_2O	2.63	2.44	2.42	2.23	1.72	1.07	2.28	2.16	2.45	2.69	2.57	2.59	2.20	2.05
K_2O	0.80	0.39	0.62	1.16	1.10	0.56	0.54	0.44	0.52	0.39	0.38	0.44	0.47	0.78
P_2O_5	0.17	0.13	0.25	1.25	1.04	0.20	0.17	0.32	0.19	0.15	0.18	0.16	0.16	0.16
CO_2	0.60	0.07	0.07	0.11	0.07	0.42	0.11	0.07	0.26	0.26	0.15	0.19	0.33	0.22
S	0.09	0.06	0.15	0.19	0.29	0.16	0.13	0.13	0.13	0.12	0.14	0.14	0.13	0.08
SUM	100.00	99.42	99.58	99.58	99.71	99.52	99.59	99.77	99.75	99.74	99.75	99.70	99.64	99.56
LOI	1.2	0.8	0.9	0.2	0.4	2.5	1.3	0.1	0.4	0.5	0.3	0.5	0.4	0.8
Li	8.3	4.7	4.7	5.2	3.5	13.2	4.9	2.0	3.3	4.2	4.0	4.8	3.2	5.3
Be	0.5	0.4	0.5	1.5	1.4	0.5	0.4	0.7	0.6	0.5	0.5	0.4	0.6	0.4
Sc	40	39	40	35	36	46	44	41	41	42	41	43	42	41
V	269	256	343	46	89	332	320	497	369	400	397	421	454	302
Cr	240	287	95	8	9	180	141	25	180	121	126	191	130	178
Co	42	41	43	29	37	50	49	49	45	54	44	50	45	41
Ni	74	66	36	2	4	63	67	22	49	40	40	63	42	49
Cu	52	32	67	39	62	10	110	78	76	87	80	84	76	87
Zn	90	85	94	105	97	103	97	137	96	134	113	109	113	106
Ga	19	18	21	28	28	21	20	24	20	21	20	20	21	18
Rb	27	8	10	31	33	16	7	9	16	6	9	13	11	15
Sr	195	154	169	144	123	200	110	109	149	166	119	119	109	142
Y	34	27	39	127	108	38	33	57	41	38	38	31	38	35
Zr	117	83	132	460	398	124	106	220	140	134	139	103	139	95
Nb	10.1	5.9	16.4	43.6	36.3	8.9	8.6	18.4	11.8	9.7	9.5	8.2	9.7	11.0
Mo	0.31	0.59	0.46	0.89	1.40	0.39	0.32	1.73	0.53	0.61	0.33	0.45	0.19	0.24
Sn	1.19	0.91	1.25	3.34	3.59	1.15	1.03	1.75	1.56	1.53	1.41	1.04	1.68	1.15
Cs	0.94	0.22	0.22	0.48	0.83	0.50	0.14	0.04	0.28	0.11	0.15	0.30	0.12	0.56
Ba	118	67	68	208	205	58	37	96	95	56	75	78	86	101
La	9.0	5.3	13.3	35.4	30.9	7.8	6.9	15.4	9.9	9.4	8.6	7.0	9.2	8.1
Ce	21.6	13.3	30.1	87.3	76.2	19.7	17.6	37.6	24.0	22.5	21.3	17.7	22.5	19.0
Pr	3.08	1.96	3.95	12.44	10.91	2.85	2.55	5.35	3.41	3.21	3.06	2.56	3.22	2.62
Nd	14.5	9.7	17.7	60.2	52.6	13.8	12.5	25.5	16.3	15.3	14.3	12.4	15.4	12.4
Sm	4.16	3.01	4.99	17.47	15.20	4.19	3.78	7.30	4.77	4.49	4.34	3.69	4.55	3.75
Eu	1.37	1.08	1.64	4.68	4.18	1.39	1.32	2.27	1.49	1.50	1.34	1.29	1.42	1.24
Gd	4.97	3.93	6.10	21.13	18.23	5.34	4.74	8.78	5.93	5.59	5.46	4.67	5.69	4.83
Tb	0.86	0.69	1.04	3.50	3.01	0.94	0.83	1.49	1.01	0.95	0.94	0.80	0.97	0.88
Dy	5.62	4.55	6.85	22.19	19.32	6.17	5.40	9.86	6.87	6.30	6.36	5.14	6.40	5.74
Ho	1.18	0.97	1.46	4.63	4.01	1.34	1.14	2.10	1.49	1.33	1.36	1.11	1.36	1.25
Er	3.33	2.78	4.16	13.01	11.37	3.85	3.22	5.92	4.26	3.85	3.91	3.15	3.86	3.63
Tm	0.49	0.42	0.62	1.92	1.69	0.59	0.49	0.89	0.64	0.57	0.59	0.47	0.58	0.55
Yb	3.07	2.60	3.93	11.92	10.47	3.69	3.08	5.57	4.00	3.62	3.73	3.00	3.67	3.50
Lu	0.46	0.39	0.58	1.75	1.54	0.54	0.46	0.83	0.60	0.53	0.54	0.44	0.55	0.53
Hf	3.1	2.3	3.6	12.8	11.0	3.4	2.9	6.0	3.8	3.7	3.8	2.8	3.8	2.6
Ta	0.53	0.31	0.81	2.29	1.96	0.48	0.48	1.00	0.63	0.52	0.54	0.44	0.54	0.64
Pb	2.9	3.9	2.4	2.8	3.3	11.5	1.9	0.7	3.4	3.3	5.4	3.9	3.6	14.6
Th	0.89	0.40	1.38	2.91	2.47	0.68	0.58	1.72	0.82	0.97	1.01	0.57	1.01	1.16
U	0.43	0.15	0.39	0.88	0.78	0.25	0.21	0.62	0.28	0.29	0.28	0.19	0.29	0.65
Nb/La	1.1	1.1	1.2	1.2	1.2	1.1	1.2	1.2	1.2	1.0	1.1	1.2	1.0	1.4
La_n/Sm_n	1.4	1.1	1.7	1.3	1.3	1.2	1.1	1.3	1.3	1.3	1.2	1.2	1.3	1.3

localities. Most Sætra dikes from the Oppdal area (fig. 16A) have La_n/Sm_n ratios between 1.3 and 1.7, and Nb/La ratios between 0.9 and 1.4. In figure 17A, most Oppdal dikes are moderately LREE-enriched, with no or very small negative Eu anomalies. The patterns for all 13 LREE-enriched samples are slightly Z-shaped: Slightly convex upward for LREE and slightly convex downward for HREE. Samples

Table 2

(continued)

Sample	111	104	105	67†	69†	70	71	72	78	79	93	183	184	185
Place	Skår	Sunnaland	Sunnaland	Lauvøy	Lauvøy	Lepsøy	Lepsøy	Lepsøy	Lepsøy	Lepsøy	Lepsøy	Midøy	Midøy	Midøy
SiO_2	48.22	47.32	48.66	50.99	51.01	49.62	50.74	49.95	50.52	50.65	47.84	50.96	49.12	49.80
TiO_2	1.72	1.30	1.62	1.62	1.83	1.52	1.58	1.31	1.63	1.46	2.18	1.99	1.47	1.83
Al_2O_3	15.19	16.35	14.83	14.03	13.68	14.65	14.15	14.30	14.20	14.41	14.62	14.38	14.59	14.49
Fe_2O_3	12.32	10.89	11.77	12.01	12.41	12.06	11.62	9.89	11.73	11.27	12.88	12.91	11.65	12.82
MnO	0.18	0.19	0.19	0.20	0.18	0.20	0.19	0.17	0.18	0.18	0.18	0.22	0.20	0.19
MgO	7.18	7.93	7.09	6.88	6.36	8.15	7.48	7.70	7.38	6.95	6.70	6.04	7.18	6.68
CaO	10.79	11.86	11.04	10.74	10.38	9.37	8.84	11.81	9.45	10.22	10.42	9.68	11.24	10.01
Na_2O	1.01	1.35	2.60	2.55	2.59	2.52	2.22	2.21	2.96	2.95	2.43	1.30	1.55	1.82
K_2O	2.61	1.83	0.65	0.33	0.54	1.12	1.64	0.81	0.66	0.79	0.54	1.12	1.12	0.80
P_2O_5	0.18	0.14	0.20	0.17	0.22	0.16	0.16	0.11	0.19	0.14	0.27	0.24	0.14	0.20
CO_2	0.08	0.32	0.71	0.07	0.41	0.19	0.78	1.41	0.71	0.63	1.12	0.34	1.15	0.52
S	0.06	0.03	0.18	0.12	0.14	0.12	0.30	0.10	0.15	0.12	0.29	0.36	0.18	0.27
SUM	99.54	99.51	99.54	99.71	99.75	99.68	99.70	99.77	99.76	99.77	99.47	99.54	99.59	99.43
LOI	1.3	2.2	1.5	0.3	0.4	0.4	1.1	1.5	1.1	1.1	1.5	1.0	1.6	0.2
Li	16.1	15.1	5.5	4.6	7.1	5.4	8.5	2.8	3.3	3.3	2.9	9.5	11.7	8.5
Be	0.7	0.4	0.6	0.5	0.6	1.0	0.7	0.4	0.6	0.4	0.7	1.0	0.9	0.7
Sc	44	37	39	40	41	42	45	43	45	44	41	41	43	42
V	328	248	281	371	420	309	355	302	353	344	365	356	320	340
Cr	114	212	23	149	119	165	90	189	121	105	55	94	99	128
Co	41	37	45	42	45	45	46	46	48	47	50	43	38	45
Ni	38	63	41	48	46	57	39	62	44	42	43	40	37	47
Cu	34	37	87	74	94	45	53	24	31	48	60	83	32	55
Zn	98	86	81	83	85	155	112	91	109	111	121	123	110	119
Ga	21	19	18	20	21	20	21	19	20	20	22	21	19	21
Rb	81	55	14	7	6	23	47	9	6	12	7	27	24	18
Sr	195	196	211	73	95	108	152	172	140	197	241	113	135	173
Y	37	24	23	41	44	31	33	28	34	30	32	42	32	40
Zr	118	85	116	133	156	97	99	93	108	91	149	154	96	136
Nb	10.7	6.2	26.0	11.9	16.4	9.2	9.0	7.1	10.2	8.0	18.8	14.1	9.5	13.5
Mo	0.21	0.41	0.41	0.60	0.48	0.61	0.33	0.27	0.18	0.19	0.52	0.24	0.37	0.28
Sn	1.49	0.92	1.15	1.45	1.98	1.17	1.04	0.89	1.09	0.87	1.19	4.69	1.55	1.65
Cs	1.93	1.73	0.18	0.03	0.06	0.29	0.77	0.06	0.14	0.19	0.09	0.54	0.29	0.41
Ba	258	271	102	52	59	120	221	119	72	129	57	115	125	129
La	9.3	5.6	18.5	9.4	12.7	6.9	7.5	6.0	8.2	6.7	13.3	12.6	8.9	12.5
Ce	22.3	14.0	39.1	22.4	28.9	17.6	18.4	14.6	19.9	16.5	32.3	29.6	20.1	29.0
Pr	3.14	2.10	4.81	3.17	3.97	2.59	2.66	2.19	2.91	2.41	4.49	4.14	2.85	3.98
Nd	15.2	10.3	19.9	14.8	18.4	12.4	13.0	10.4	13.9	11.8	20.3	19.1	13.4	18.0
Sm	4.37	3.13	4.38	4.46	5.18	3.75	4.01	3.17	4.09	3.48	5.28	5.37	3.88	4.96
Eu	1.54	1.14	1.56	1.48	1.68	1.35	1.47	1.16	1.45	1.26	1.78	1.80	1.35	1.66
Gd	5.37	3.85	4.37	5.67	6.43	4.65	4.97	4.05	5.02	4.41	5.66	6.46	4.77	5.87
Tb	0.92	0.65	0.68	1.00	1.12	0.80	0.87	0.68	0.88	0.77	0.93	1.10	0.83	1.00
Dy	5.95	4.12	4.05	6.52	7.31	5.20	5.60	4.51	5.59	4.95	5.66	7.09	5.41	6.43
Ho	1.28	0.87	0.82	1.42	1.55	1.09	1.20	0.95	1.17	1.06	1.15	1.52	1.15	1.35
Er	3.68	2.44	2.20	4.02	4.40	3.07	3.40	2.75	3.29	2.97	3.06	4.30	3.24	3.79
Tm	0.54	0.37	0.31	0.60	0.66	0.45	0.50	0.40	0.49	0.44	0.43	0.64	0.48	0.56
Yb	3.41	2.40	1.93	3.85	4.23	2.84	3.20	2.55	3.04	2.83	2.69	4.01	3.01	3.43
Lu	0.50	0.37	0.28	0.58	0.63	0.42	0.48	0.38	0.46	0.41	0.39	0.60	0.46	0.52
Hf	3.1	2.3	2.9	3.6	4.2	2.6	2.8	2.4	2.9	2.5	3.8	4.1	2.6	3.6
Ta	0.57	0.34	1.37	0.61	0.85	0.49	0.50	0.36	0.54	0.43	1.03	0.72	0.49	0.68
Pb	7.3	6.9	1.9	0.8	3.0	23.7	12.3	9.9	7.7	10.3	9.2	9.4	8.8	8.5
Th	0.68	0.44	1.88	1.03	1.25	0.65	0.62	0.49	0.70	0.54	1.17	1.28	0.90	1.52
U	0.31	0.14	0.53	0.31	0.52	0.25	0.27	0.19	0.22	0.17	0.39	0.50	0.38	0.50
Nb/La	1.2	1.1	1.4	1.3	1.3	1.3	1.2	1.2	1.2	1.2	1.4	1.1	1.1	1.1
La_n/Sm_n	1.3	1.1	2.6	1.3	1.5	1.2	1.2	1.2	1.3	1.2	1.6	1.5	1.4	1.6

300 and 304, in contrast, have the flattest REE patterns (La_n/Sm_n = 1.0-1.1) of any Sætra dikes reported here or elsewhere (see below). Excepting these two samples, REE concentrations vary by a factor of ~2. Most patterns are approximately parallel, suggesting that the concentration range is controlled mainly by low-pressure crystal fractionation (modeling not shown, as in Hollocher, 1993), supported by a negative correlation between MgO and La (not shown). Sample 313 has a negative Ce anomaly,

TABLE 2

(continued)

Sample	285	286	287	288	289	323*	316	317
Place	Ystland	Ystland	Ystland	Ystland	Ystland	Ura	Åsbøen	Åsbøen
SiO_2	50.65	51.07	50.86	50.61	50.90	50.17	44.99	46.28
TiO_2	1.33	1.25	1.29	1.27	1.16	2.80	1.66	1.72
Al_2O_3	15.30	15.11	15.41	15.91	14.92	13.09	16.70	16.61
Fe_2O_3	10.23	9.90	10.30	9.73	9.13	13.59	12.68	12.70
MnO	0.16	0.17	0.16	0.16	0.15	0.17	0.17	0.20
MgO	7.18	7.46	6.96	6.84	8.00	6.07	9.01	8.12
CaO	11.10	10.97	11.10	11.29	10.94	10.36	9.66	9.17
Na_2O	2.24	2.17	1.87	2.37	2.56	1.96	2.52	2.93
K_2O	0.98	0.95	1.03	1.02	1.39	0.54	1.51	1.35
P_2O_5	0.20	0.19	0.18	0.19	0.20	0.39	0.25	0.25
CO_2	0.22	0.41	0.41	0.30	0.38	0.30	0.23	0.19
S	0.13	0.11	0.16	0.07	0.08	0.15	0.09	0.06
SUM	99.72	99.76	99.73	99.76	99.81	99.59	99.47	99.58
LOI	1.4	1.6	1.9	1.5	1.7	0.8	1.4	1.1
Li	3.3	3.4	3.9	4.3	6.6	8.4	28.1	28.6
Be	0.5	0.6	0.5	0.5	0.6	0.9	0.6	0.6
Sc	35	36	34	35	35	44	24	26
V	277	269	236	225	214	448	201	206
Cr	117	176	117	132	329	73	83	85
Co	41	38	39	37	39	44	62	55
Ni	45	60	44	46	75	40	167	126
Cu	69	58	73	24	36	81	62	69
Zn	84	84	99	93	69	57	108	102
Ga	18	18	18	18	17	24	21	21
Rb	22	23	26	23	38	9	48	42
Sr	280	316	299	309	333	160	319	344
Y	25	25	25	24	24	71	26	28
Zr	102	101	102	97	110	260	114	122
Nb	16.3	17.3	15.2	13.8	15.1	6.1	8.8	9.4
Mo	0.31	0.24	0.36	0.81	2.71	0.27	0.43	1.38
Sn	0.89	0.93	0.98	0.83	1.02	2.31	1.18	1.32
Cs	0.40	0.37	0.41	0.45	0.78	0.17	4.01	3.35
Ba	124	137	202	172	293	49	292	276
La	12.8	13.4	12.5	11.0	15.4	9.4	10.4	11.2
Ce	27.9	29.0	26.7	24.0	33.1	28.4	25.3	26.1
Pr	3.63	3.75	3.49	3.16	4.24	4.77	3.54	3.75
Nd	15.9	15.9	15.3	14.0	17.5	24.3	16.2	16.8
Sm	3.91	3.79	3.94	3.74	4.03	8.09	4.11	4.36
Eu	1.33	1.27	1.32	1.28	1.26	2.47	1.43	1.54
Gd	4.24	3.99	4.23	4.10	4.01	10.36	4.39	4.71
Tb	0.71	0.67	0.69	0.68	0.65	1.83	0.71	0.77
Dy	4.41	4.20	4.33	4.18	3.99	11.95	4.43	4.70
Ho	0.91	0.85	0.89	0.85	0.81	2.54	0.90	0.97
Er	2.51	2.38	2.48	2.38	2.26	7.23	2.50	2.65
Tm	0.37	0.35	0.36	0.35	0.34	1.09	0.37	0.39
Yb	2.29	2.18	2.25	2.13	2.08	6.74	2.32	2.44
Lu	0.34	0.33	0.33	0.32	0.31	0.98	0.34	0.36
Hf	2.7	2.7	2.6	2.5	2.8	6.6	3.0	3.2
Ta	0.86	0.87	0.81	0.72	0.74	0.35	0.46	0.50
Pb	3.3	2.7	3.5	3.4	4.6	4.5	11.3	8.8
Th	1.21	1.28	1.14	1.03	1.60	0.65	0.82	0.88
U	0.38	0.40	0.38	0.30	0.62	0.31	0.47	0.46
Nb/La	1.3	1.3	1.2	1.3	1.0	0.6	0.8	0.8
La_n/Sm_n	2.0	2.2	2.0	1.8	2.4	0.7	1.6	1.6

which is not unusual for altered or metamorphosed basalts (for example, Grauch, 1989, his fig. 26; Shikazono, 1999; Verma, 2000, Cocos plate samples). In figure 18A, three multi-element patterns are shown for typical, LREE-enriched Oppdal dikes (299, 306, 313). These patterns are nearly parallel, like the REE patterns. Notable features include small positive P and small negative Zr-Hf anomalies. Important is the absence of negative Nb-Ta anomalies, suggesting that these dikes are unrelated to arcs and have

TABLE 3

Chemical analyses of mafic dikes in basement gneiss, Lepsøy, Midsund and Geita

Sample	73	74	75	76	77	80	81	82	83	84	85	86	170	176
Place	Lepsøy	Lepsøy	Lepsøy	Lepsøy	Lepsøy	Lepsøy	Lepsøy	Lepsøy	Lepsøy	Lepsøy	Lepsøy	Lepsøy	Dryna	Dryna
SiO_2	50.79	50.54	51.48	51.03	49.85	51.44	50.07	51.12	50.95	50.38	49.96	51.53	50.81	51.17
TiO_2	1.41	0.93	1.56	1.54	1.25	1.45	1.43	1.57	1.15	1.24	1.14	1.01	1.47	1.36
Al_2O_3	15.20	15.91	14.09	14.39	16.50	14.49	14.40	14.67	15.59	14.89	15.88	15.56	15.18	15.00
Fe_2O_3	10.08	8.45	11.63	11.56	8.98	11.42	11.84	10.61	9.56	10.00	8.75	8.00	9.80	9.62
MnO	0.14	0.11	0.22	0.20	0.15	0.18	0.17	0.22	0.15	0.16	0.14	0.13	0.16	0.21
MgO	6.79	8.75	6.85	6.51	6.76	6.44	7.06	6.92	7.16	8.12	7.65	8.12	6.90	7.34
CaO	11.24	11.95	11.08	11.15	11.36	10.44	10.59	11.34	11.32	10.84	11.57	10.30	10.34	10.59
Na_2O	2.38	2.43	1.77	2.17	2.73	2.03	1.99	2.16	2.27	2.36	2.20	2.47	2.80	2.81
K_2O	1.35	0.47	0.44	0.83	1.49	1.37	1.68	0.75	1.14	1.42	1.48	1.77	1.88	1.25
P_2O_5	0.18	0.08	0.17	0.25	0.15	0.24	0.15	0.18	0.14	0.15	0.15	0.15	0.18	0.19
CO_2	0.07	0.04	0.19	0.07	0.37	0.15	0.22	0.07	0.22	0.15	0.70	0.52	0.11	0.07
S	0.09	0.01	0.07	0.05	0.11	0.06	0.05	0.08	0.07	0.05	0.11	0.11	0.03	0.05
SUM	99.72	99.67	99.55	99.75	99.70	99.71	99.65	99.69	99.72	99.76	99.73	99.67	99.66	99.66
LOI	0.1	0.2	0.2	0.3	0.5	0.6	0.8	0.4	0.4	0.6	0.5	1.0	0.6	0.5
Li	4.6	6.9	3.3	3.9	5.5	5.8	7.4	6.5	4.7	6.1	6.3	9.3	6.5	2.0
Be	0.4	0.3	0.5	0.6	0.6	0.7	0.8	0.4	0.7	0.4	0.4	0.6	0.9	0.6
Sc	36	35	40	40	33	36	41	37	36	37	34	30	35	35
V	293	257	421	494	343	473	319	287	241	257	212	191	252	242
Cr	224	470	92	51	260	146	85	102	228	312	299	381	197	205
Co	41	40	40	46	37	41	44	41	39	44	37	38	39	40
Ni	45	114	32	37	48	43	40	36	43	78	75	89	39	70
Cu	37	6	52	98	64	84	47	71	13	65	24	25	24	19
Zn	91	84	80	95	84	93	104	94	88	78	85	83	82	95
Ga	19	17	20	20	18	19	20	20	18	18	18	16	20	18
Rb	19	17	16	17	16	20	38	11	15	44	22	62	27	19
Sr	295	249	184	256	225	252	157	278	206	213	228	213	219	196
Y	28	17	31	33	24	32	30	31	23	24	23	23	29	25
Zr	105	58	102	124	95	136	94	113	78	76	90	103	112	107
Nb	12.4	5.8	11.8	27.0	10.5	19.3	11.2	13.9	9.3	10.1	8.2	10.8	12.1	11.8
Mo	0.46	0.23	0.71	0.54	0.49	0.48	0.38	0.58	0.71	0.43	0.42	0.21	0.32	0.58
Sn	0.98	0.68	1.08	1.06	0.99	1.22	1.46	1.09	0.87	0.83	0.91	0.84	1.01	1.03
Cs	0.09	0.04	0.06	0.09	0.28	0.15	0.49	0.13	0.49	0.30	0.50	1.62	0.89	0.27
Ba	108	119	123	133	84	173	173	81	112	116	98	243	371	81
La	10.3	5.6	9.4	19.7	8.8	17.6	9.9	11.7	8.2	7.7	8.2	13.2	11.1	10.0
Ce	23.4	12.9	22.2	40.8	20.4	38.8	22.1	26.5	18.6	18.0	19.1	28.6	25.7	23.3
Pr	3.20	1.76	3.19	5.06	2.84	5.02	3.05	3.63	2.56	2.49	2.66	3.70	3.58	3.24
Nd	14.7	8.0	14.9	20.6	13.3	21.4	13.9	16.5	11.7	11.7	12.6	15.6	16.2	14.7
Sm	3.98	2.26	4.38	4.82	3.56	4.96	3.81	4.53	3.22	3.23	3.43	3.65	4.41	3.91
Eu	1.35	0.85	1.51	1.58	1.25	1.55	1.41	1.51	1.14	1.14	1.16	1.05	1.51	1.34
Gd	4.52	2.64	5.15	5.19	4.09	5.26	4.59	5.14	3.67	3.76	3.80	3.79	5.01	4.34
Tb	0.75	0.45	0.86	0.85	0.66	0.86	0.79	0.85	0.62	0.65	0.62	0.62	0.83	0.72
Dy	4.75	2.86	5.47	5.46	4.20	5.36	5.14	5.44	3.97	4.11	3.88	3.97	5.20	4.49
Ho	0.98	0.58	1.13	1.14	0.87	1.11	1.08	1.11	0.82	0.86	0.79	0.82	1.06	0.92
Er	2.73	1.61	3.10	3.20	2.38	3.11	2.98	3.06	2.24	2.37	2.17	2.28	2.96	2.54
Tm	0.40	0.23	0.45	0.49	0.35	0.46	0.44	0.45	0.33	0.35	0.32	0.34	0.44	0.37
Yb	2.56	1.48	2.89	3.13	2.23	2.96	2.75	2.78	2.05	2.17	2.02	2.13	2.74	2.35
Lu	0.37	0.22	0.42	0.47	0.32	0.44	0.41	0.41	0.30	0.33	0.29	0.32	0.39	0.35
Hf	2.8	1.6	2.8	3.2	2.5	3.5	2.5	3.0	2.1	2.1	2.4	2.7	3.0	2.8
Ta	0.70	0.33	0.65	1.25	0.58	0.91	0.57	0.72	0.49	0.56	0.44	0.58	0.70	0.66
Pb	4.1	3.9	3.5	3.3	8.5	7.4	7.7	3.9	5.4	6.4	11.8	11.6	5.2	4.6
Th	0.97	0.75	0.88	2.12	0.81	1.81	0.86	1.16	0.77	0.69	0.71	2.39	0.98	0.96
U	0.30	0.30	0.46	0.59	0.34	0.55	0.41	0.40	0.24	0.25	0.22	0.64	0.35	0.68
Nb/La	1.2	1.0	1.2	1.4	1.2	1.1	1.1	1.2	1.1	1.3	1.0	0.8	1.1	1.2
La_n/Sm_n	1.6	1.5	1.3	2.6	1.5	2.2	1.6	1.6	1.6	1.5	1.5	2.3	1.6	1.6

no significant component of typical continental crust (for example, Thompson and others, 1984; Sun and McDonough, 1989; Pearce and others, 1995; Rudnick and Gao, 2003).

Almost all samples from seven other probable Sætra localities, figures 16B-H, are compositionally similar to those at Oppdal (fig. 16A). The data from these samples plot on top of the Oppdal data with respect to La_n/Sm_n and Nb/La ratios, with the

TABLE 3
(continued)

Sample	177	186	193	194	195	196	255	256	257	258	259
Place	Dryna	Midøy	Otrøy	Otrøy	Otrøy	Otrøy	Geita	Geita	Geita	Geita	Geita
SiO_2	50.43	47.78	49.92	52.17	49.40	51.24	49.10	49.83	49.76	50.15	46.16
TiO_2	1.38	3.11	1.06	1.19	1.41	1.32	1.03	0.98	1.58	1.49	0.92
Al_2O_3	15.96	13.39	17.03	14.95	15.16	14.98	16.55	17.05	14.13	14.15	15.03
Fe_2O_3	9.60	15.03	8.78	8.67	10.11	9.73	8.37	8.00	12.65	12.43	7.95
MnO	0.18	0.23	0.15	0.15	0.17	0.17	0.16	0.14	0.22	0.24	0.23
MgO	6.79	6.23	7.01	7.95	8.87	7.11	8.30	7.29	6.69	6.71	6.51
CaO	10.60	9.95	12.26	10.71	11.32	11.28	12.10	11.02	10.69	10.56	9.20
Na_2O	2.88	1.97	2.47	2.26	2.49	2.76	2.21	1.69	1.76	1.78	3.08
K_2O	1.16	1.53	0.87	1.37	0.75	1.05	1.39	2.78	1.82	1.85	4.61
P_2O_5	0.20	0.28	0.11	0.18	0.20	0.18	0.14	0.13	0.21	0.17	0.12
CO_2	0.37	0.11	0.30	0.30	0.07	0.07	0.34	0.79	0.04	0.11	6.12
S	0.08	0.17	0.09	0.06	0.03	0.06	0.10	0.07	0.15	0.11	0.01
SUM	99.63	99.78	100.05	99.96	99.98	99.95	99.79	99.77	99.70	99.75	99.94
LOI	0.8	1.1	1.2	1.3	1.1	0.8	1.5	2.1	1.3	1.2	7.9
Li	4.5	8.6	11.8	14.0	20.8	10.4	6.9	11.6	6.5	8.9	33.5
Be	0.6	0.7	0.4	0.6	0.5	0.6	0.4	0.6	1.1	0.8	2.5
Sc	34	43	35	36	31	38	31	29	40	42	26
V	250	609	207	222	249	253	199	174	324	331	172
Cr	252	79	256	319	394	130	323	310	96	104	258
Co	37	46	39	38	43	42	40	34	44	43	28
Ni	58	44	44	83	146	33	75	86	36	37	58
Cu	45	56	85	52	11	62	57	28	77	59	1
Zn	89	136	85	93	90	92	79	107	102	110	123
Ga	19	23	17	17	18	20	17	17	19	20	16
Rb	11	41	17	20	20	15	28	79	39	40	160
Sr	199	117	298	284	254	245	315	1225	342	359	422
Y	28	37	21	24	30	27	20	19	33	32	17
Zr	107	161	65	111	124	108	78	77	106	103	66
Nb	13.0	21.8	6.9	12.6	14.2	13.7	7.5	7.2	13.9	13.1	7.3
Mo	0.32	0.86	0.26	0.33	0.42	0.40	0.51	0.94	0.37	0.72	4.66
Sn	1.09	1.67	0.81	0.90	1.22	1.04	0.72	0.76	1.14	0.94	0.63
Cs	0.25	0.13	0.27	0.56	0.38	0.48	0.74	1.63	0.83	0.85	6.14
Ba	89	132	93	98	170	96	258	440	374	412	936
La	11.1	16.7	6.2	12.0	12.1	12.4	7.4	7.7	11.0	10.7	7.2
Ce	25.6	38.7	14.5	26.9	28.1	27.9	17.2	17.8	25.2	24.3	16.3
Pr	3.50	5.17	2.05	3.49	3.89	3.69	2.43	2.48	3.39	3.28	2.26
Nd	15.8	22.6	9.8	14.7	17.5	16.3	11.2	11.3	15.4	15.0	10.1
Sm	4.13	5.64	2.84	3.52	4.52	4.05	3.03	3.09	4.18	4.02	2.72
Eu	1.41	1.88	1.04	1.04	1.47	1.35	1.06	1.11	1.45	1.40	0.95
Gd	4.66	6.24	3.34	3.76	4.94	4.47	3.34	3.33	4.92	4.79	2.92
Tb	0.78	1.06	0.58	0.64	0.84	0.73	0.55	0.55	0.85	0.84	0.49
Dy	4.96	6.62	3.73	4.13	5.31	4.69	3.44	3.34	5.52	5.35	3.00
Ho	1.03	1.35	0.78	0.87	1.09	0.95	0.71	0.69	1.16	1.14	0.61
Er	2.89	3.75	2.14	2.49	3.03	2.65	1.94	1.87	3.26	3.13	1.67
Tm	0.42	0.54	0.32	0.37	0.44	0.38	0.28	0.27	0.48	0.47	0.24
Yb	2.71	3.33	2.01	2.32	2.79	2.38	1.71	1.67	2.99	2.92	1.47
Lu	0.40	0.48	0.30	0.34	0.41	0.35	0.26	0.25	0.45	0.44	0.22
Hf	2.9	4.2	1.8	2.9	3.3	2.8	2.1	2.1	2.9	2.7	1.8
Ta	0.72	1.13	0.38	0.66	0.76	0.71	0.42	0.40	0.71	0.68	0.40
Pb	4.2	4.0	3.0	2.8	2.9	4.6	12.6	18.3	11.4	13.8	10.5
Th	1.09	1.97	0.57	2.12	1.28	1.40	0.69	0.70	1.04	1.03	0.73
U	0.40	0.55	0.28	0.57	0.45	0.41	0.24	0.23	0.32	0.31	0.22
Nb/La	1.2	1.3	1.1	1.0	1.2	1.1	1.0	0.9	1.3	1.2	1.0
La_n/Sm_n	1.7	1.9	1.4	2.1	1.7	1.9	1.5	1.5	1.6	1.7	1.7

exception of sample 105 from the Moldefjord syncline near Sunnaland (fig. 16E), which has an anomalously high La_n/Sm_n ratio of 2.6 instead of 1.0 to 1.8 for the others. Data from sample 105 plots in the same general area as all five samples from Ystland (fig. 16I), which have La_n/Sm_n ratios of 1.8 to 2.6, but Nb/La ratios of 0.8 to 1.4 like other Sætra samples. The Sætra Nappe is well constrained by consistent lithotectonic stratigraphy at Ystland on the southeast limb of the Lensvik syncline (Tucker, 1986;

TABLE 4

Chemical analyses of Sætra-like dikes in the Risberget Nappe

Sample	260	262	263	264	265	321	322	103	68	108	125	135
Place	Kjøra	Kjøra	Kjøra	Kjøra	Kjøra	Ura	Ura	Øygardsneset	Lauvøy	Skår	Brattvåg	Sunnaland
SiO_2	50.44	49.79	50.52	49.26	50.35	45.10	45.90	46.31	50.83	46.82	50.84	49.38
TiO_2	1.22	1.10	1.33	1.11	1.14	1.94	2.48	1.31	0.97	2.48	1.77	1.30
Al_2O_3	15.66	17.31	15.64	18.00	15.94	15.42	16.58	16.83	14.83	15.51	14.63	15.71
Fe_2O_3	9.21	9.31	9.96	8.31	9.09	14.05	14.21	10.99	8.68	14.35	12.05	10.54
MnO	0.15	0.14	0.15	0.14	0.15	0.20	0.22	0.20	0.18	0.23	0.22	0.19
MgO	8.44	7.34	7.38	7.04	7.45	9.65	5.86	8.90	9.35	6.99	6.62	8.50
CaO	12.27	11.20	10.95	11.88	10.97	9.35	9.98	9.85	8.97	9.09	10.20	10.81
Na_2O	1.50	2.53	0.84	2.63	1.68	2.13	2.83	0.93	1.76	2.51	0.76	2.69
K_2O	0.53	0.74	2.63	1.19	2.55	1.09	0.77	3.74	3.75	0.83	2.21	0.45
P_2O_5	0.17	0.15	0.19	0.15	0.14	0.26	0.32	0.15	0.12	0.39	0.23	0.13
CO_2	0.07	0.15	0.11	0.07	0.26	0.19	0.15	0.26	0.11	0.15	0.15	0.09
S	0.03	0.03	0.01	0.06	0.04	0.15	0.12	0.02	0.01	0.10	0.11	0.04
SUM	99.69	99.79	99.71	99.84	99.76	99.53	99.42	99.49	99.56	99.45	99.79	99.83
LOI	1.0	1.2	1.2	1.3	1.5	2.2	0.5	1.8	1.0	1.0	1.9	0.8
Li	9.9	8.8	18.3	10.0	13.3	37.9	15.4	33.7	43.2	17.0	34.8	10.3
Be	0.5	0.4	1.0	0.4	0.8	0.7	0.8	0.6	1.7	0.9	0.8	0.5
Sc	34	31	34	30	34	26	31	27	33	31	40	38
V	248	229	228	188	214	207	266	307	250	471	350	397
Cr	348	334	260	252	192	131	128	186	545	140	70	267
Co	37	36	40	33	39	67	50	53	44	54	38	46
Ni	76	68	59	69	37	248	76	169	159	111	32	92
Cu	23	20	15	19	14	149	210	77	2	166	58	14
Zn	75	66	123	85	107	116	109	114	105	115	110	97
Ga	19	17	19	19	18	21	24	18	16	23	22	18
Rb	10	15	79	26	68	45	16	167	146	15	82	6
Sr	497	230	252	274	282	201	394	236	141	274	206	246
Y	26	24	28	21	22	26	33	20	22	36	37	23
Zr	103	85	121	86	80	132	165	85	87	194	136	77
Nb	11.7	9.8	12.6	8.1	8.4	10.3	13.3	6.8	8.1	14.2	16.7	8.1
Mo	1.18	5.29	2.76	0.56	0.67	0.84	0.35	0.18	0.20	0.19	0.62	0.21
Sn	0.93	0.82	0.98	1.00	0.74	1.34	1.72	0.87	0.78	1.66	1.28	0.82
Cs	0.28	0.44	2.79	0.73	1.00	1.39	0.77	5.97	4.81	0.52	4.92	0.14
Ba	137	75	322	137	295	189	174	294	540	269	206	92
La	12.8	9.3	12.4	8.8	9.1	11.6	15.2	7.6	9.5	17.0	16.3	7.4
Ce	28.7	21.0	28.4	20.7	20.7	27.8	36.2	17.9	21.2	40.2	34.9	17.0
Pr	3.86	2.89	3.82	2.82	2.80	3.89	4.96	2.48	2.82	5.48	4.51	2.39
Nd	16.4	13.0	17.0	13.0	12.8	17.1	22.4	11.4	12.0	24.2	19.1	11.2
Sm	3.94	3.47	4.33	3.32	3.39	4.37	5.54	3.12	3.00	5.97	5.03	3.24
Eu	1.38	1.20	1.43	1.23	1.13	1.51	1.88	1.11	0.97	1.90	1.65	1.07
Gd	4.20	3.99	4.79	3.67	3.69	4.68	5.90	3.48	3.40	6.30	5.83	3.81
Tb	0.71	0.66	0.78	0.59	0.61	0.77	0.96	0.58	0.59	1.04	0.99	0.63
Dy	4.47	4.21	4.93	3.77	3.86	4.78	5.98	3.65	3.75	6.37	6.47	4.01
Ho	0.94	0.87	1.00	0.76	0.78	0.97	1.22	0.74	0.80	1.28	1.35	0.84
Er	2.67	2.44	2.80	2.14	2.15	2.64	3.32	2.04	2.27	3.48	3.81	2.33
Tm	0.39	0.35	0.42	0.31	0.31	0.39	0.48	0.30	0.34	0.51	0.58	0.35
Yb	2.39	2.22	2.56	1.93	1.95	2.44	3.05	1.86	2.14	3.18	3.59	2.18
Lu	0.35	0.33	0.38	0.28	0.29	0.36	0.45	0.27	0.32	0.47	0.54	0.33
Hf	2.8	2.3	3.1	2.3	2.2	3.3	4.2	2.4	2.3	4.8	3.7	2.1
Ta	0.63	0.55	0.64	0.45	0.46	0.57	0.72	0.38	0.43	0.75	0.88	0.42
Pb	13.5	8.8	11.4	9.2	14.3	6.0	9.1	17.9	13.8	5.4	40.8	5.3
Th	1.54	0.95	1.18	0.76	0.90	1.00	1.29	0.63	1.59	1.59	1.56	0.63
U	0.49	0.28	0.34	0.25	0.26	0.35	0.44	0.20	0.43	0.38	0.65	0.21
Nb/La	0.9	1.1	1.0	0.9	0.9	0.9	0.9	0.9	0.9	0.8	1.0	1.1
La_n/Sm_n	2.0	1.7	1.8	1.7	1.7	1.7	1.7	1.5	2.0	1.8	2.0	1.4

Solli and others, 1997, Stop 5), and there is little doubt that it represents Sætra quartzite and dikes. We therefore interpret the five anomalous samples from Ystland, and sample 105 from Sunnaland, to be a more LREE-enriched variety of Sætra dikes.

Figures 17B-H show REE patterns for amphibolites in Sætra quartzites. Most of the patterns are somewhat straighter than those at Oppdal, lacking their slight Z-shaped curvature. Otherwise, REE patterns at other localities largely overlap those of Oppdal

TABLE 5

Chemical analyses of mafic rocks within the Risberget Nappe that are unlike those of the Sætra Nappe

Sample	261	329	391	393	152	168	102	62	106	107	109
Place	Kjøra	Årnes	Oppdal	Oppdal	Bolsøy	Bolsøy	Øygardsneset	Tennøy	Skår	Skår	Skår
SiO_2	48.95	50.23	59.40	51.22	63.65	51.36	52.68	49.54	50.44	46.54	47.24
TiO_2	0.63	1.17	1.10	0.20	0.83	0.97	1.97	1.18	1.08	0.98	2.09
Al_2O_3	18.84	18.39	16.73	17.40	16.21	16.20	15.34	16.09	15.83	15.80	16.03
Fe_2O_3	8.75	9.19	7.35	7.55	5.46	10.17	11.24	10.25	11.64	11.40	13.73
MnO	0.13	0.13	0.12	0.16	0.11	0.18	0.18	0.16	0.19	0.17	0.20
MgO	8.14	5.09	2.65	9.72	1.28	7.17	4.77	7.71	7.48	10.55	6.59
CaO	9.43	8.62	5.58	10.47	3.51	9.26	6.34	11.09	8.14	10.21	8.69
Na_2O	3.46	3.86	3.99	2.49	3.37	2.81	2.01	2.16	2.97	2.24	3.10
K_2O	1.19	2.08	2.38	0.22	5.09	1.04	4.12	1.02	1.24	0.74	1.09
P_2O_5	0.24	0.46	0.34	0.03	0.31	0.29	0.59	0.14	0.24	0.15	0.50
CO_2	0.04	0.19	0.11	0.23	0.07	0.07	0.15	0.22	0.19	0.75	0.19
S	0.06	0.17	0.04	0.01	0.09	0.03	0.10	0.11	0.10	0.02	0.09
SUM	99.86	99.58	99.79	99.70	99.98	99.55	99.49	99.67	99.54	99.55	99.54
LOI	1.1	1.1	1.4	2.1	0.8	1.0	1.0	0.7	1.1	2.1	0.6
Li	16.5	16.3	10.7	8.3	8.4	13.7	27.3	10.8	15.9	20.4	15.5
Be	0.5	1.0	0.9	0.5	1.4	0.9	1.1	0.4	0.8	0.3	0.6
Sc	21	22	21	30	12	35	20	35	34	29	29
V	128	191	115	105	35	263	266	324	322	348	289
Cr	135	85	48	119	15	95	55	254	121	191	89
Co	39	30	20	44	9	46	40	46	53	58	54
Ni	82	48	24	155	8	104	73	108	110	182	107
Cu	31	56	35	1	17	175	57	86	110	21	154
Zn	69	109	88	95	77	90	109	74	108	85	117
Ga	17	25	25	16	22	19	21	19	20	17	23
Rb	25	43	68	1	95	24	136	36	24	17	22
Sr	665	1059	523	453	260	258	319	291	327	278	444
Y	14	23	33	11	45	32	32	20	29	17	31
Zr	48	111	543	16	608	121	182	71	104	51	134
Nb	2.5	6.5	11.9	0.5	20.0	6.9	11.5	4.4	5.6	2.6	6.8
Mo	0.82	0.05	0.37	0.03	0.25	0.07	0.50	0.19	0.04	0.08	0.21
Sn	0.45	1.71	1.35	0.56	1.07	1.18	1.70	0.74	1.02	0.65	1.31
Cs	1.06	1.54	1.26	0.02	1.05	0.66	4.31	2.77	0.62	0.19	0.69
Ba	391	1107	1128	38	1501	438	905	169	450	237	577
La	8.9	24.4	36.9	5.5	54.8	23.2	23.8	7.8	16.1	5.8	16.9
Ce	19.9	55.0	81.0	13.4	116.4	49.7	55.9	18.5	35.3	14.3	40.0
Pr	2.70	7.61	10.27	1.93	14.70	6.52	7.11	2.55	4.69	2.00	5.70
Nd	11.5	32.6	42.0	8.6	58.0	26.4	29.4	11.6	20.1	9.6	25.3
Sm	2.43	6.71	8.17	1.95	11.48	5.61	6.42	3.04	4.73	2.51	6.10
Eu	0.86	1.99	3.11	0.55	3.52	1.48	1.86	1.08	1.37	1.00	2.14
Gd	2.35	5.49	6.83	1.79	9.40	5.44	5.97	3.37	4.82	2.89	6.16
Tb	0.37	0.76	1.03	0.29	1.48	0.88	0.94	0.57	0.77	0.47	0.93
Dy	2.32	4.24	5.93	1.84	8.74	5.52	5.64	3.57	5.04	2.90	5.65
Ho	0.48	0.83	1.17	0.39	1.76	1.17	1.13	0.74	1.04	0.60	1.12
Er	1.34	2.15	3.18	1.11	4.83	3.34	3.09	2.01	2.93	1.64	3.09
Tm	0.20	0.30	0.46	0.17	0.70	0.50	0.44	0.29	0.44	0.24	0.45
Yb	1.23	1.80	2.88	1.10	4.36	3.07	2.73	1.83	2.82	1.49	2.71
Lu	0.19	0.26	0.42	0.16	0.65	0.47	0.40	0.27	0.42	0.22	0.40
Hf	1.3	2.9	12.3	0.6	14.6	3.2	4.6	2.0	2.8	1.5	3.6
Ta	0.10	0.21	0.47	0.03	0.80	0.29	0.59	0.23	0.25	0.13	0.36
Pb	8.9	8.7	11.7	4.4	18.0	7.1	14.6	5.0	6.8	2.9	5.3
Th	0.56	0.14	2.88	0.07	5.27	0.70	4.02	0.87	0.92	0.46	0.93
U	0.31	0.13	0.66	0.01	1.12	0.21	0.91	0.28	0.36	0.12	0.27
Nb/La	0.3	0.3	0.3	0.1	0.4	0.3	0.5	0.6	0.3	0.5	0.4
La_n/Sm_n	2.3	2.3	2.8	1.7	3.0	2.6	2.3	1.6	2.1	1.4	1.7

Table 5
(continued)

Sample	123	124	126	127	136
Place	Brattvåg	Brattvåg	Brattvåg	Brattvåg	Sunnaland
SiO_2	46.25	47.12	56.73	52.42	49.98
TiO_2	2.08	1.80	1.38	1.04	1.21
Al_2O_3	16.09	15.79	15.47	15.86	16.61
Fe_2O_3	13.45	12.87	9.98	9.96	10.88
MnO	0.36	0.21	0.21	0.18	0.21
MgO	6.98	7.70	4.40	7.31	7.21
CaO	8.30	8.73	6.17	8.45	9.26
Na_2O	0.20	2.48	2.88	2.80	2.68
K_2O	5.29	2.42	1.75	1.36	1.21
P_2O_5	0.49	0.45	0.44	0.26	0.42
CO_2	0.11	0.11	0.11	0.07	0.08
S	0.24	0.16	0.17	0.09	0.11
SUM	99.84	99.84	99.69	99.80	99.86
LOI	2.4	1.7	0.9	1.1	1.3
Li	46.6	22.5	17.9	21.2	16.3
Be	1.0	0.5	1.3	0.8	1.0
Sc	32	29	27	31	30
V	383	322	284	313	249
Cr	96	94	92	165	154
Co	47	53	31	44	42
Ni	84	108	54	134	122
Cu	130	80	134	113	126
Zn	396	116	110	101	112
Ga	24	20	22	19	20
Rb	255	75	41	35	22
Sr	464	455	336	319	461
Y	30	27	35	30	29
Zr	104	99	332	157	153
Nb	5.3	4.5	14.6	8.0	7.7
Mo	0.23	0.15	0.04	0.26	0.29
Sn	1.20	1.01	2.07	1.30	1.49
Cs	14.54	5.28	1.50	2.12	0.64
Ba	1179	707	775	493	548
La	16.6	14.6	40.2	21.7	23.9
Ce	38.8	34.2	84.0	46.9	52.7
Pr	5.51	4.91	10.80	6.05	6.90
Nd	25.0	22.5	43.3	24.9	29.3
Sm	6.07	5.38	8.55	5.22	6.02
Eu	2.13	1.88	2.06	1.27	1.69
Gd	6.19	5.40	7.36	5.05	5.51
Tb	0.93	0.81	1.08	0.80	0.84
Dy	5.63	4.97	6.21	4.99	5.14
Ho	1.14	1.00	1.26	1.03	1.05
Er	3.09	2.69	3.48	2.90	2.92
Tm	0.44	0.39	0.50	0.43	0.43
Yb	2.65	2.38	3.20	2.72	2.71
Lu	0.39	0.35	0.49	0.41	0.41
Hf	2.9	2.6	8.1	3.8	3.9
Ta	0.25	0.23	0.58	0.36	0.30
Pb	66.2	22.5	7.4	7.5	8.1
Th	1.18	0.71	1.38	1.39	0.41
U	0.27	0.19	0.38	0.44	0.14
Nb/La	0.3	0.3	0.4	0.4	0.3
La_n/Sm_n	1.7	1.7	2.9	2.6	2.5

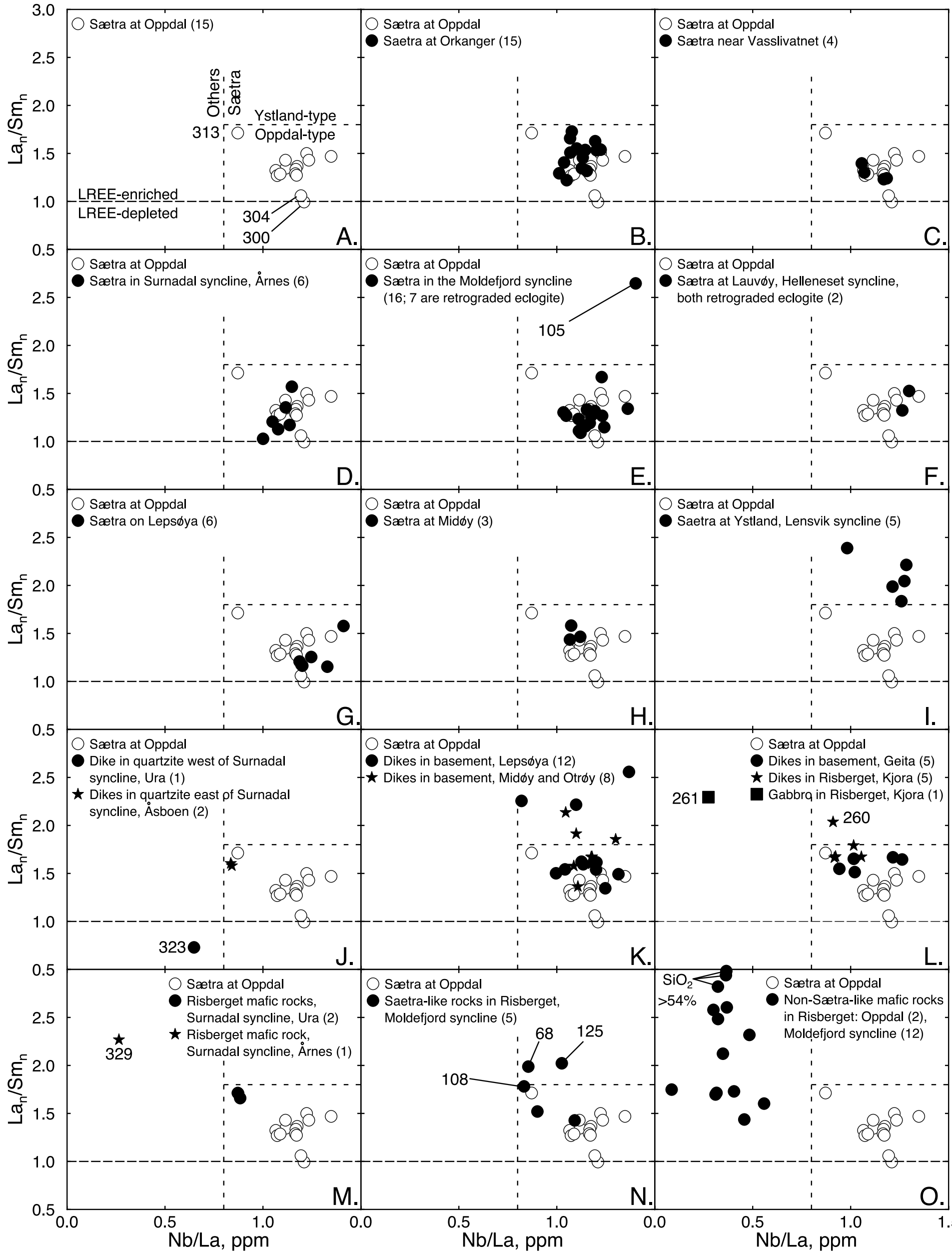

Fig. 16. Nb/La vs. La_n/Sm_n graphs showing all rocks analyzed in this study. Sætra samples from Oppdal are shown in panel A, and in all subsequent panels for comparison. Reference lines at Nb/La = 0.8 and La_n/Sm_n = 1.0 and 1.8 are used to differentiate between different Sætra dike compositional groups. Chondrite normalizing factors for La and Sm are from McDonough and Sun (1995).

(excepting samples 300 and 304, fig. 17A). Sample 93, one of six samples from Lepsøya (fig. 17G), has a REE pattern shape identical to those at Oppdal. This sample demonstrates that the Z-shaped Oppdal REE patterns are not unique. Relatively high REE concentrations are found in samples 334 at Årnes (fig. 17D) and samples 60, 96, and 97 in the Moldefjord syncline (fig. 17E). These REE patterns are essentially parallel to other samples at their respective localities, suggesting that these samples acquired their high REE concentrations by crystal fractionation. This inference is supported by the fact that these samples have progressively larger negative Eu anomalies and lower MgO and CaO contents, with increasing REE concentration, than any other samples at their respective sample areas, and by simple fractional crystallization modeling (not shown, as in Hollocher, 1993). Sample 105 from Sunnaland (fig. 17E) and the five samples from Ystland (fig. 17I), noted as being anomalous in figure 16, all have concave upward REE patterns that are distinct from patterns from the other localities.

Figures 18B-H show multi-element patterns for Sætra amphibolites in comparison to Oppdal. Most patterns are similar to those from Oppdal: Generally enriched in the less compatible elements, no to small negative Zr-Hf anomalies, no to small positive U and P anomalies, and lack of Ta-Nb anomalies. These features hold for most samples, the only exceptions being samples already noted as having undergone substantial crystal fractionation. Samples 96 (not shown) and 97 (fig. 18E) have large positive P and negative Ti anomalies, indicative of magma that had evolved to fractionate Fe-Ti oxides but not to the point of apatite crystallization. U anomalies range from small negative to moderate positive, and do not correlate with other chemical characteristics. This may be the result of U mobility.

In summary, most amphibolites from the Sætra correlatives (figs. 16-18, panels A–I have La_n/Sm_n (1.0 – 1.8) and Nb/La (0.8 – 1.4) ratios nearly identical to those from the Oppdal area (figs. 16-18, panel A). These will be referred to as Oppdal-like compositions. A second, distinct compositional group includes all samples from Ystland (figs. 16-18, panel I) and sample 105 from the Moldefjord syncline (figs. 16-18, panel E). These six rocks are characterized by higher La_n/Sm_n ratios (1.8 – 2.6), and hence steeper REE patterns, than the Oppdal-like Sætra dikes. These are referred to as Ystland-like compositions. The flat REE pattern samples 300 and 304 (fig. 17A) form a separate group. We conclude that geochemistry supports lithotectonic stratigraphic correlation of quartzites from all these locations with the Sætra Nappe.

Mafic Rocks in Quartzites Having Unusual Tectonostratigraphic Positions

Panel J, figures 16, 17, and 18, show samples from two unusual localities near the Surnadal syncline. One sample was collected at Ura from a quartzite mapped as Sætra by Krill (1987). This quartzite is part of a separate narrow thrust slice (as shown by Krill, 1987) or syncline southwest of the southwestern limb of the Surnadal syncline near Stangvik (fig. 3). The Risberget augen gneiss along the axis of this structure is flanked on both sides by quartzite and then by basement, unusual compared to the usual arrangement of Risberget augen gneiss between basement and the Sætra Nappe. The Ura sample has La_n/Sm_n and Nb/La ratios of 0.7 and 0.6, respectively (fig. 16J), lower than any Sætra amphibolites we or others (Appendix 1) report. This sample is LREE-depleted, but has higher HREE concentrations than any other sample we report (fig. 17J). It also has a larger positive P anomaly than any but the most evolved Sætra samples (96, 97), and a moderate negative Nb-Ta anomaly not seen in any Sætra sample (fig. 18J). The unusual structural position of this quartzite, and the composition of this mafic rock, is unlike any other Sætra sample reported here or elsewhere (see below). We suggest that this unit may instead be correlative with the Neoproterozoic Åmotsdal Quartzite, from the proximal part of the Baltican margin.

Two additional samples are shown in figures 16, 17, and 18, panel J, from a 12 m thick quartzite layer associated with augen gneiss at Åsbøen (fig. 3), east of the east limb of the Surnadal syncline in a region mapped by Krill (1987) as undifferentiated basement. These two samples plot at a marginally lower Nb/La ratio (0.84, fig. 16J)

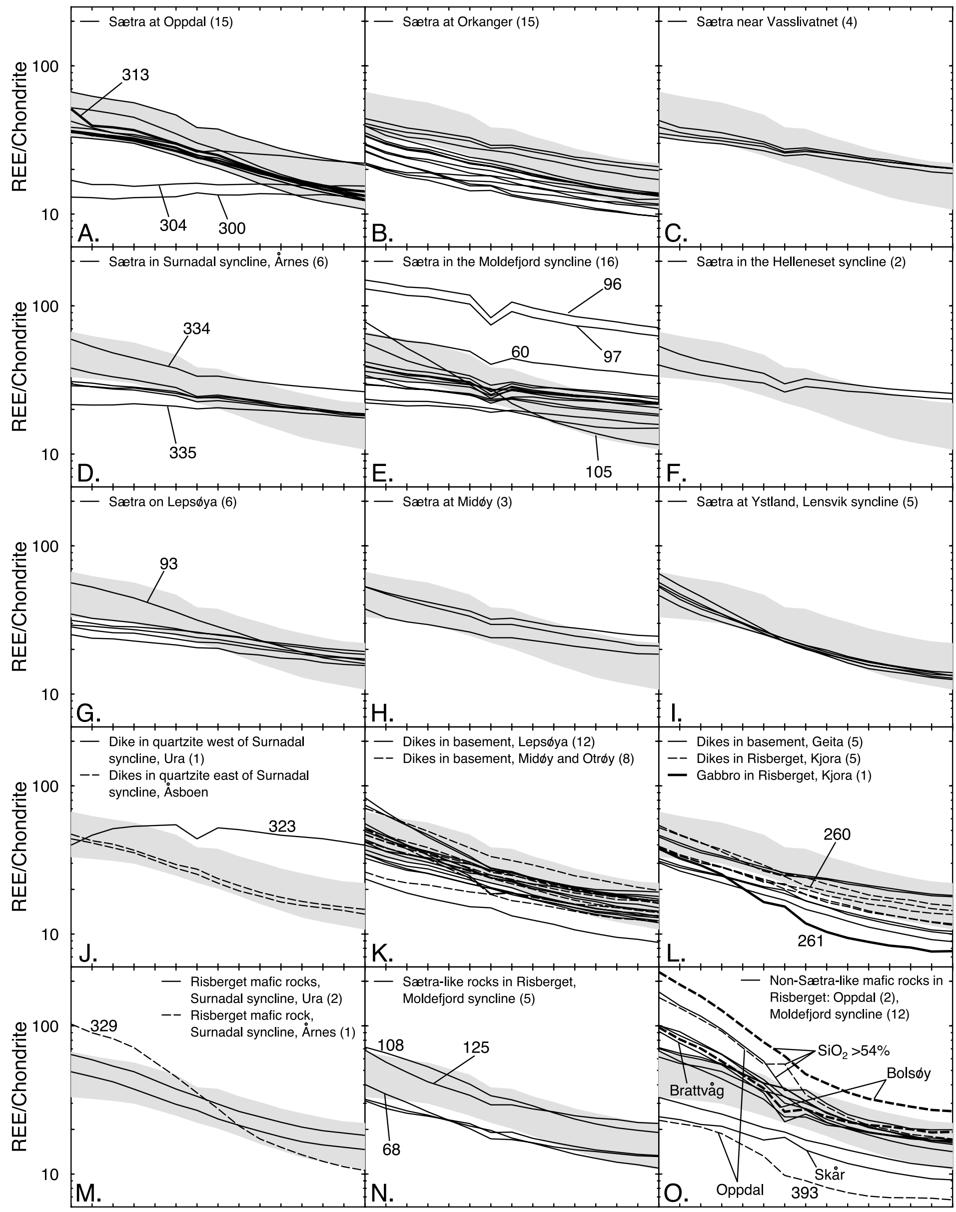

Fig. 17. Chondrite-normalized REE diagrams showing all samples analyzed in this study. The range of Sætra samples at Oppdal in (A), excluding samples 300 and 304, is shown as a shaded field in all panels for comparison. Chondrite normalizing factors are from McDonough and Sun (1995).

than sample 313 (0.87) from Oppdal, but are otherwise similar to the common Sætra Nappe amphibolites discussed above. They have positive U anomalies slightly larger than most Sætra samples, but similar to samples 304 at Oppdal (fig. 18A), 247 at Orkanger (fig. 18B), and 184 at Midsund (fig. 18H). We suspect that these rocks are part of the Sætra quartzite, but must await additional mapping before reaching a firm conclusion.

Mafic Dikes in Basement Sausage Rock

The samples in figure 16K are from basement sausage rock on the north coast of Lepsøy and on the south coast of Dryna, Midøy, and Otrøy. Fourteen of the 20 samples plot within the Oppdal data range, and six in the range of Ystland-like compositions at La_n/Sm_n ratios >1.8. REE patterns of these 20 amphibolites (fig. 17K) include Oppdal-like patterns and concave upward Ystland-like patterns. The multi-element patterns (fig. 18K) are similar to most Sætra rocks of both types. Based on this and on other chemical comparisons and cluster and discriminant analysis (discussed above), we conclude that the basement sausage rock dikes are indistinguishable from dikes in Sætra Nappe quartzites.

Mafic Dikes in Basement Gneiss and Risberget Augen Gneiss, Geita and Kjora

Ten dike samples from layered basement gneiss and Risberget Nappe augen gneiss were taken from Geita and Kjora on Trondheimsfjord. The mineralogy, similar thickness, and metamorphic mineralogy and textures of these dikes, particularly a fine-grained epidote amphibolite matrix hosting large biotite crystals and white spots of polycrystalline clinozoisite, suggest that they were emplaced contemporaneously in both units. In figure 16L, nine of the 10 samples plot within the range of Oppdal data. Sample 260 plots at a slightly higher, Ystland-like La_n/Sm_n ratio of 2.0. The REE patterns (fig. 17L) resemble the relatively straight Sætra dike patterns at Orkanger, with the steepest pattern (260, in augen gneiss) resembling patterns from Ystland. The multi-element patterns (fig. 18L) are all similar to those of Sætra dikes. We conclude that these dikes are compositionally indistinguishable from those of the Sætra Nappe, and are probably related to them.

Also plotted in panel L is sample 261 (table 5), from a large, coarse-grained, hornblende-rich amphibolite boudin in the Risberget Nappe augen gneiss at Kjora. This rock and its foliation are cut by one of the fine-grained epidote amphibolite dikes discussed immediately above (260), and we plot it here for comparison purposes. This coarse-grained rock has a Nb/La ratio of 0.3 (fig. 16L), much lower than any Sætra dike. It is LREE-enriched (La_n/Sm_n=2.3), like the Ystland-like Sætra dikes, but with flatter and lower HREE concentrations and a positive Eu anomaly (fig. 17L). The multi-element pattern of this rock (fig. 18L) has large negative Nb-Ta and Zr-Hf anomalies, not found in Sætra dikes, and a positive P anomaly larger than any but the most fractionated Sætra (samples 96 and 97; fig. 18E). We conclude that this rock is unrelated to the Sætra dikes.

Other Mafic Rocks in Risberget Augen Gneiss

Figures 16, 17, and 18, panels M-O, show 22 mafic rocks from augen gneisses of the Risberget Nappe taken from three major areas: The Surnadal syncline, the Moldefjord syncline, and Oppdal. Seven samples compositionally resemble Sætra dikes: Two from Ura (fig. 16M) and five from the Moldefjord syncline (fig. 16N). The two Ura and one Moldefjord syncline samples (108) have La_n/Sm_n ratios of 1.7 to 1.8 and slightly Z-shaped REE patterns exactly like Sætra dikes at Oppdal (fig. 16 and fig. 17, panels A, M, N). Two from the Moldefjord syncline (samples 68, 125) are Ystland-like with La_n/Sm_n ratios >1.8 and concave-up REE patterns (fig. 16 and fig. 17, panels I, M). The remaining two Moldefjord syncline samples have La_n/Sm_n ratios of 1.4 to 1.5 and straight REE patterns like those at Orkanger (fig. 16 and fig. 17, panels B, N). These seven samples have multi-element patterns that resemble those from Sætra dikes (fig. 18 M, N).

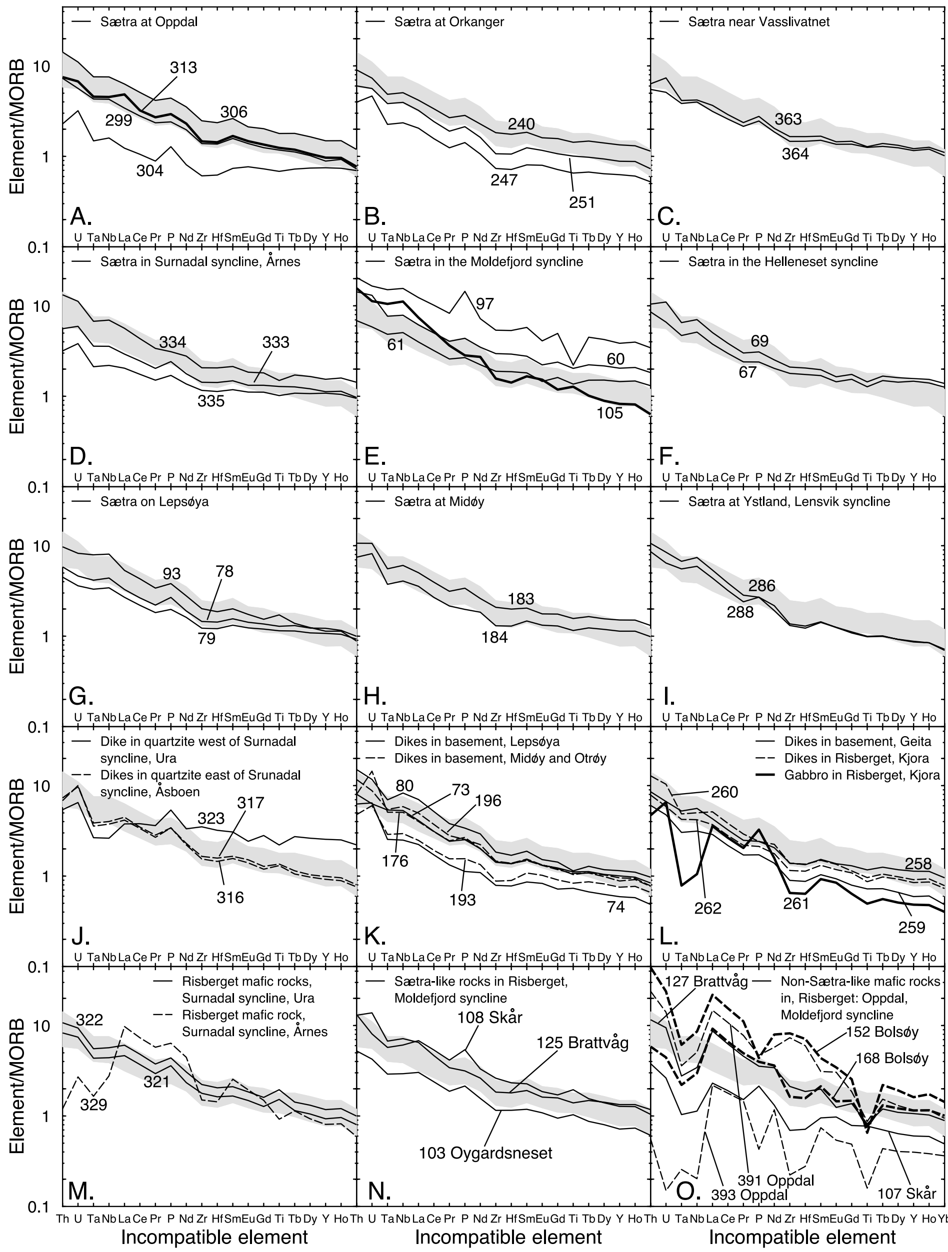

Fig. 18. MORB-normalized multi-element diagrams for selected samples analyzed in this study. The range of Sætra compositions at Oppdal (A), exclusive of samples 300 and 304, is shown in gray for comparison in all panels. Plotted samples were selected to be representative of the range of compositions for the rock groups in each panel, and to show unusual compositions (for example, sample 304 in A). In panel O, different line thicknesses and dashed lines simply differentiate crossing lines. MORB normalizing factors are from Pearce and Parkinson (1993).

The remaining 15 mafic rocks from the Risberget Nappe are shown in figures 16, 17, and 18: Sample 329 from Årnes on the southwest limb of the Surnadal syncline in panel M, and 12 from the Moldefjord syncline and two from Oppdal in panel O. These rocks come from a large geographic area and span a wide compositional range with La_n/Sm_n ratios of 1.4 to 3.0, but all have large negative Ta-Nb anomalies and Nb/La ratios <0.6, compared to >0.8 for all Sætra dikes. Sample 261 from augen gneiss at Kjora, discussed above for panel L, is compositionally similar. Three silica-rich samples (SiO_2 $>54\%$, 126, 152, 391), all from different locations, have the highest REE concentrations and the highest La_n/Sm_n ratios. Though not basaltic, all are dark-gray amphibolites.

Figures 16, 17, and 18, panels M-O, therefore show that seven mafic rocks from augen gneiss in the Risberget Nappe are similar to Sætra Nappe dike compositions; five Oppdal-like and two Ystland-like. This suggests that the Risberget Nappe contains members of the same Neoproterozoic Ottfjället dike swarms that cut the Sætra Nappe quartzites. Compositionally identical dikes from the Geita-Kjora area on Trondheimsfjord support this conclusion. In contrast, the 16 remaining mafic rocks in the Risberget augen gneiss (with 261 at Kjora), have compositional characteristics of arc magmas (for example, Pearce, 1982) or substantial contamination with continental crust (for example, Thompson and others, 1984; Glass and Phillips, 2006) and so have a very different genesis.

Tectonic Environment of Magma Production

Figures 19A and 19B show all our Sætra, Risberget, and basement samples plotted on tectonic setting discriminant diagrams. The Sætra samples plot mostly in transition regions between N-MORB and within-plate alkali basalts, with some plotting in the N-MORB fields at one end and a few plotting in the more alkaline E- or P-MORB and within-plate tholeiite fields at the other end. The Ystland-like Sætra plot in the E- or P-MORB and more alkaline within-plate fields.

The more alkaline end of Oppdal-like Sætra (figs. 19A and 19B) is almost obscured by samples from Oppdal-like mafic rocks in basement sausage rock and Risberget Nappe augen gneiss, plotting very close to or within the E- or P-MORB and within-plate tholeiite fields. Most Ystland-like samples from basement and Risberget augen gneiss plot near the Ystland-like Sætra, but three plot in the calc-alkaline arc basalt field in figure 19A (circled) a result of somewhat elevated Th concentrations rather than low Ta. Non-Sætra-like mafic rocks in the Risberget plot in extended belts from the depleted end of the N-MORB field into calc-alkaline fields. Sample 323 from quartzite in Ura, southwest of the Surnadal syncline, plots in the N-MORB field in both diagrams far from any analyzed Sætra. The two samples from quartzites at Åsbøen, east of the Surnadal syncline, plot with the Sætra in the E-MORB/within-plate tholeiite field in figure 19A, but in figure 19B plot in the within-plate alkali basalt field joined by only one or two Ystland-like Sætra. We remain uncertain that this quartzite belongs to the Sætra.

We now discuss in more detail the tectonic implications of Sætra-like dike chemistry by comparison with modern igneous rocks. Figure 20 summarizes Sætra data on figures 16–18 panels A-I, plotted along with several reference basaltic compositions from five tectonic environments: Mid-ocean ridges, flood basalts, oceanic islands, continental rifts, and island arcs. We acknowledge that the reference compositions are mere points representing extensive fields of data, but the object is to compare typical compositions from these environments with the Sætra dikes.

In figure 20A, Sætra dikes plot at higher Nb/La ratios (median 1.2) than arcs (0.14 – 0.7) and continental flood basalts (0.6 – 0.8), although the Deccan flood basalt reference composition plots just barely within the nominal range of Sætra dike compositions. The field of Oppdal-like Sætra occurs between N-MORB, and E-MORB

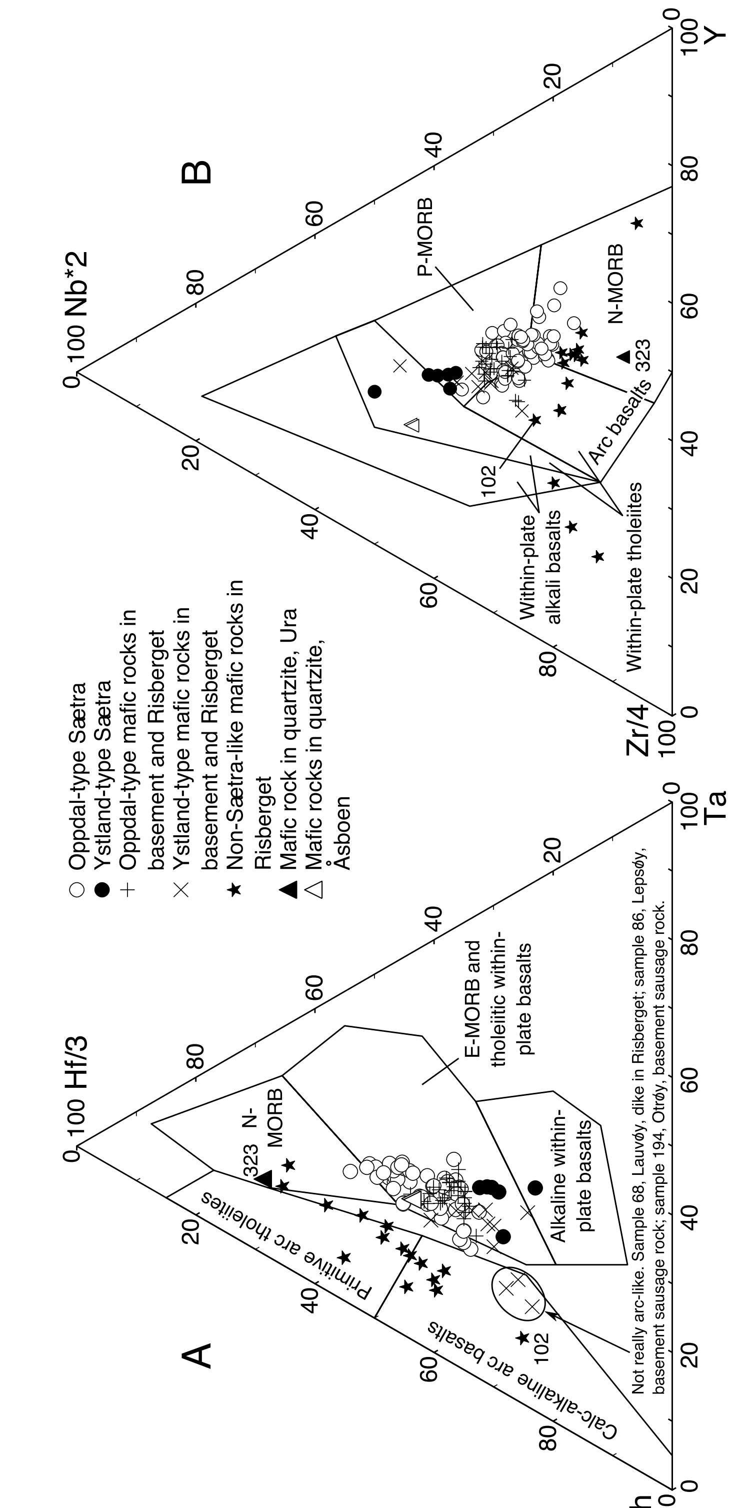

Fig. 19. Tectonic setting classification diagrams from Wood (1980; A) and Meschede (1986; B), showing all samples analyzed in this study.

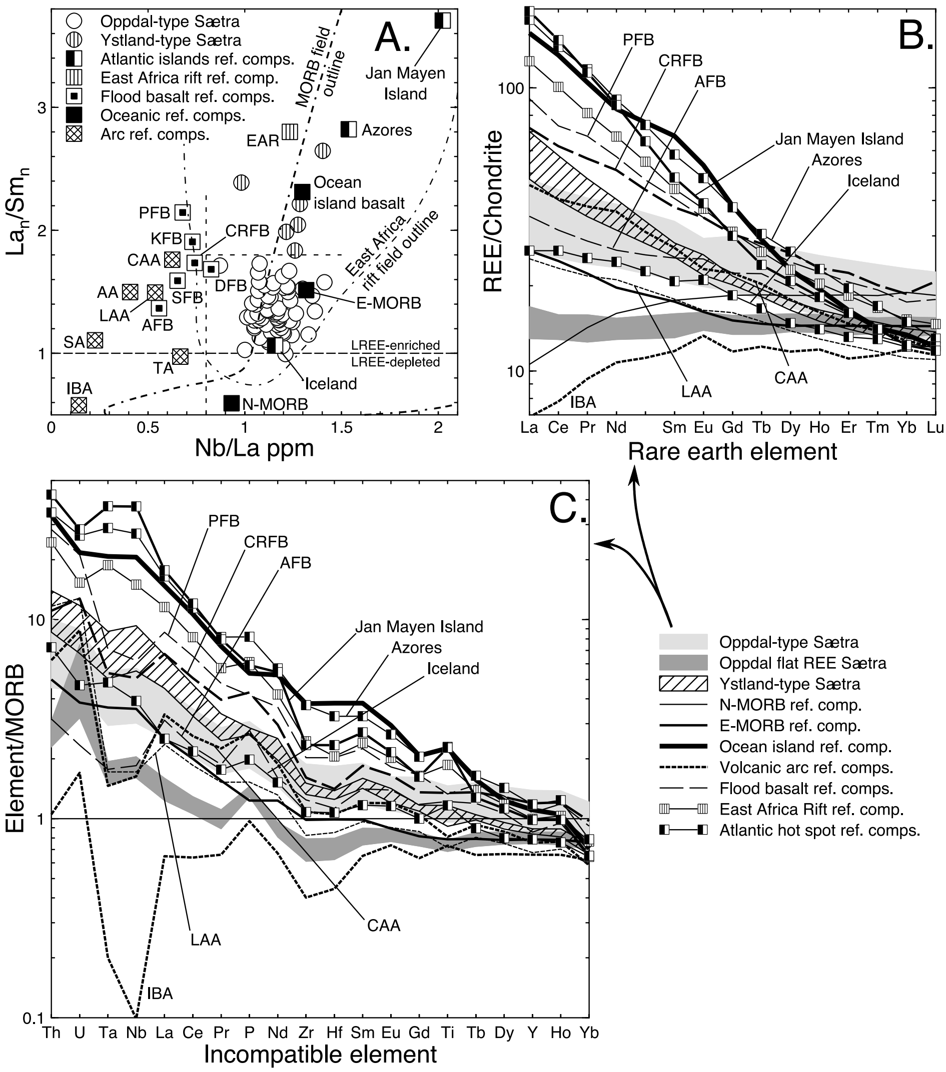

Fig. 20. Diagrams comparing our Sætra dike data with reference basalt compositions from volcanic arcs, flood basalts, MORB, ocean islands, and the East Africa rift system. (A) Nb/La vs. La_n/Sm_n diagram showing all of our Sætra data compared with reference compositions and composition fields (East Africa rift field; MORB field). (B) REE diagram showing reference compositions from A, but omitting the fields. Only selected arc and flood basalt patterns are shown to avoid confusion. Sætra compositions are shown with shaded fields: Light gray is average Oppdal-type Sætra ($\pm 1\ \sigma$; all samples in fig. 17, panels A-H, excluding flat REE samples 300 and 304, high REE samples 96 and 97, and Ystland-type sample 105); dark gray is Oppdal samples 96 and 97 only; hatched pattern is average Ystland-type samples ($\pm 1\ \sigma$; all samples in fig. 17, panel I, plus sample 105). (C) Multi-element diagram showing our Sætra data and reference compositions as in B. MORB and multi-element normalizing factors are as in figures 17 and 18, respectively. N-MORB, E-MORB, and ocean island basalt reference compositions are from Sun and McDonough (1989), but P values were divided by 1.6 to make them consistent with Pearce and Parkinson (1993) MORB normalizing factors. Arc, flood basalt, East Africa rift, Iceland, Azores, and the Jan Mayen Island reference compositions are medians derived from the GEOROC public compositional database (http://georoc.mpch-mainz.gwdg.de/georoc/), and the MORB field is derived from the PETDB public compositional database (http://www.petdb.org/). For database descriptions see Lehnert and others (2000) and references therein. Database analyses were filtered to be volcanic rocks having a 97–102% sum of the 11 major, non-volatile oxides (all iron calculated as FeO), 45–52% SiO_2, U and Eu present in the analysis, and U concentrations <3 ppm to avoid highly evolved magmas. Flood basalt abbreviations: AFB, Antarctic, Dronning-Maud land (96 analyses in A); CRFB, Columbia River (66); DFB, Deccan (180); KFB, Karoo (71); PFB, Paraná (45); SFB, Siberian (146). Arc basalt abbreviations: AA, Aleutian (38); CAA, Central American

reference compositions, though it plots partially outside the field of mid-ocean ridge basalts. The field of Ystland-like Sætra compositions plot in the vicinity of the ocean island reference composition, though the Iceland reference composition plots at the low La_n/Sm_n end of the field of Oppdal-type Sætra, and the Azores and Jan Mayen island reference compositions plot at somewhat higher La_n/Sm_n and Nb/La ratios. All of the Sætra data plot within the field of basalts from the East Africa rift system.

Figure 20B shows REE patterns for the reference compositions with respect to the Sætra compositional groups. There is considerable variation in REE pattern shapes and REE concentrations in each of the tectonic settings, certainly for individual rocks but also in the reference compositions. Basalts from different arcs can range from typically LREE-depleted (Izu-Bonin) to LREE-enriched (Central American). All flood basalt reference compositions are LREE-enriched, ranging from weakly (Antarctic) to strongly (Paraná). Ocean island and East Africa rift basalts are typically strongly LREE-enriched, and also tend to be slightly concave upward, like the Ystland-type Sætra dikes. REE patterns are not sufficiently diagnostic to reach strong conclusions.

Figure 20C compares multi-element patterns of the three Sætra groups with the reference compositions. As with the REE patterns, there is considerable variation within each tectonic setting and there are no exact matches with the Sætra dike groups. However, the arc reference compositions all have moderate to large negative Nb-Ta anomalies, not present in any of the Sætra samples. The arc reference compositions also generally have larger negative Zr-Hf anomalies than do Sætra dikes. The flood basalt reference compositions also have moderate negative Nb-Ta anomalies, larger than those in the Sætra, and Zr-Hf anomalies that range from moderate to small, larger than or similar to those in the Sætra dikes. The N-MORB, E-MORB, and Ocean island reference compositions have no substantial anomalies (none by definition for N-MORB), so it is tempting to suggest that E-MORB in particular is substantially similar in pattern shape especially to the Oppdal-type Sætra. However, hot spot-related Iceland and the East Africa rift system reference compositions have no Nb-Ta anomaly and yet have small negative Zr-Hf anomalies, and thus are in detail more like Sætra dikes in pattern shape. In contrast, patterns for the Azores and Jan Mayen Island have positive Nb-Ta anomalies and small negative Zr-Hf anomalies.

Figure 20 therefore indicates that the Sætra dikes are not arc-related, and are probably also not continental flood basalts of the sort represented in the reference compositions. They appear to be compositionally most similar to E-MORB, Iceland hot spot basalts, and the less LREE-enriched end of East Africa rift system basalts. This conclusion is consistent with the continental rift tectonic interpretation for the emplacement of the Sætra dikes (Gee, 1975; Gee and others, 1985; Siedlecka and others, 2004), and also consistent, in part, with conclusions reached by Solyom and others (1985) who used major elements and a few selected trace elements to show that the Särv (~Sætra) dikes were not arc-related, and spanned a composition range including flood, continental rift, and ocean floor basalts.

---

(65); IBA, Izu-Bonin (74); LAA, Lesser Antilles (91); SA, Scotia (39); TA, Tonga (80). Other abbreviations and numbers of analyses: East Africa rift and rift field, EAR (229); Jan Mayen Island (12); Iceland (441); Azores (55); MORB field (518). Missing concentration values for some elements result in fewer samples used to calculate reference patterns in B and C by ~5% and ~35%, respectively. Missing lanthanide values were linearly interpolated before calculating median REE and multi-element patterns. Missing Ta or Nb values were calculated from the available value by the MORB relationship: Nb x 0.056 = Ta (Pearce and Parkinson, 1993).

Comparisons with Sætra from Other Workers

Our Sætra data set is derived from the northwestern flank of the Western Gneiss Region, but most previous geochemical studies of dikes in correlative quartzites are from the Sætra, Leksdal, and Särv Nappes in central and eastern Norway and west-central Sweden (Andréasson and others, 1979; Solyom and others, 1979, 1985; Krill, 1983; Beckholmen and Roberts, 1999).

Figure 21A is analogous to figure 16 and shows that the Leksdal and Särv Nappe dikes include samples with high La_n/Sm_n ratios of 2.5 to 4.0 and Nb/La ratios of ~0.9 (one at 0.6), and some with low La_n/Sm_n ratios of ~1.1 to 2.0 and Nb/La ratios up to 2.3. In contrast, our Sætra data set has La_n/Sm_n ratios of 1.0 to 2.6 and Nb/La ratios of 0.9 to 1.4. The Leksdal and Särv rocks with high La_n/Sm_n ratios are generally alkaline, whereas the others are tholeiitic (Andréasson and others, 1979; Solyom and others, 1985; Mitchell and Roberts, 1986; Beckholmen and Roberts, 1999). The fact that most of the tholeiitic samples plot at higher Nb/La ratios (>1.4) than our Sætra data is a concern. Examination of figure 21C shows that several Leksdal and Särv Nappe samples from Leksdal, Ottfjället, and Sylarna have anomalously high Nb compared to adjacent Ta (Solyom and others, 1985). In terrestrial basaltic magmas, Nb/Ta ratios are usually very close to 17.9 (Pearce and others, 1984; Thompson and others, 1984; Sun and McDonough, 1989; Pearce and Parkinson, 1993; McDonough and Sun, 1995), and bulk Nb and Ta solid/liquid partition coefficients during melting and crystallization are low and similar (for example, Thompson and others, 1984; Sun and McDonough, 1989; Pearce and others, 1995; but see Münker, 1998). Because Nb/Ta ratios in the Leksdal and Särv Nappe tholeiitic rocks are up to 28, we therefore suspect that the Nb concentrations reported by Solyom and others (1985) are too high. We suspect Nb because Ta is consistent with La, Th, and U in figure 21C, as is Nb for the high La_n/Sm_n rocks. Plotting Ta/0.056 as a proxy for Nb in figure 21A (not shown; see caption for fig. 20) moves the tholeiitic Särv samples within or immediately adjacent to the field of our data. We conclude that Sætra dike equivalents from other areas span a composition range from that of our Oppdal-like Sætra at low La_n/Sm_n ratios, through Ystland-like Sætra to still higher La_n/Sm_n ratios for the most alkaline rocks.

Figure 21B shows available REE patterns for Sætra Nappe correlatives from other workers, compared with our Oppdal and Ystland data fields. Many Leksdal Nappe dikes are alkaline and strongly LREE-enriched. One sample from the Särv Nappe at Ottfjället is also strongly LREE-enriched, but three others have REE concentrations somewhat lower than our Oppdal-type data field and are more like Sætra from Orkanger (fig. 16B). Three Särv Nappe samples from Sylarna completely overlap the Oppdal field, and two have lower REE concentrations and so are more like our Sætra dikes from Orkanger (fig. 16B).

In figure 21C, most Leksdal and Särv Nappe samples have anomaly patterns like those of the Sætra dikes we report, including small negative Zr-Hf anomalies, absent to moderate positive P anomalies, and lack of Nb-Ta anomalies (when corrected for anomalous Nb, not shown, see discussion above for fig. 21A). The four samples with analyzed U (fig. 21C, caption) have small, slightly negative to positive U anomalies, similar to most Sætra samples we report. The one anomalous pattern (Beckholmen and Roberts, 1999, sample 75-87) is from a rock in the Leksdal Nappe. It is the most LREE-rich sample from the Ottfjället dike swarms for which analyses are available. This alkaline rock has large negative Zr-Hf and Nb-Ta anomalies, not found elsewhere in the Sætra or equivalents. It is difficult to reach firm conclusions from a single analysis, but we speculate that the anomalies of this sample stem from an unusually large amount of contamination with continental crust material.

In figure 21D, the few available data from the Leksdal and Särv Nappes are largely coincident with the more alkaline end of our data set in the E-MORB field, with a few

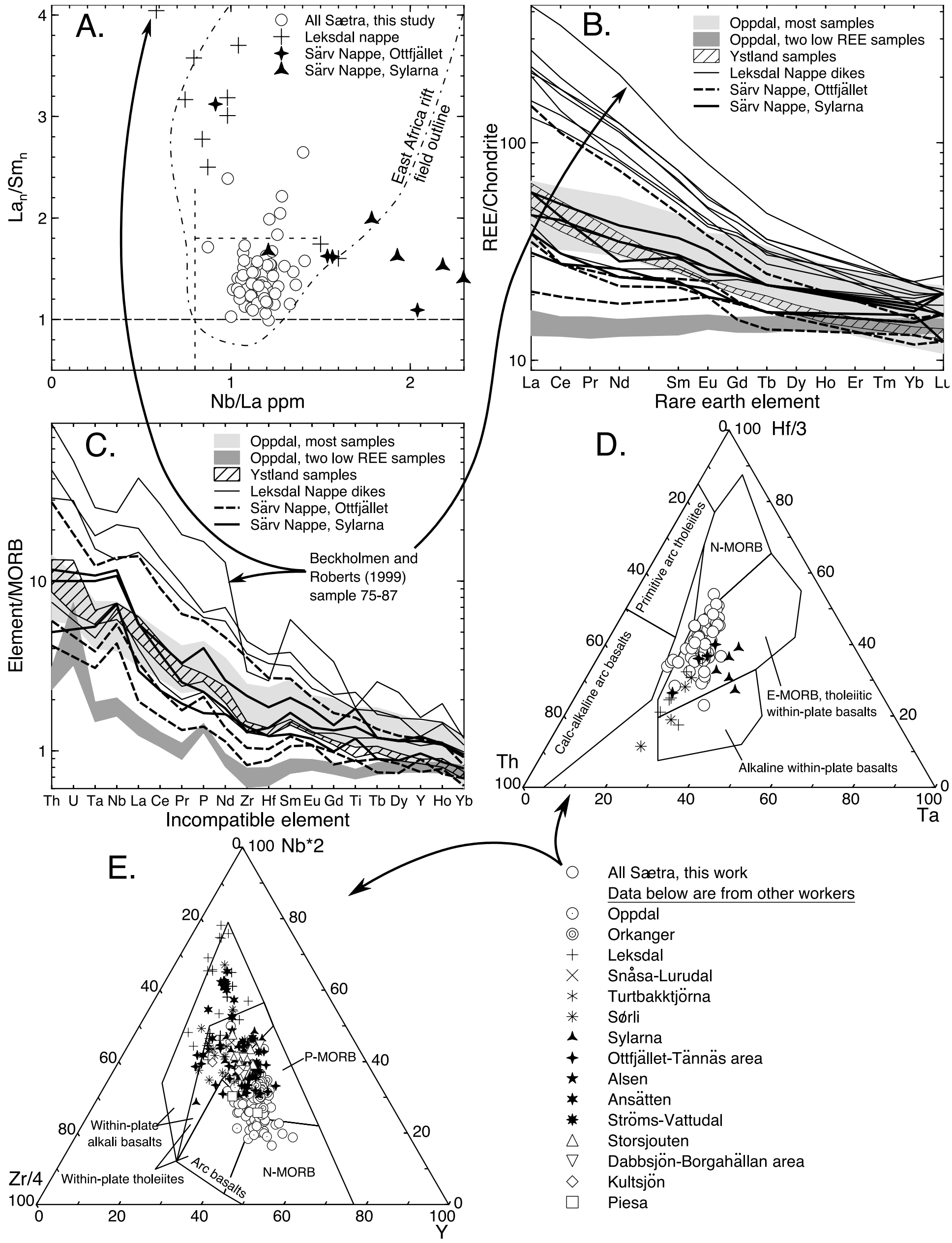

Fig. 21. Five diagrams comparing our Sætra data with Sætra Nappe and equivalent dikes analyzed by others (see figs. 1 and 22 for locations and Appendix 1 for data sources; chondrite and multi-element normalizing factors as in figs. 17 and 18, respectively). The East Africa rift field (A) is from figure 20A. Gray and hatched composition fields in B and C are our Sætra data are from figures 20B and C. In C only the four Leksdal Nappe samples had analyzed U, all others are shown with interpolated straight lines between Ta and Th. Tectonic setting discriminant diagrams are from Wood (1980; D) and Meschede (1986; E). Because of available data, few or no samples are plotted from some areas in some diagrams. See text regarding possible errors in Nb values for samples from Ottfjället and Sylarna.

samples plotting in the field of within-plate alkali basalts. In figure 21E, rocks most similar to our Oppdal-like dikes, plotting closest to and even within the N-MORB field, include samples from the Oppdal, Orkanger, Piesa, Ottfjället-Tännäs, and Dabbsjön-Borgahällan areas. Samples from the Snåsa-Lurudal, Turtbakktjörna, Sylarna, Ströms-Vattudal, and Storsjouten areas plot toward and within the within-plate alkali basalt fields, analogous to our Ystland-like samples (hidden under other plotted points, see fig. 19B). The samples that tend to plot in the within-plate alkali basalt field are from the Ansätten, Alsen, Sørli, and especially the Leksdal areas. Our Sætra data set extends farther into N-MORB fields than any of the other plotted data sets (totaling 225 samples).

Geographic Variations in Dike Composition

From figure 21, we see that dikes in the Sætra Nappe quartzite and equivalents have REE patterns that range from flat (transitional MORB-like) to strongly LREE-enriched (alkaline). Though each sample area yielded a range of basaltic rock compositions, there are systematic geographic variations (fig. 22A). The composition vector illustrated in figure 22A is:

$$100(2Nb/(2Nb + Zr/4 + Y))$$

hereafter referred to as the NbZrY value. The NbZrY values plotted on figure 22A are medians for each sample area, effectively representing the median vertical position of data from each location on figures 19B and 21E. This compositional vector was chosen because it uses relatively immobile elements that were commonly analyzed by other workers, and it appears to vary smoothly across the Sætra compositional spectrum. It is also a relatively sensitive indicator of tholeiitic versus alkaline character in the absence of arc-like negative Nb anomalies.

Figure 22A shows that Sætra, Leksdal, and Särv dikes sampled near the southern and northern extremes of central Norway and west-central Sweden are most N-MORB-like, in the sense of figure 21E, with NbZrY values $\leq$30. NbZrY values generally increase northeastward from Årnes and Oppdal and southwards from Piesa, toward a central region 150 to 200 km northeast of Trondheim. There, median values of samples from Leksdal, Ansätten, and Alsen have NbZrY values $\geq$51, and thus have the most alkaline compositions. In addition, carbonatites have been discovered in the Särv Nappe at Prästrun and Åkersjön (figs. 1 and 22A; Jonsson and Stephens, 2006), plotting perfectly within the region of the most alkaline Neoproterozoic dikes.

Sætra-like dikes in basement on Lepsøy and in the Midsund area, figure 22A, do not have NbZrY values identical to nearby Sætra dikes, but instead have values more like those found at Oppdal to the east or Orkanger to the northeast. The dikes cutting basement and Risberget augen gneiss in the Geita-Kjora area have NbZrY values like those at Orkanger and Oppdal to the south, rather than those at Ystland to the north (see fig. 1 for location detail). This may illustrate differential transport between the Sætra Nappe and underlying parts of the Middle Allochthon (Risberget Nappe, basement sausage rock) during Scandian thrusting.

Concept for the Origin of Geographic Differences in Dike Compositions

It seems likely that the geographic distribution of different Sætra and equivalent dike compositions in Scandian thrust slices in some way represents their earlier distribution in the original dike swarms emplaced during Neoproterozoic rifting of the Baltica margin. Geographic variation of compositionally diverse magmas has been associated with rifting elsewhere, and we note three examples.

McHone (2000) reviewed the compositional and geographic diversity of dikes and lavas associated with Mesozoic rifting of Gondwanaland to form the Atlantic Ocean. He noted three compositionally and geographically large but distinct, if somewhat overlap-

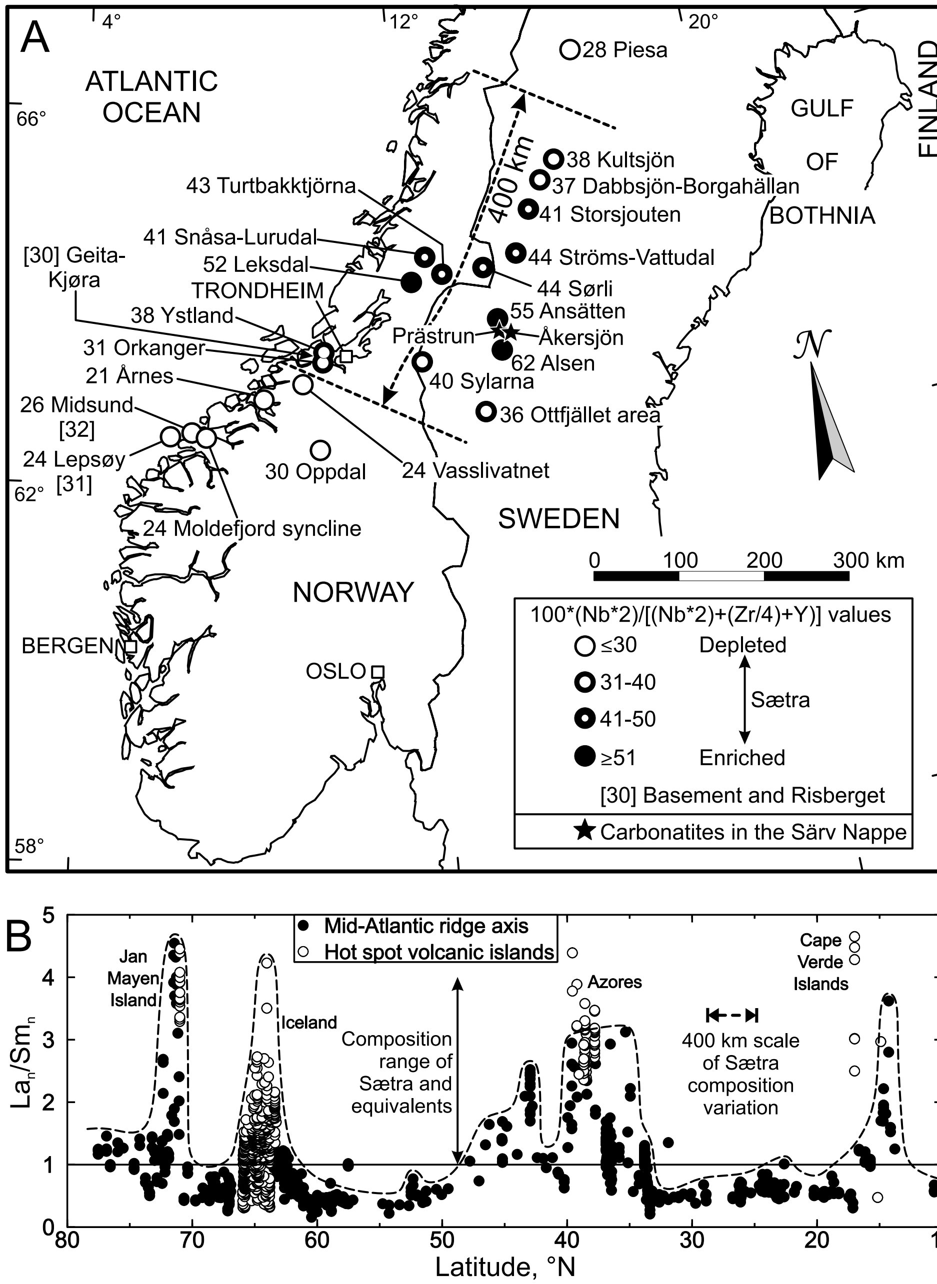

Fig. 22. (A) Map showing the locations of different Sætra Nappe (and equivalent) dike study areas, including our data and data of others (Appendix 1). Round symbols and numbers represent the median NbZrY value (see text and inset) for mafic rocks at each location. High values northeast and east of Trondheim (~64°N) are areas dominated by alkaline dikes, including carbonatites in the Särv Nappe (stars) at Prästrun and Åkersjön, Sweden, for which analytical data are unavailable. Dashed lines and arrow represent the 400 km geographic span of dikes having median NbZrY values >30. (B) Graph showing La_n/Sm_n variations along the Mid-Atlantic Ridge, 10°–80°N after Schilling and others (1983), redrafted to include additional data from the PETDB and GEOROC databases (see fig. 20 for citation; filtered as in fig. 20, but requiring only the trace elements La, and Sm in the analyses; rare rocks with La_n/Sm_n >5 were omitted). Curved dashed line indicates the approximate upper limit of La_n/Sm_n ratios for ocean ridge basalts along the ridge axis. Range of La_n/Sm_n ratios for Sætra and equivalent dikes, and the 400 km scale of Sætra dikes having median NbZrY values >30, are indicated.

ping, groups: Low-Ti, high-Mg magmas in southeastern and southern U.S.A.; intermediate-Ti, low Mg magmas in northeastern North America, Iberia, west and northwest Africa, and Brazil; and high-Ti, high Fe magmas in Liberia and northern South America. Each geographic region has a particular range of basalt compositions, as is found in the Sætra Nappe and equivalents, but the scale of these compositional provinces (>1000 km) is considerably larger than what we describe in the Caledonides (~400 km, fig. 22A).

Puffer (2002) examined regional geochemical distributions of Neoproterozoic dike swarms and lavas in eastern North America that are related to the opening of Iapetus, and are similar in age to the Sætra dikes. Puffer (2002) described three different compositional groups: An early (615 –564 Ma) flood basalt-type group; a younger group (554 – 550 Ma) geographically overlapping the first that is similar in composition to ocean-island basalts; and a MORB-like group of latest Proterozoic to early Paleozoic age (also see Coish, 1997). The contours of site average TiO_2 and Zr concentrations define an elongate shape that is probably, in part, the result of Taconian (Ordovician) collapse of Iapetus and thrusting onto the Laurentian continental margin. We note that the range of magma compositions discussed by Puffer (2002), and the scale of the contoured regions *perpendicular* to the Laurentian Iapetan margin, is similar to the scale of the Sætra compositional and geographic variations in figure 22A. The scale of the Laurentian compositional variations *parallel* to the Laurentian Iapetan margin, however, is thousands of kilometers.

Lastly, we consider an example involving compositional variations along the modern Mid-Atlantic Ridge. Schilling and others (1983; fig. 22B) illustrated La/Sm ratio variations with latitude along the northern Mid-Atlantic Ridge. For over half of the latitude range the La_n/Sm_n ratios are <1, characteristic of N-MORB-type magmas. However, at the latitudes of the Jan Mayen Islands, Iceland, the Azores, and the Canary Islands, and at 45°N, basalt La_n/Sm_n ratios range from 1 to 3.5. These regions were interpreted as having ocean-ridge magma sources that had been enriched by hot-spot-related mantle associated with the islands. Ridge segments having elevated La_n/Sm_n ratios range in length from ~400 km (Jan Mayen Islands, Iceland) to 600 km (Azores), comparable to the ~400 km scale of the Sætra dike compositional variations illustrated in figure 22A.

We suggest that, at the time of Late Neoproterozoic rifting of the Baltican margin, a hot spot on the scale of those presently influencing Mid-Atlantic Ridge lava compositions was present west or northwest of the Leksdal region (current coordinates). Mantle material associated with this hot spot influenced magma compositions for hundreds of kilometers along the rift axis at the incipient Baltica continental margin. Caledonian thrust transport of the Sætra Nappe and its correlative thrust sheets over 200 to 300 kilometers (Gee, 1975; Gee and Sturt, 1985; Siedlecka and others, 2004), was insufficient in degree or in diversity of direction to destroy this preexisting large-scale compositional pattern. Alkaline magmas in the Middle Allochthon in the Øksfjord region, 850 km north of Trondheim (Reginiussen and others, 1995), may have a similar origin.

CONCLUSIONS

Dikes cutting quartzites are extensively exposed in the Sætra and correlative nappes of the Middle Allochthon of the Caledonides of central Norway and Sweden. Using the chemical compositions of well correlated exposures of dikes in the Sætra at Oppdal and Orkanger, our data supports mapping evidence that assigns quartzites in six other regions to the Sætra: Vasslivatnet, Årnes, an extensive along-strike belt in the Moldefjord syncline, in the Helleneset syncline, on Lepsøy, in the Midsund area, and possibly also at Åsbøen. The Moldefjord belt includes both eclogites and amphibolites in quartzite that are compositionally typical of Sætra at most other localities, and one more strongly LREE-enriched sample (105, at Sunnaland). This dike is compositionally almost identical to those from quartzites at Ystland on the southeast limb of the Lensvik syncline on Trondheimsfjord, showing that the Ystland dike compositions are not unique. Despite differences between Oppdal and Ystland-like groups, their multi-element patterns and other aspects of their chemistry are remarkably similar. We conclude that the quartzites at all of these localities are correlative with the Sætra Nappe, and that the dikes represent the same Late Neoproterozoic dike swarms related to rifting of the Baltoscandian continental margin of Baltica. These are part of the same dike swarms characterized by others in the Särv and Leksdal nappes of Sweden and Norway. The compositional range of our dike set extends farther toward N-MORB-like compositions than any other Ottfjället dikes thus far reported.

There is a remarkably clear geographic distribution of dike compositions in the Sætra and equivalent nappes. The dikes are most LREE-enriched and alkaline at about the latitude of northern Trondheimsfjord (~64°N), and become progressively more N-MORB-like to the north and southwest. We interpret this central region of relatively alkaline compositions as having been influenced by a nearby source of hot-spot-enriched mantle during Neoproterozoic rifting.

An additional, important result of this work is that the dikes cutting basement on Lepsøy and on the southeastern shores of Dryna, Midøy, and Otrøy, dikes cutting basement and the Risberget Nappe in the Geita-Kjora area, and a few other mafic rocks in the Risberget Nappe, are essentially identical in composition to those of the Sætra Nappe. This suggests that the dike-rich basement, Risberget Nappe, and Sætra Nappe were cut by the same dike swarms that were emplaced during Late Neoproterozoic rifting of Baltoscandia during initial opening of the Iapetus Ocean. This conclusion implies that the dike-rich basement on Lepsøy, in the Midsund area, and at Geita is allochthonous, having been injected by dikes closer to the rifting axis compared to dike-poor parts of Baltican basement broadly exposed in the Western Gneiss Region.

This point is emphasized by comparisons in these three areas: 1) Though dikes dominate two belts of gneissic basement of the central segment on Lepsøy and Haramsøy (Terry and Robinson, 2003a, 2003b, 2004), they appear to be absent from the northern segment of Ulla Gneiss and related gneisses on Haramsøy, Flemsøy, and Fjørtoft, and absent from the southern segment of gneisses on Lepsøy, and Haramsøy. 2) Dike swarms also appear to be absent from gneisses on the north side of the islands surrounding Midsund, though they dominate gneisses on the southern coast. The dike swarms have also not been identified in basement areas closer to the Baltoscandian foreland. 3) Basement and Risberget augen gneiss in the Geita-Kjora area are cut by the same Sætra-like dike set. The Risberget Nappe and Sætra Nappe in these areas are both assigned to the Middle Allochthon, implying that the dike-rich basement is also part of the Middle Allochthon. This new recognition of basement areas with extensive Late Neoproterozoic dikes as part of the Middle Allochthon is a new framework for detailed bedrock geologic mapping, leading toward a more comprehensive understanding of the complex evolution of this major mountain belt.

ACKNOWLEDGMENTS

Field work and sample collecting by Hollocher in 2004 was supported by a grant from the American Scandinavian Foundation. For acknowledgment of support for early field work by Robinson, see Robinson (1995a). Most recently, mapping and field work was supported by Norges geologiske undersøkelse (Geological Survey of Norway). For acknowledgment of field work by Terry, see Terry and Robinson (2003). Union College provided support for major- and trace-element chemical analyses. Trace element analyses were also supported by National Science Foundation grant DUE-9952410. Alexandra McEnroe assisted with sample collecting. The paper benefited from informal reviews by Øystein Nordgulen, Arne Solli, Bauke Zwaan, and David Roberts, and formal reviews by Alan G. Krill, Victoria Pease, and John H. Puffer. To each of these institutions and persons we express our grateful acknowledgment.

Appendix 1

List of areas where data were used from the Sætra Nappe and its equivalents, with citations

Sample Area	Country	Reference
Alsen	Sweden	Solyom and others, 1985
Ansätten	Sweden	Solyom and others, 1985
Åkersjön	Sweden	Jonsson and Stephens, 2006
Dabbsjön-Borgahällan	Sweden	Solyom and others, 1985
Kultsjön	Sweden	Solyom and others, 1985
Leksdal	Norway	Andreasson and others, 1979; Solyom and others, 1985
Oppdal (Engan quarries)	Norway	Krill, 1983; Solyom and others, 1985; also this work
Orkanger	Norway	Solyom and others, 1985; also this work
Ottfjället-Tännäs	Sweden	Solyom and others, 1979; Solyom and others, 1985
Piesa	Sweden	Solyom and others, 1985
Prästrun	Sweden	Jonsson and Stephens, 2006
Snåsa-Lurudal	Norway	Solyom and others, 1985
Sørli	Norway	Beckholmen and Roberts, 1999
Storsjouten	Sweden	Solyom and others, 1985
Ströms-Vattudal	Sweden	Solyom and others, 1985
Sylarna	Sweden	Solyom and others, 1985
Turtbakktjörna	Norway	Solyom and others, 1985

Appendix 2

Notes for samples in tables 2–5

No.	PR Loc.	Place	Notes for samples in Table 2 – Mafic rocks in quartzites, mostly of the Sætra Nappe
299	NA	Oppdal	Eidsvoll flagstone quarry, NGU97.132 Stop 1-2, see fig. 1.
300	NA	Oppdal	As above.
301	NA	Oppdal	Eidsvoll quarry access road, NGU97.132 Stop 1-2, see photo fig. 2A.
302	NA	Oppdal	E side of Rt. E6 road cut adjacent to Eidsvoll quarry access road. Dark greenish-gray, fine-grained amphibolite dike 0.5 m thick.
303	NA	Oppdal	As above, 0.4 m thick dike structurally 15 cm above sample 302 dike.
304	NA	Oppdal	As above, medium-grained, 25 cm thick dike structurally 1.3 m below sample 302 dike. Plagioclase phenocrysts, sparse pyrite cubes.
305	NA	Oppdal	As above, 0.5 m thick dike, dark-gray.
306	NA	Oppdal	As above, 0.4 m thick dike, dark-gray.
307	NA	Oppdal	As above, 25 cm thick dike, dark greenish-gray.
308	NA	Oppdal	As above, 15 cm thick dike, dark yellowish-gray but fresh.
309	NA	Oppdal	As above, boudin near the N end of the road cut, medium-grained, biotite-rich, plagioclase streaks.
310	NA	Oppdal	Driva River, 1 m thick boudin, fine-grained, dark-gray, on W side of E6 below the western quarry, 50 m S of quarry access bridge over river.
311	NA	Oppdal	As above, 2 m thick boudin with plagioclase phenocrysts, 55 m S of quarry access bridge over river.
312	NA	Oppdal	As above, 9 m thick boudin with plagioclase phenocrysts, 40 m N of quarry access bridge over river.
313	NA	Oppdal	Fine-grained, medium grayish-green, 5 cm thick amphibolite layer. From quarry west of Driva River near Eidsvoll.
240	NA	Orkanger	Orkdalsfjord, Almlia quarry, map fig. 1. Fine-grained greenish-gray margin of composite dike 2 m thick.
241	NA	Orkanger	As above, center of composite 2 m thick dike.
242	NA	Orkanger	Orkdalsfjord, Almlia quarry, map fig. 1. Fine-grained greenish-gray dike.
243	NA	Orkanger	As above.
244	NA	Orkanger	As above, plagioclase phenocrysts.
245A	NA	Orkanger	As above, medium-grained, greenish-gray dike with plagioclase phenocrysts.
245B	NA	Orkanger	As above, plagioclase phenocrysts.
246	NA	Orkanger	As above, plagioclase phenocrysts.
247	NA	Orkanger	As above, plagioclase phenocrysts.
248	NA	Orkanger	As above, plagioclase streaks.
249	NA	Orkanger	As above, plagioclase streaks, sparse coarse hornblende crystals.
250	NA	Orkanger	As above, plagioclase phenocrysts.
251	NA	Orkanger	As above, plagioclase phenocrysts.
252	NA	Orkanger	As above, plagioclase phenocrysts.
253	NA	Orkanger	As above, plagioclase phenocrysts.
363	NA	Vasslivatnet	N side of Rt. 71, Flaugknebba, map fig. 1. Medium-grained dark-green dike 5 cm thick.
364	NA	Vasslivatnet	As above. Med.-grained dark greenish-gray dike 20 cm thick.
365	NA	Vasslivatnet	As above. Med.-grained dark greenish-gray dike 5 cm thick.
366	NA	Vasslivatnet	As above. Med.-grained dark greenish-gray dike 7 cm thick.

Appendix 2

(continued)

No.	PR Loc.	Place	Notes for samples in Table 2 (continued) – Mafic rocks in quartzites, mostly of the Sætra Nappe
333	NA	Årnes	Between Årnes and Kjergroneset, map figs. 1, 3. Medium-gray boudin 0.3 m thick, 1.5 m from contact with Blåhø Nappe.
334	NA	Årnes	As above. Fine-grained, dark-gray, from a 1.5 m thick section of quartzite, with sparse garnet.
335	NA	Årnes	As above. Biotite along foliation planes.
336	NA	Årnes	As above. Biotite along foliation planes.
337	NA	Årnes	As above. Biotite along foliation planes.
338	NA	Årnes	As above. Biotite along foliation planes.
94	354	Dragneset	S limb, Moldefjord syncline, map fig. 5. Fine-grained medium-gray, layer 1 m thick. 3.2 m in 34.6 m measured section.
95	354	Dragneset	As above. Medium-gray, fine-grained layer 1.2 m thick with sparse garnets, fresh pyrite. 7.65 m in 34.6 m measured section
96	354	Dragneset	As above. Fine-grained medium-gray layer 30 cm thick, very sparse garnet, some pyrite. 11.05 m in 34.6 m measured section.
97	354	Dragneset	As above. Fine-grained medium-gray layer 0.8 m thick, sparse garnet, pyrite. Near but not touching quartz vein. 14 m in 34.6 m measured section.
98	354	Dragneset	As above. Fine-grained medium greenish-gray boudin 0.6 m thick, epidote, some pyrite. 28.5 m in 34.6 m measured section.
99	354	Dragneset	As above. Fine-grained dark-gray, porphyry boudin 1.5 m thick. 25 cm from lower contact. Abundant pyrite. 32.5 m in 34.6 m measured section.
60†	170	Tennøya	S limb Moldefjord syncline, map fig. 6, point NE of station 170. Fine-grained retrograde boudin ~1 m-thick. small garnet; rusty fractures.
61†	170	Tennøya	As above, photo fig. 7C, at station 170. Retrograde eclogite boudin 2.4 m thick. Secondary hornblende veins, rusty fractures.
63†	171	Tennøya	As above. Very fresh, medium-gray, S-central part of 6 m-thick retrograded eclogite boudin, also yielded 64 and 66. Garnets to 4 mm, minor amphibolitized veins.
64†	171	Tennøya	As above. Very fresh, medium-gray, N part, same boudin 6 m-thick, ~2.5 m NE of sample 63. Garnets to 4 mm, minor amphibole veins.
65†	171	Tennøya	As above. Very fresh, dark-gray, center part, separate boudin 0.9 m-thick, NE of sample 64. Garnets to 2 mm, minor amphibole veins.
66†	171	Tennøya	As above. Very fresh, medium-gray, N part, same 6m-thick boudin, ~2.5 m NW of sample 63. Garnets to 4 mm, amphibolitized veins.
110†	138	Skår	S limb, Moldefjord syncline, map fig. 6, photo fig. 7B, at hammer handle. Very fresh, dark greenish-black, fine-grained tail of retrograded eclogite boudin 0.95 m thick, no surviving garnets. 0.3 m from contact with sheared augen gneiss in photo.
111	138	Skår	As above. Left (N) of photo fig. 7A. Dark-gray, fine-grained plagioclase porphyry. Last mafic layer 5-15 cm from Blåhø contact.
104	195	Sunnaland	Juvik near Skulmeisterneset, fault slice, S limb of Moldefjord syncline, map fig. 8. Med.-grained gray-green, plagioclase porphyry boudin 60 cm thick. 3.8-4.4 m in 7 m measured section of Sætra, 3 m S of marble on Blåhø contact.
105	195	Sunnaland	As above. Fine-grained greenish-gray, homogeneous, lacking phenocrysts. 1.5 m in 7 m measured thickness of Sætra, near Risberget contact.
67†	843	Lauvøy	N limb Helleneset syncline, map fig. 6, photo fig. 7D. South-central section, ~10 m thick, fresh retrograded layered eclogite boudin.
69†	843	Lauvøy	As above. East-central section, same boudin as sample 67, amphibolitized layered eclogite, 10 m NE of sample 67.
70	2245	Lepsøy	Bryggja, NW coast, fig. 9. Fine-grained, dark-gray layer 10-cm thick, 10 cm N of Blåhø contact. Slight rust, minor biotite, quartz veins.
71	2245	Lepsøy	As above. Hard, slightly weathered layer, east end of outcrop, ~0.7 m S of contact with gneiss. Traced W to where 25 cm below sample 70 layer.
72	2245	Lepsøy	As above. Fine-grained from small boudins in 2 m thick infold of Sætra in Blåhø, south from samples 70 and 71.
78	1265	Lepsøy	Hellevik, N coast, fig. 9. Fine-grained Dark-gray layer, in infold of Sætra in Blåhø, 1.3 m N of Blåhø contact. Sparse garnet, rusty cracks.
79	1265	Lepsøy	As above. Very fresh, fine-grained, medium-gray layer 30 cm thick, within thin infold of Sætra in Blåhø, 50 cm from Blåhø contact to S.
93	1265	Lepsøy	As above, photo fig. 7E. Center of layer with minor garnet 40 cm thick from the N Sætra belt folded to ~3 m at basement contact.
183	989	Midøy	Oksvollneset on S coast, map fig. 10, photo fig. 11. Medium-grained dark gray layer with garnets up to 6 mm, Sætra is 1 m thick, between Blåhø and sausage basement.

Appendix 2

(continued)

No.	PR Loc.	Place	Notes for samples in Table 2 (continued) – Mafic rocks in quartzites, mostly of the Sætra Nappe
184	989	Midøy	As above. Medium-grained layer from fold hinge in 7.6-cm-thick layer with 5 mm garnets.
185	989	Midøy	As above. Dark-gray, medium-gray layer with garnet, SW end of outcrop below high tide line. 12.7 cm below calc-silicate rock near contact with gneiss as in fig. 11.
285	NA	Ystland	Lensvik syncline, map fig. 1. Fine-grained dark greenish-gray layer 20-30 cm thick in quartzite near middle of quartzite section.
286	NA	Ystland	As above. Fine-grained dark greenish-gray layer 20-30 cm thick in quartzite near middle of quartzite section.
287	NA	Ystland	As above. Fine-grained dark greenish-gray layer 20-30 cm thick in quartzite near middle of the quartzite section.
288	NA	Ystland	As above. Fine-grained dark greenish-gray layer 20-30 cm thick in quartzite near the middle of quartzite section.
289	NA	Ystland	As above. Dark greenish-gray, fine-grained layer from lower in quartzite section than samples 285-288, 7 m above contact with basement.
323‡	NA	Ura	Belt SW of Surnadal syncline (Åmotsdal?), map fig. 3. Dark-gray, medium-grained biotite-, garnet-bearing boudin 0.4 m thick among several in road cut.
316	NA	Åsbøen	SE limb, Surnadal syncline, map fig. 3. Medium-gray, dark-gray, hornblende-rich boudin 1.5 m thick in 12 m thick quartzite section.
317	NA	Åsbøen	As above. Medium-grained, dark-gray, biotite-bearing boudin 0.6 m thick, 4 m above sample 316.

* Amphibolite except where eclogite is indicated. † Eclogite, retrograded to varying degrees. ‡ Composition not Sætra-like.

No.	PR Loc.	Place	Notes for samples in Table 3 – Mafic dikes in basement gneiss at Lepsøy, islands of Midsund (Dryna, Midøya, Otrøy) and Geita
73	2245	Lepsøy	Bryggja, NW coast, map fig. 9. Center of a 1 m thick layer in gneiss. Medium-grained with white feldspar streaks.
74	2245	Lepsøy	As above. From near the center of a body ~4 m thick with pyroxene-cored hornblende lumps several cm across.
75	2245	Lepsøy	Aa above. From 2 m N of sample 74. Darker garnet-bearing boudins within the larger boudin of sample 74.
76	3362	Lepsøy	Northernmost point of Lepsøy, fig. 9. 6 m-thick boudin with garnet.
77	3362	Lepsøy	As above. From NE side of the highest pointed block in vicinity. Medium-grained.
80	1265	Lepsøy	Hellevik lighthouse area, Fig. 9. Coarse with abundant plagioclase streaks. ~9 m N from N contact of northern Sætra belt.
81	1264	Lepsøy	As above. From 30-cm thick layer, ~10 m from shore, 80 m E of lighthouse. Very fresh, tough, medium-gray and fine-grained
82	1264	Lepsøy	As above. Med.-gray, fine-grained, very fresh center of 3 m boudin. Has quartz veins, avoided for sample. 70 m NE of lighthouse.
83	1264	Lepsøy	As above. 70 m SW of the lighthouse, middle of 0.5 m thick boudin in some less shredded gneiss. Medium-gray, very fresh.
84	1264	Lepsøy	As above. Center of medium-grained, medium-gray, large plagioclase-streaked boudin like sample 80. W-facing wall 10 m W of lighthouse.
85	1264	Lepsøy	As above. Center of 0.4 m thick layer. Dark-gray, medium-grained, very fresh from 20 m W of lighthouse, 1 m N of sample 84.
86	1264	Lepsøy	As above. Medium-grained, dark-gray layer, 40 m N of lighthouse.
170	910	Dryna	SW point of island, W from Dryna ferry terminal, map fig. 10. Coarse-grained, dark-gray boudin 1.4 m thick.
176	2564	Dryna	SE side, road cut, E point of Dryna, near bridge to Midøy, fig. 10. Coarse-grained, medium-gray.
177	2564	Dryna	NW side, road cut, E point of Dryna, near bridge to Midøy, fig. 10. Coarse-grained, medium-gray.
186	989	Midøy	Oksvollneset, S Midøy coast, map fig. 10. Boudin 1 m thick, 0.6 m where sampled. Medium-gray with sparse garnet. 14 m S from Sætra contact.
193	1449	Otrøy	Coast E. of Arnesklubben, SW Otrøy, map fig. 10. Amphibolite 4 m thick cutting gneiss layering. Medium-grained and medium-gray with plagioclase streaks.

APPENDIX 2

(continued)

No.	PR Loc.	Place	Notes for samples in Table 3 (continued) – Mafic dikes in basement gneiss at Lepsøy, islands of Midsund (Dryna, Midøya, Otrøy) and Geita
194	1449	Otrøy	As above. No plagioclase streaks. Medium-grained, medium-gray, 0.7 m thick layer. 6 m from 193 toward lighthouse.
195	1449	Otrøy	As above. 67 m NE on shore from 193. Coarse interior with pale hornblende, not fully fresh, fine chilled margins.
196	518	Otrøy	Point east of Juvika, SW Otrøy, map fig. 10. 3 m thick layer, very coarse-grained, medium-gray on fresh surfaces. Epidote veins but not in sample.
255	NA	Geita	Geita to Kjøra shore traverse, map fig. 1. Dike 1.5 m thick, cuts gneiss foliation (fig. 13A). Coarse-grained, dark gray with plagioclase phenocrysts, abundant biotite.
256	NA	Geita	As above. Boudin of dike 0.5 m thick, pitted weathered, biotite-rich, medium greenish-gray, medium-grained.
257	NA	Geita	As above. Dike 2 m thick, very fresh greenish-gray, fine-grained rock with 4 mm biotite scattered like gas vesicles.
258	NA	Geita	As above. Dike 2 m thick with graded layering. Very fresh, dark greenish-gray, fine-grained with 4 mm biotite grains.
259	NA	Geita	As above. Very fresh, biotite-rich, dark gray medium-grained dike 0.5 m thick. Local felsic melt.

No.	PR Loc.	Place	Notes for samples in Table 4 – Sætra-like mafic dikes, all amphibolites, in the Risberget Nappe
260	NA	Kjøra	Geita to Kjøra shore traverse, map fig. 1. Dike 1 m thick cutting both enclosing augen gneiss and dark-gray amphibolite sample 261.
262	NA	Kjøra	As above. Dike 0.5 m thick cutting Dark-gray amphibolite. Dark greenish-gray, fine-grained except 4 mm biotite crystals.
263	NA	Kjøra	As above. 0.7 m thick, cutting augen gneiss. Medium greenish-gray, medium-grained with biotite streaks.
264	NA	Kjøra	As above. 3 m thick, cutting fabric in augen-rich gneiss. Medium greenish-gray, fine-grained except for plagioclase phenocrysts to 1 cm.
265	NA	Kjøra	As above. Dike 0.5 m thick, cutting augen gneiss near shore. Medium greenish-gray and medium-grained
321	NA	Ura	Map fig. 2. Coarse-grained, biotite-rich hornblendite boudin 1 m thick in augen gneiss.
322	NA	Ura	As above. Medium-grained biotite-bearing boudin 4 m thick.
103	333	Øygardsneset	Map fig. 5. Fine-grained dark greenish-gray amphibolite dike cutting coarse augen gneiss, containing abundant black tourmaline.
68	842	Lauvøy	N limb Helleneset syncline, map fig. 6, photo fig. 13B. 25 cm-thick layer in sheared augen gneiss, 20 m N from Sætra contact.
108	138	Skår	Map fig. 6, photo fig. 15. Medium-grained medium greenish-gray 30 cm thick homogeneous layer within mapped layered “gabbro unit” in which non-Sætra compositions predominate.
125	189	Brattvåg	Quarry behind factory, ferry access road, map fig. 8, photograph fig. 14. Fine-grained, greenish-gray, biotite-bearing 25 cm dike in augen gneiss, 7.6 m S of Risberget “gabbro” contact.
135	195	Sunnaland	Point inside Juvik, S of Skulmeisterneset, map fig. 8. Coarse-grained medium-grained near N contact of mapped mafic unit.

Appendix 2

(continued)

No.	PR Loc.	Place	Notes for samples in Table 5 – Mafic rocks within Risberget Nappe that are unlike those of the Sætra Nappe
261	NA	Kjøra	Map fig. 1. Geita to Kjøra shore traverse. Mafic body cut by dike sample 260. Coarse-grained medium-gray, Different from all nearby dikes.
329	NA	Årnes	Map fig. 3. Between Årnes and Kjergroneset. Biotite-rich, dark-gray, medium-grained layer up to 1 m thick. Hard to collect, fractures and veins.
391	NA	Oppdal	Map fig. 1. Old Rt. E6, NGU97.132 Stop 1-3A. Strongly layered mafic schist. SE end of road cut, 11m SE from anorthosite contact.
393	NA	Oppdal	As above. Mafic porphyry layer NW structurally below (33 m NW of) base of anorthosite, mingled with schistose mafic rocks and sheared Risberget augen gneiss.
152	8	Bolsøy	Low outcrop on N shore of augen gneiss point, Robinson (1995a, his fig. 3). Fine-grained med.-gray, looks more felsic on broken edges.
168	-	Bolsøy	New road cut, Dragvågen Road. Collected 2004, dynamited in housing development 2005. Dark-gray, coarse-grained rock from mapped mafic section in Risberget augen gneiss, Robinson (1995a, his fig. 3).
102	333	Øygardsneset	Map fig. 5. Fine-grained medium-gray 35 cm-thick layer very rich in biotite amongst fine-grained gray Risberget rock.
62	138	Tennøy	Tennøy, NW coast, map fig. 6. Gray ~0.5 by 1.5 m boudin in Risberget augen gneiss, part of string of boudins up to 2 m thick. No garnet. Lies within obvious augen gneiss, not in extremely mylonitic contact zone.
106	138	Skår	Map fig. 6. Medium-grained, homogeneous layer 12 m from SW-most exposure of mafic rocks.
107	138	Skår	As above. Medium greenish-gray, coarse-grained from boudin 5 m by 15 m.
109	138	Skår	As above. From west point of mafic rock, 18 m from contact with Sætra. Medium-grained medium-gray.
123	189	Brattvåg	Ferry access road, quarry behind factory, map fig. 8. Fine-grained greenish-gray biotite-rich dike 30 cm thick in augen gneiss. 22 m S of contact with Risberget gabbro.
124	189	Brattvåg	As above. Fine-grained greenish-gray biotite-rich dike 20 cm thick in augen gneiss. 18 m S of contact with Risberget gabbro.
126	189	Brattvåg	As above. Fine-grained dark-gray. Sample from 6 m N of augen gneiss contact.
127	189	Brattvåg	As above. Coarse-grained first collectable gabbro, 0.6 m N of augen gneiss contact.
136	196	Sunnaland	Point near Kvithaugen, W of Juvik, map fig. 8. Medium-grained homogeneous pyrite-bearing rock, 365 m W of sample 135, 10.6 m S of contact with augen gneiss, exposed on water side of outcrop.

Appendix 3

Sample locations in latitude and longitude by global positioning system (GPS; decimal degrees) and elevation (meters above mean sea level; estimated along shorelines, by GPS at inland locations). In general, estimated error is <10 m

Samples	Quadrangle	GPS position			Samples	Quadrangle	GPS position		
		Longitude	Latitude	Elevation			Longitude	Latitude	Elevation
60	Brattvåg	6.58881	62.62934	3	136	Brattvåg	6.40830	62.60862	5
61	Brattvåg	6.58816	62.62911	3	152	Vestnes	7.28371	62.72573	2
62	Brattvåg	6.58729	62.62894	2	168	Vestnes	7.29144	62.72696	13
63	Brattvåg	6.58760	62.62891	4	170	Brattvåg	6.51889	62.63991	4
64	Brattvåg	6.58959	62.62968	4	176-177	Brattvåg	6.55937	62.64901	4
65-66	Brattvåg	6.58970	62.62970	3	183-186	Brattvåg	6.63224	62.65508	4
67-69	Brattvåg	6.58677	62.61007	4	193-195	Brattvåg	6.68944	62.66283	4
70	Vigra	6.12820	62.63161	6	196	Brattvåg	6.70202	62.66569	4
71	Vigra	6.12860	62.63161	6	240-253	Orkanger	9.86844	63.33942	9
72	Vigra	6.12830	62.63127	3	255	Orkanger	9.97652	63.43587	3
73	Vigra	6.12842	62.63186	4	256	Orkanger	9.97562	63.43509	4
74-75	Vigra	6.12837	62.63202	4	257	Orkanger	9.97531	63.43365	3
76-77	Vigra	6.14241	62.63784	6	258	Orkanger	9.97451	63.43242	2
78	Vigra	6.17376	62.63726	3	259	Orkanger	9.97335	63.43060	3
79	Vigra	6.17381	62.63725	3	260-261	Orkanger	9.97285	63.42938	3
80	Vigra	6.17300	62.63743	4	262	Orkanger	9.97287	63.42852	3
81	Vigra	6.17224	62.63756	3	263	Orkanger	9.97012	63.42101	3
82	Vigra	6.17173	62.63762	4	264	Orkanger	9.97038	63.42080	3
83	Vigra	6.17103	62.63703	5	265	Orkanger	9.97001	63.41915	4
84	Vigra	6.17128	62.63722	6	285-289	Rissa	9.80819	63.51858	7
85	Vigra	6.17111	62.63728	4	299-300	Snøhetta	9.57782	62.45822	716
86	Vigra	6.17161	62.63761	4	301	Snøhetta	9.57804	62.46132	670
93	Vigra	6.17336	62.63734	3	302-309	Snøhetta	9.57760	62.46236	661
94	Vestnes	6.79878	62.65261	2	310-311	Snøhetta	9.57064	62.45984	638
95-98	Vestnes	6.79870	62.65265	2	312-313	Snøhetta	9.57117	62.46095	643
99	Vestnes	6.79826	62.65280	3	316-317	Stangvik	8.60728	62.89653	88
102-103	Brattvåg	6.70090	62.63965	5	321	Stangvik	8.47001	62.90586	51
104-105	Brattvåg	6.41560	62.60942	3	322	Stangvik	8.46760	62.90700	32
106	Brattvåg	6.53311	62.61917	4	323	Stangvik	8.46434	62.90802	40
107-109	Brattvåg	6.53230	62.61917	5	329	Stangvik	8.49015	62.97227	19
110-111	Brattvåg	6.53187	62.61947	4	333-338	Stangvik	8.49143	62.97136	16
123-127	Brattvåg	6.44616	62.62664	5	363-366	Løkken	9.27764	63.22197	281
135	Brattvåg	6.41499	62.60912	3	391-393	Snøhetta	9.62500	62.43040	700

References

Andréasson, P. G., Solyom, Z., and Roberts, D., 1979, Petrochemistry and tectonic significance of basic and alkaline-ultrabasic dykes in the Leksdal Nappe, northern Trondheim region, Norway: Norges geologiske undersøkelse Bulletin, v. 348, p. 47–72.

Andréasson, P. G., Svenningsen, O. M., and Albrecht, L., 1998, Dawn of Phanerozoic Orogeny in the North Atlantic tract; evidence from the Seve-Kalak Superterrane, Scandinavian Caledonides: GFF, v. 120, p. 159–172.

Becker, H., Jochum, K., and Carlson, R., 2000, Trace element fractionation during dehydration of eclogites from high-pressure terranes and the implications for element fluxes in subduction zones: Chemical Geology, v. 163, p. 65–99.

Beckholmen, M., and Roberts, D., 1999, Mafic dykes in the Leksdal Nappe at Sørli, central Norwegian Caledonides: geochemistry and paleotectonic implications: Norges geologiske undersøkelse Bulletin, v. 435, p. 59–67.

Carswell, D. A., and Harvey, M. A., 1981, Molde-Otrøy-Midøy, *in* Griffin, W. L., and Mørk, M. B. E., editors, Excursions in the Scandinavian Caledonides (Uppsala Caledonide Symposium), Excursion B1: Oslo, Norway, Geologisk Museum.

——— 1985, The intrusive history and tectonometamorphic evolution of the Basal Gneiss Complex in the Moldefjord area, west Norway, *in* Gee, D. G., and Sturt, B. A., editors, The Caledonide Orogen–Scandinavia and Related Areas: London, John Wiley and Sons, p. 843–857.

Coish, R. A., 1997, Rift and ocean floor volcanism from the Late Proterozoic and early Paleozoic of the Vermont Appalachians; p. 129–145, *in* Sinha, A. K., Whalen, J. B., and Hogan, J. P., editors, The Nature of Magmatism in the Appalachian Orogen: Geological Society of America, Memoir 191, 429 p.
Dupuy, C., Vidal, P., Maury, R., and Guille, G., 1993, Basalts from Mururoa, Fangataufa and Gambier islands (French Polynesia): geochemical dependence on age of the lithosphere: Earth and Planetary Science Letters, v. 117, p. 89–100.
Finlow-Bates, T., and Stumpfl, E. F., 1981, The behavior of so-called immobile elements in hydrothermally altered rocks associated with volcanogenic submarine-exhalative ore deposits: Mineralium Deposita, v. 16, p. 319–328.
Gee, D. G., 1975, A tectonic model for the central part of the Scandinavian Caledonides: American Journal of Science, v. 275-A, p. 468–515.
——— 1977, Extension of the Offerdal and Särv Nappes and Seve Supergroup into northern Trondelag: Norsk Geologisk Tidsskrift, v. 57, p. 163–170.
——— 1978, Nappe displacement in the Scandinavian Caledonides: Tectonophysics, v. 47, p. 393–419.
——— 1980, Basement-cover relationships in the central Scandinavian Caledonides: Geologiska Föreningen i Stockholm Förhandlingar, v. 102, p. 523–530.
Gee, D. G., and Kumpulainen, R., 1980, An excursion through the Caledonian mountain chain in central Sweden from Östersund to Storlien: Sverges geologiska undersökning, C774, 66 p.
Gee, D. G., and Sturt, B. A., 1985, editors, The Caledonide Orogen – Scandinavia and Related Areas: Chichester, John Wiley and Sons, 1266 p.
Gee, D. G., and Wolff, F. C., 1981, The Central Scandinavian Caledonides – Östersund to Trondheim: Uppsala Caledonide Symposium 1981, excursion guide A2, 85 p.
Gee, D. G., Guezou, J. C., Roberts, D., and Wolff, F. C., 1985, The central-southern part of the Scandinavian Caledonides, *in* Gee, D. G., and Sturt, B. A., editors, The Caledonide Orogen – Scandinavia and Related Areas: Chichester, John Wiley and Sons, p. 109–133.
Glass, L. M., and Phillips, D., 2006, The Kalkarindji continental flood basalt province: a new Cambrian large igneous province in Australia with possible links to faunal extinctions: Geology, v. 34, p. 461–464.
Grauch, R. I., 1989, Rare earth elements in metamorphic rocks, *in* Lipin, B. R., and McKay, G. A., editors, Geochemistry and Mineralogy of Rare Earth Elements: Mineralogical Society of America, Reviews in Mineralogy, v. 21, p. 147–167.
Greenough, J. D., Fryer, B. J., and Robinson, P. T., 1990, Geochemical effects of alteration on mafic rocks from Indian Ocean site 706, *in* Duncan, R., Backman, J., Peterson, L., Baker, P., Baxter, A., Boersma, A., Cullen, J., Droxler, A., Fisk, M., Greenough, J., Hargraves, R., Hempel, P., Hobart, M., Hurley, M., Johnson, D., Macdonald, A., Mikkelsen, N., Okada, H., Rio, D., Robinson, S., Schneider, D., Swart, P., Tatsumi, Y., Vandamme, D., Vilks, G., Vincent, E., and Barbu, E., editors: Proceedings of the Ocean Drilling Program, Scientific Results, v. 115, p. 85–92.
Griffin, W. L., Austrheim, H., Brastad, K., Bryhni, I., Krill, A. G., Krogh, E. J., Mørk, M. B. E., Qvale, H., and Tørudbakken, B., 1985, High-pressure metamorphism in the Scandinavian Caledonides, *in* Gee, D. G., and Sturt, B. A., editors, The Caledonide Orogen–Scandinavia and Related Areas: Chichester, John Wiley and Sons, p. 783–801.
Grammeltvedt, G., 1995, Løkken Berggrunnskart 1521-III: Norges geologiske undersøkelse, scale 1:50,000.
Handke, M. J., Tucker, R. D., and Robinson, P., 1995, Contrasting U-Pb Ages for the Risberget Augen Gneiss in the Norwegian Caledonides: Getting to the Root of the Problem: Geological Society of America Abstracts with Programs, v. 27, n. 6, p. A–226.
Hollocher, K., 1985, Geochemistry of Metamorphosed volcanic rocks in the Middle Ordovician Partridge Formation, and amphibole dehydration reactions in the high-grade metamorphic zones of central Massachusetts: Amherst, Massachusestts, Department of Geology and Geography, University of Massachusetts, Ph. D. thesis, Contribution 56, 275 p.
——— 1993, Geochemistry and origin of volcanics in the Ordovician Partridge Formation, Bronson Hill anticlinorium, west-central Massachusetts: American Journal of Science, v. 293, p. 671–721.
Humphris, S. E., and Thompson, G., 1978, Trace element mobility during hydrothermal alteration of oceanic basalts: Geochimica et Cosmochimica Acta, v. 42, p. 127–136.
Jonsson, E., and Stephens, M. B., 2006, Metamorphosed U-Nb-Ta-REE-bearing alkaline rocks from the Swedish Caledonides in Jämtland: Bulletin of the Geological Society of Finland, Special Issue 1, p. 63.
Knoll, A. H., Walter, M. R., Narbonne, G. M., and Christie-Blick, N., 2006, The Ediacaran Period: a new addition to the geologic time scale: Lethaia, v. 39, p. 13–30.
Krill, A. G., 1980, Tectonics of the Oppdal area, central Norway: Geologiska Föreningen i Stockholm Förhandlingar, v. 102, p. 523–530.
——— 1983, Rb-Sr study of dolerite dikes and psammite from the Western Gneiss Region of Norway: Lithos, v. 16, p. 85–93.
——— 1986, Eidsvoll quarry, Oppdal, South Norway; a one-outcrop model for some aspects of Trollheimen-Dovrefjell tectonics: Norges geologiske undersøkelse Bulletin, v. 404, p. 21–30.
——— 1987, Stangvik Berggrunnskart 1420-IV: Norges geologiske undersøkelse, scale 1:50,000.
Krill, A. G., and Röshoff, K., 1981, Basement-cover relationships in the central Scandinavian Caledonides: Uppsala Caledonide Symposium, Mineralogisk–Geologisk Museum, Excursion B-5, 88 p.
Krill, A. G., and Sigmond, E. M. O., 1986, Surnadalens dekkalagfolge og dens fortsettelse mot vest: Geonytt, v. 21, p. 35.
Kumpulainen, R., and Nystuen, J. P., 1985, Late Proterozoic basin evolution and sedimentation in the westernmost part of Baltoscandia, *in* Gee, D. G., and Sturt, B. A., editors, The Caledonide Orogen – Scandinavia and Related Areas: Chichester, John Wiley and Sons, p. 213–232.
Lehnert, K., Su, Y., Langmuir, C. H., Sarbas, B., and Nohl, U., 2000, A global geochemical database structure for rocks: Geochemistry, Geophysics, Geosystems, v. 1, paper no. 1999GC000026.

Ludden, J., and Thompson, G., 1979, An evaluation of the behavior of the rare earth elements during the weathering of sea-floor basalt: Earth and Planetary Science Letters, v. 43, p. 85–92.
Lutro, O., Robinson, P., Solli, A., Tucker, R. D., Wain, A., Terry, M. P., and Krabbendam, M., 1997, Proterozoic geology and Scandian high-pressure overprinting in the Western Gneiss Region: COPENA Conference (Correlation of Proterozoic of Europe and the North Atlantic Region): Guidebook for Field Trip A-3 (August 14–17), Norges geologiske undersøkelse Report 97.132, 86 p.
McDonough, W. F., and Sun, S. S., 1995, The Composition of the Earth: Chemical Geology, v. 120, p. 223–253.
McHone, J. G., 2000, Non-plume magmatism and rifting during the opening of the central Atlantic Ocean: Tectonophysics, v. 316, no. 3-4, p. 287–296.
Meschede, M., 1986, A method of discriminating between different types of mid-ocean ridge basalts and continental tholeiites with the Nb-Zr-Y diagram: Chemical Geology, v. 56, p. 207–218.
Mitchell, J. B., and Roberts, D., 1986, Ages of lamprophyre dykes from Ytterøy and Lerkehaug, near Steinkjer, central Norwegian Caledonides: Norsk Geologisk Tidsskrift, v. 66, p. 255–261.
Mocek, B., 2001, Geochemical evidence for arc-type volcanism in the Aegean Sea; the blueschist unit of Siphnos, Cyclades (Greece): Lithos, v. 57, p. 263–289.
Münker, C., 1998, Nb/Ta fractionation in a Cambrian arc/back arc system, New Zealand: source constraints and application of refined ICPMS techniques: Chemical Geology, v. 144, p. 23–45.
Pearce, J. A., 1976, Statistical analysis of major element patterns in basalts: Journal of Petrology, v. 17, p. 15–37.
——— 1982, Trace element characteristics of lavas from destructive plate boundaries, *in* Thorpe, R. S., editor, Andesites: New York, John Wiley and Sons, Publishers, p. 525–548
Pearce, J. A., and Parkinson, I. J., 1993, Trace element models for mantle melting: application to volcanic arc petrogenesis, *in* Prichard, H. M., Alabaster, T., Harris, N. B. W., and Neary, C. R., editors, Magmatic Processes and Plate Tectonics: London, Geological Society Special Publication, no. 76, p. 373–403.
Pearce, J. A., and Peate, D. W., 1995, Tectonic implications of the composition of volcanic arc magmas: Annual Reviews of Earth and Planetary Sciences, v. 23, p. 251–285.
Pearce, J. A., Harris, N. B. W., and Tindle, A. G., 1984, Trace element discrimination diagrams for the tectonic interpretation of granitic rocks: Journal of Petrology, v. 25, p. 956–983.
Pearce, J. A., Baker, P. E., Harvey, P. K., and Luff, I. W., 1995, Geochemical evidence for subduction fluxes, mantle melting and fractional crystallization beneath the South Sandwich Island arc: Journal of Petrology, v. 36, p. 1073–1109.
Polat, A., Hofmann, A., Muenker, C., Regelous, M., and Appel, P., 2003, Contrasting geochemical patterns in the 3.7-3.8 Ga pillow basalt cores and rims, Isua greenstone belt, southwest Greenland; implications for postmagmatic alteration processes: Geochimica et Cosmochimica Acta, v. 67, p. 441–457.
Puffer, J. H., 2002, A late Neoproterozoic eastern Laurentian superplume: location, size, chemical composition, and environmental impact: American Journal of Science, v. 302, p. 1–27.
Reginiussen, H., Krogh-Ravna, E. J., and Berglund, K., 1995, Mafic dikes from Øksfjord, Seiland Igneous Province, northern Norway: geochemistry and paleotectonic significance: Geological Magazine, v. 132, p. 667–681.
Rickard, M. J., 1985, The Surnadal Synform and basement gneisses in the Surnadal-Sunndal District of Norway, *in* Gee, D. G., and Sturt, B. A., editors, The Caledonide Orogen – Scandinavia and Related Areas: Chichester, John Wiley and Sons, p. 485–497.
Roberts, D., and Gee, G. H., 1985, An introduction to the structure of the Scandinavian Caledonides, *in* Gee, D. G., and Sturt, B. A., editors, The Caledonide Orogen–Scandinavia and Related Areas: Chichester, John Wiley and Sons, p. 55–68.
Robinson, P., 1995a, Extension of Trollheimen tectono-stratigraphic sequence in deep synclines near Molde and Brattvåg, Western Gneiss Region, southern Norway: Norsk Geologisk Tidsskrift, v. 75, p. 181–197.
——— 1995b, Evidence for Caledonide thrust nappes in the high-grade eclogite-facies area northwest of Moldefjord syncline, Western Gneiss Region: Geonytt 1–95, p. 61.
——— 2003, Day 3: Structural-metamorphic relationships between Caledonide Nappes and Fennoscandian basement on the mainland near Brattvåg. Guidebook for Post-Meeting Excursion, Alice Wain Memorial West Norway Eclogite Field Symposium, Selje, Norway: Norges geologiske undersøkelse, Report 2003.057, p. 71–86.
Robinson, P., and Panish, P. T., 1994, Trapping a prograde eclogite-facies P-T path in deformed diabase dikes of the Sætra and Risberget Nappes adjacent to high-grade eclogite-facies Baltic basement, western gneiss region, Norway: Eos, v. 75, p. 175.
Robinson, P., Krogh, T., and Carswell, T., 2003, Geology from Nordøyane-Midsund to Trondheim. Guidebook for Post-Meeting Excursion, Alice Wain Memorial West Norway Eclogite Field Symposium, Selje, Norway: Norges geologiske undersøkelse, Report 2003.057, p. 125–142.
Röshoff, K., 1978, Structures of the Tännäs Augen Gneiss Nappe and its relation to the underlying and overlying units in the central Scandinavian Caledonides: Sveriges geologiska undersökning, Series C739, 35 p.
Rudnick, R. L., and Gao, S., 2003, Composition of the continental crust, *in* Holland, H. D., and Turekian, K. K., editors, Treatise on Geochemistry: Elsevier, Amsterdam, v. 3, p. 1–64.
Schilling, J. G., Zajac, M., Evans, R., Johnston, T., White, W., Devine, J. D., and Kingsley, R., 1983, Petrologic and geochemical variations along the Mid-Atlantic Ridge from 29 degrees N to 73 degrees N: American Journal of Science, v. 283, p. 510-586.
Shikazono, N., 1999, Rare earth element geochemistry of Kuroko ores and hydrothermally altered rocks; implication for evolution of submarine hydrothermal system at back-arc basin, *in* Shikazono, N., Shimizu, M., Inoue, A., and Utada, M., editors, The Japanese Island Arc; its Hydrothermal and Igneous Activities: Resource Geology, special monograph, v. 20, p. 23–30.

Siedlecka, A., Roberts, D., Nystuen, J. P., and Olovyanishnikov, V. G., 2004, Northeastern and northwestern margins of Baltica in Neoproterozoic time: evidence from the Timanian and Caledonian Orogens, *in* Gee, D. G., and Pease, V., editors, The Neoproterozoic Timanide Orogen of Eastern Baltica: London, Geological Society Memoir No. 30, p. 169–190.
Solli, A., Robinson, P., and Tucker, R. D., 1997, Proterozoic basement and Scandian geology of the outer Trondheimsfjord region: Norges geologiske undersøkelse, Report 97.133, 21 p.
Solyom, Z., Gorbatschev, R., and Johansson, I., 1979, The Ottfjäll dolerites: Geochemistry of the dyke swarm in relation to the geodynamics of the Caledonide Orogen of central Scandinavia: Sveriges geologiska undersökning, Series C756, Årsbok, no. 72, 38 p.
Solyom, Z., Andréasson, P. G., and Johansson, I., 1985, Petrochemistry of Late Proterozoic rift volcanism in Scandinavia. II: The Särv dolerites (SD) - volcanism in the constructive arms of Iapetus: Lund Publications in Geology, no. 35, 42 p.
Sun, S. S., and McDonough, W. F., 1989, Chemical and isotopic systematics of oceanic basalts: implications for mantle composition and processing, *in* Saunders, A. D., and Norry, M. J., editors, Magmatism in the Ocean basins: London, Geological Society Special Publication, no. 42, p. 313–345.
Terry, M. P., and Robinson, P., 2003a, Evolution of amphibolite-facies structural features and boundary conditions for deformation during exhumation of HP and UHP rocks, Nordøyane, Western Gneiss Region, Norway: Tectonics, v. 22, p. 1036–1058.
——— 2003b, Day 2: Geology of Haramsøya, Flemsøya and Lepsøya. Guidebook for Post-Meeting Excursion, Alice Wain Memorial West Norway Eclogite Field Symposium, Selje, Norway: Norges geologiske undersøkelse Report 2003.057, p. 33–70.
——— 2004, Geometry of eclogite facies structural features; implications for production and exhumation of ultrahigh-pressure and high-pressure rocks, Western Gneiss Region, Norway: Tectonics, v. 23, p. 1–23.
Terry, M. P., Robinson, P., and Ravna, E. K., 2000, Kyanite eclogite thermobarometry and evidence for thrusting of UHP over HP metamorphic rocks, Nordøyane, Western Gneiss Region, Norway: American Mineralogist, v. 85, p. 1637–1650.
Thompson, R. N., Morrison, M. A., Hendry, G. L., and Parry, S. J., 1984, An assessment of the relative roles of crust and mantle in magma genesis: an elemental approach: Philosophical Transactions of the Royal Society of London, v. A310, p. 549–590.
Tucker, R. D., 1986, Geology of the Hemnefjord-Orkanger area, south-central Norway: Norges geologiske undersøkelse Bulletin, v. 404, p. 1–24.
Tucker, R. D., Krogh, T. E., and Råheim, A., 1990, Proterozoic evolution and age-province boundaries in the central part of the Western Gneiss Regon, Norway: Results of U-Pb dating of accessory minerals from Trondheimsfjord to Geiranger, *in* Gower, C. F., Ryan, B., and Rivers, T., editors, Middle Proterozoic Geology of the Southern Margin of Proto Laurentia-Baltica: Geological Association of Canada Special Paper 38, p. 149–173.
Tucker, R. D., Robinson, P., Solli, A., Gee, D. G., Thorsnes, T., Krogh, T. E., Nordgulen, Ø., and Bickford, M. E., 2004, Thrusting and extension in the Scandian hinterland, Norway: new U-Pb ages and tectonostratigraphic evidence: American Journal of Science, v. 304, p. 477–532.
Verma, S. P., 2000, Geochemistry of the subducting Cocos Plate and the origin of subduction-unrelated mafic volcanism at the volcanic front of the central Mexican volcanic belt, *in* Delgado-Granados, H., Aguirre-Diaz, G. J., and Stock, J. M., editors, Cenozoic Tectonics and Volcanism of Mexico: Geological Society of America, Special Paper, v. 334, p. 195–222.
Vidal, G., and Moczydłowska, M., 1995, The Neoproterozoic of Baltica—stratigraphy, paleobiology and general geological evolution: Precambrian Research, v. 73, p. 197–216.
Wood, D. A., 1980, The application of a Th-Hf-Ta diagram to problems of tectonomagmatic classification and to establishing the nature of crustal contamination of basaltic lavas of the British Tertiary Volcanic Province: Earth and Planetary Science Letters, v. 50, p. 11–30.